University of São Paulo
"Luiz de Queiroz" College of Agriculture

Remote and proximal sensing applications for soil conservation and management

Henrique Bellinaso

Thesis presented to obtain the degree of Doctor in Science. Area: Soil and Plant Nutrition

Piracicaba
2022

Henrique Bellinaso
Agronomist

Remote and proximal sensing applications for soil conservation and management

versão revisada de acordo com a Resolução CoPGr 6018 de 2011

Advisor:
Prof. Dr. **JOSÉ ALEXANDRE MELO DEMATTÊ**

Thesis presented to obtain the degree of Doctor in Science. Area: Soil and Plant Nutrition

Piracicaba
2022

Dados Internacionais de Catalogação na Publicação
DIVISÃO DE BIBLIOTECA – DIBD/ESALQ/USP

Bellinaso, Henrique

Remote and proximal sensing applications for soil conservation and management / Henrique Bellinaso. - - versão revisada de acordo com a Resolução CoPGr 6018 de 2011. - - Piracicaba, 2022.

109 p.

Tese (Doutorado) - - USP / Escola Superior de Agricultura “Luiz de Queiroz”.

1. Mapeamento de solos 2. Pedometria 3. Sensoriamento remoto 4. Erosão I. Título

DEDICATÓRIA

À Gladys e Maria

Por todo suporte, incentivo e apoio incondicional

Dedico.

AGRADECIMENTOS

Primeiramente agradeço a Deus e a Jesus onde deposito minha fé, e de quem recebo todo proposito para minha vida.

A minha esposa, amiga companheira Gladys, por todo apoio e incentive que recebi nesses anos e a Maria nossa filha, que é uma fonte de alegria e amor inexplicável.

A meus pais Ivo e Maria, por todo incentivo que me deram e sacrifícios por que passaram para permitir que pudesse estudar e conseguir chegar até aqui. A meus irmãos Letícia e Filipe, meu cunhado Pedro e meus sobrinhos Mateus e Amanda, por também sempre me incentivarem e pela amizade.

Ao meu sogro e sogra, Geraldo e Ademair, Glenio, Lilia, Ester e João Pedro, também por todo incentivo e amizade.

Aos professors do Departamento de Ciência do Solo e do PPG Solos e Nutrição de Plantas, assim como de outros departamentos de quem recebi os mais diferentes ensinos e conselhos.

A ESALQ/USP, ao Departamento de Ciência do Solo e ao PPG Solos e Nutrição de Plantas por toda estrutura e apoio necessários.

Aos professores Gerd Sparovek (ESALQ/USP), Peterson Ricardo Fiorio (ESALQ/USP) e Mara de Andrade Marinho (UNICAMP), por todo auxílio e apoio referente as informações da Microbacia do Córrego do Ceveiro.

Ao professor Marcos Rafael Nanni e ao GALeS, da Universidade Estadual de Maringá, pela disponibilização das imagens AISA-FÊNIX, utilizadas no presente trabalho.

A Fundação de Amparo a Pesquisa do Estado de São Paulo - FAPESP, pelos recursos financeiros para desenvolvimento do projeto através do Projeto Temático 14/22262-0.

A todos os colegas do Geocis com quem pude conviver por algum momento durante esses 4 anos: Fellipe, Nélida, Raul, Rodnei, Jorge, Nicolas, José Lucas, André Dotto, Soledad, Mah, Salman, Danilo, Ariane, Wanderson, Benito, Luiz Ruiz, Andrés, Lucas Greschuk, Natasha Valadares, Claudia, Diego, Bruna Gallo, Arnaldo, e também aos ic´s Merylin, Lucas Rabelo, Gabriel Pimenta, Ana, Fabio, Bruno, Renan, obrigado pelos ensinos, ajudas e espírito de trabalho em grupo.

Meu Muito Obrigado!!

CONTENTS

RESUMO

Aplicações de sensoriamento remoto e proximal para conservação e manejo do solo

A presente tese de doutorado teve por objetivo desenvolver técnicas de sensoriamento remoto e próximo e mapeamento digital do solo aplicadas ao manejo e conservação dos solos. O Capítulo 1 expõe uma introdução geral do trabalho. No Capítulo 2 objetivou-se avaliar a utilização de diferentes sistemas sensores na predição do teor de um dos mais importantes atributos do solo que a argila, para apoiar práticas de manejo em uma pequena propriedade agrícola. Para isso, foram usados dados provenientes dos sensores hiperespectrais de laboratório FieldSpec e aerotransportado AISA-FÊNIX, e dos sensores ópticos orbitais do LANDSAT 8-OLI, Sentinel 2-MSI e PlanetScope. No terceiro capítulo uma abordagem semelhante foi adotada, no entanto, adotou-se uma área de estudo de maior extensão (regional) para mapear a erodibilidade do solo, um importante parâmetro utilizado em modelagens da predição de perda do solo por erosão hídrica. Para isso foi obtida uma imagem multi-temporal de solo exposto denominada SYSI. No quarto capítulo, uma coleção de imagens Landsat (1985 a 2019) foi utilizada para entender a dinâmica espaço-temporal de exposição dos solos (descobertos) cultivados com cana-de-açúcar cobrindo a região de Piracicaba. No segundo capítulo os resultados encontrados mostraram melhores desempenhos de predição para os sensores de laboratório e a bordo de aeronave, seguido pelos sensores Landsat 08-OLI e Sentinel 2-MSI. O sensor PlanetScope apresentou a menor performance de predição (R^2 0,26 e 0,14). No terceiro capítulo as técnicas utilizadas permitiram a criação de mapas digitais da erodibilidade do solo mais adequados para a utilização em pequenas áreas do que mapas de erodibilidade gerados a partir de mapas de solos legados atualmente disponíveis. No quarto capítulo foi possível identificar o impacto positivo do fim da queima da cana-de-açúcar, na redução da área de solo desprotegido durante o ano. Entretanto, se constatou que solos arenosos são mais frequentemente desprotegidos devido ao seu menor potencial produtivo. Essa maior frequência de exposição pode potencializar a perda de carbono orgânico do solo, uma vez que está associada a práticas convencionais de preparo do solo para um novo plantio da cultura da cana-de-açúcar. Solos mais argilosos apresentam menor frequência de exposição devido ao maior potencial produtivo dos mesmos, o que leva a uma menor necessidade de renovação do canavial. Finalmente o capítulo 5, faz considerações gerais e conclusões sobre o trabalho como um todo.

Palavras-chave: Mapeamento digital do solo, Sensoriamento remoto, Sensoriamento próximo, Erosão, USLE, Séries temporais de imagens de satélites, Manejo do solo, Pedometria

ABSTRACT

Remote and proximal sensing applications for soil conservation and management

This doctoral thesis aimed to develop techniques for remote and proximal sensing and digital soil mapping applied to soil management and conservation. Chapter 1 provides a general introduction to the work. In Chapter 2, the objective was to evaluate the use of different sensor systems in predicting the content of one of the most important attributes of the soil than clay, to support management practices in a small agricultural property. For this, data from the FieldSpec laboratory and airborne AISA-FÉNIX hyperspectral sensors, and from the orbital optical sensors of LANDSAT 8-OLI, Sentinel 2-MSI and PlanetScope were used. In the third chapter a similar approach was adopted, however, a larger (regional) study area was adopted to map soil erodibility, an important parameter used in modeling the prediction of soil loss by water erosion. For this, a multi-temporal image of exposed soil called SYSI was obtained. In the fourth chapter, a collection of Landsat images (1985 to 2019) was used to understand the spatio-temporal dynamics of exposure of (discovered) soils cultivated with sugarcane covering the Piracicaba region. In the second chapter, the results found showed better prediction performance for the laboratory and on-board sensors, followed by the Landsat 08-OLI and Sentinel 2-MSI sensors. The PlanetScope sensor presented the lowest prediction performance (R^2 0.26 and 0.14). In the third chapter, the techniques used allowed the creation of digital maps of soil erodibility more suitable for use in small areas than erodibility maps generated from currently available legacy soil maps. In the fourth chapter, it was possible to identify the positive impact of the end of the sugarcane burning, in the reduction of the area of unprotected soil during the year. However, it was found that sandy soils are more often unprotected due to their lower productive potential. This higher frequency of exposure can potentiate the loss of organic carbon from the soil, since it is associated with conventional practices of soil tillage for a new planting of the sugarcane crop. More clayey soils have a lower frequency of exposure due to their greater productive potential, which leads to a lower need for sugarcane renewal. Finally, chapter 5 makes general considerations and conclusions about the work as a whole.

Keywords: Digital soil mapping, Remote sensing, Proximal sensing, Erosion, USLE, Satellite images time series, Soil management, Pedometric

1. GENERAL INTRODUCTION

Soil has importance not just in agriculture, but also in the performance of six other functions that are related to the good functioning of ecosystems and human well-being (Blum, 2005). Therefore, knowing the soil and its attributes, as well as its distribution in space, is extremely important for its proper conservation and management. One of the most practical and didactic ways to represent information on the variation of important soil characteristics is through maps. This can be a map of soil classes, or of a particular attribute, or even a map generated from basic information in order to point out where specific management practices should occur, such as maps of management zones.

However, in many places around the world soil information is difficult to obtain and is practically nonexistent, especially in developing countries and in tropical region (Minasny and Hartemink, 2011). This is more pronounced for data on an adequate scale for local soil management and conservation planning and for smallholder farming application (Lepsch, 2013). Digital Soil Mapping (DSM) (Nolasco de Carvalho et al., 2015) linked or not with remote or proximal sensing and pedotransfer functions (PTFs), is a technique that can contribute to obtain information in these situations.

Different techniques of proximal sensing (PS), such as visible, near and short-wave infrared spectroscopy (Vis-NIR-SWIR), have boosted the obtaining of faster and low cost punctual soil information, which makes it possible, for example, to increase the number of samples collected. This aspect is very important mainly for spatial predictions using geostatistical (e.g., kriging). On the other hand, remote sensing (RS) makes it possible to obtain information that can contribute to spatial predictions based on spatial association approaches (Miller, 2017), by providing information used as covariates. Satellites have the capability of imaging large areas and provide a spatial overview of possible changes in landscapes at short or longer distances (e.g., 30m of spatial resolution), with different temporal resolution, which is allowing the monitoring of changes that can associated to the spatial variability of soils (Demattê et al., 2020). Recent advances, such as the use of hyperspectral sensors aboard aircraft or satellites, further increase this potential for obtaining grided soil information.

Another important advance in recent years is the use of multi-temporal images. With an image collection obtained since the 1970s, that is, over 40 years of information, it is possible to assess changes in environment characteristics or, in the case of agricultural soil, to measure the spatial information of the exposed/bare soil. All this, driven by the advance in computational processing capacity, artifitial intellingence algorithms, cloud-based processing tools, among others.

In this thesis, we are concerned in addressing two main subjects: a) advance in the digital mapping of important soil properties for the correct management and conservation of soils, using data from remote and proximal sensing. b) to use satellite time series images as a tool for monitoring soil management practices, aiming at their adequate conservation (soil security). In the Chapter 2, spectral data from sensors located on different platforms (laboratory, aircraft and satellites) with different spatial and spectral resolutions were used as independent variables for spatial prediction of clay content. Clay is an important attribute related to soil management and conservation practices, for which a farm-geographic extension area was used as a study area. In Chapter 3 a similar prediction approach was used, using data from a Synthetic Soil Image (SYSI) obtained from Landsat time series images (1985 to 2019) and 350 to 2500 nm proximal sensing data. However, the study area was the Piracicaba region (2574 km^2), and the property predicted the soil erodibility (K factor). The results obtained were analyzed in two case studies aiming to demonstrate potential of the soil erodibility digital maps to better represent the spatial variation of

erodibility, compared to erodibility maps obtained from low-scale soil maps. Finally, Chapter 4 presented an innovative proposal, the analysis of soil exposure (discovered soil) from 1985 to 2019 for the sugarcane production area in the Piracicaba region. One of the basic factors necessary for soil loss by water born erosion, is the same being unprotected/uncovered/bare (Morgan, 2005). We demonstrate how sugarcane crop management practices are directly related to a greater number of times the soil is uncovered over time.

This thesis ends with a general discussion and a conclusion of the main findings.

References

Blum, W.E.H., 2005. Functions of soil for society and the environment. Rev. Environ. Sci. Biotechnol. 4, 75–79. https://doi.org/10.1007/s11157-005-2236-x

Demattê, J.A.M., Safanelli, J.L., Poppiel, R.R., Rizzo, R., Silvero, N.E.Q., de Mendes, W.S., Bonfatti, B.R., Dotto, A.C., Salazar, D.F.U., de Mello, F.A.O., da Paiva, A.F.S., Souza, A.B., dos Santos, N.V., Maria Nascimento, C., de Mello, D.C., Bellinaso, H., Gonzaga Neto, L., Amorim, M.T.A., de Resende, M.E.B., da Vieira, J.S., de Queiroz, L.G., Gallo, B.C., Sayão, V.M., da Lisboa, C.J.S., 2020. Bare Earth's surface spectra as a proxy for soil resource monitoring. Sci. Rep. 10, 4461. https://doi.org/10.1038/s41598-020-61408-1.

Lepsch, I.F., 2013. Status of Soil Surveys and Demand for Soil Series Descriptions in Brazil. Soil Horizons 54, sh2013-54-2-gc. 10.2136/sh2013-54-2-gc.

Miller, B.A., 2017. Chapter 5 - Geographic Information Systems and Spatial Statistics Applied for Soil Mapping: A Contribution to Land Use Management, in: Pereira, P., Brevik, E.C., Muñoz-Rojas, M., Miller, B.A.B.T.-S.M. and P.M. for S.L.U.M. (Eds.). Elsevier, pp. 127–149. https://doi.org/https://doi.org/10.1016/B978-0-12-805200-6.00005-0

Minasny, B., Hartemink, A.E., 2011. Predicting soil properties in the tropics. Earth-Science Rev. 106, 52–62. https://doi.org/10.1016/j.earscirev.2011.01.005.

Morgan, R.P.C., 2005. Soil Erosion and Conservation, 3rd edition. Blackwell Publishing, Oxford.

Nolasco de Carvalho, C.C., Nunes, F.C., Homem Antunes, M.A., Nolasco, M.C., 2015. Soil surveys in Brazil and perspectives in digital soil mapping. Soil Horizons 56. https://doi.org/10.2136/sh14-01-0002.

2. CLAY CONTENT PREDICTION USING SPECTRA DATA COLLECTED FROM THE GROUND TO SPACE PLATFORMS IN A SMALLHOLDER TROPICAL AREA

Abstract

Proximal and remote sensors are emerging as powerful sources of soil spectral information at an array of temporal and spatial resolutions. This study investigated clay content prediction at three spectral acquisition levels: laboratory, airborne, and spaceborne. Two approaches were tested, the use of prediction models developed with local and regional spectral libraries (52 samples- local scale and (950, 200 e 224 samples - regional scale), termed internal and external models respectively. A total of 52 soil samples were collected in a smallholder area, 83 ha, located in southeastern Brazil. Spectral data in the Vis-NIR-SWIR region were acquired in the laboratory using FieldSpec 3 sensor, and the clay content was determined by sedimentation technique. Afterward, bare soil images from AISA-FENIX, Planetscope, Sentinel2-MSI and Landsat8-OLI were obtained. The clay content determined in the laboratory was related to the soil spectra acquired by each of the sensors and was predicted using the Cubist regression tree algorithm. The results obtained from local spectral libraries showed good predictions using FieldSpec3 and AISA-FENIX sensors. Landsat8-OLI and Sentinel2-MSI provided satisfactory results, while PlanetScope gave poor results. For the prediction using regional spectral libraries, only lab-based FieldSpec 3 sensor provided a fair prediction, while other sensors gave poor results. This study demonstrated that soil sensing is possible at any level taking into account its advantages and limitations. This approach paves the way for acquiring soil spectra for smallholder farms.

Keywords: Remote Sensing, Hyperspectral Sensing, Proximal Sensing, Multi-temporal Images, Bare Soil Reflectance; Digital Soil Mapping

Published as: Bellinaso, H., Silvero, N.E.Q., Ruiz, L.F.C., Accorsi Amorim, M.T., Rosin, N.A., Mendes, W. de S., Sousa, G.P.B. de, Sepulveda, L.M.A., Queiroz, L.G. de, Nanni, M.R., Demattê, J.A.M., 2021. Clay content prediction using spectra data collected from the ground to space platforms in a smallholder tropical area. Geoderma 399, 115116. https://doi.org/10.1016/j.geoderma.2021.115116

2.1. Introduction

The characterization of soil physical and chemical attributes is urgently needed to optimize tropical agricultural land management (Sanchez, 2019). Environmental information is frequently demanded to assist in public policy decisions (Bouma et al., 2012; Panagos et al., 2012). The knowledge of soil physical and chemical properties as well as of soil distribution on the earth's surface is essential for land use optimization (Feizizadeh and Blaschke, 2013). However, in many places around the world soil information is difficult to obtain and is practically nonexistent, especially in developing countries and in tropical region (Mallavan et al.,2010; Minasny and Hartemink, 2011; Silatsa et al., 2018). This is more pronounced for data on an adequate scale for local soil management and conservation planning and for smallholder farming application (Arrouays et al., 2018; Lepsch, 2013; Steinmetz et al., 2018).

Digital Soil Mapping (DSM) (Arrouays et al., 2014; Nolasco de Carvalho et al., 2015) linked or not with remote (Onyango et al., 2021) or proximal sensing (Silva et al., 2020) and pedotransfer functions (PTFs) (Minasny and Hartemink, 2011), is a technique that can contribute to obtaining information in these situations. However, DSM exploitation in Latin America and Africa has been lower than developed countries (Agyeman et al., 2020; Minasny and Hartemink, 2011; van Zijl, 2019). The high cost of collecting primary input data and the lack of government policies to obtain this (Nolasco de Carvalho et al., 2015; Silva et al., 2020a; van Zijl, 2019), the need for the correct digitization and harmonization of pre-existing legacy data (Agyeman et al., 2020; Samuel-Rosa et al., 2020; Santra et al., 2021) and the difficult to establish protocols (Coelho et al., 2021; Guevara et al., 2018), are possible explanations for this greater difficulty of application. In this context, information obtained by remote and proximal

sensing becomes even more relevant for the high-resolution soil spatial information (Ben-Dor et al., 2009; Santra et al., 2021; Silva et al., 2020a; Viscarra Rossel et al., 2010).

Soil spectral information can be collected at several acquisition levels: in the laboratory, in the field onboard unmanned terrestrial or aerial vehicles or aircrafts and satellites (Lausch et al., 2019). The soil's spectral signature must be well-known to ensure that the information acquired by sensors located on different platforms is related to soil. Huete (1996) emphasized the importance of the spectral data acquired in the laboratory as a basis for field, aerial, and satellite studies, because external factors can be controlled (geometry, atmospheric condition, light, distance from the object, among others) (Nouri et al., 2017). Each spectral acquisition level will have advantages and limitations related to the equipment, like spectral and spatial resolution, the equipment or data cost, and the need for data pre-treatment (Ben-Dor et al., 2009).

Among soil properties, the clay content is one of the most commonly studied by spectral analysis (Lagacherie et al., 2020) and has a strong relationship with other soil properties and functions such as charge dynamics, soil carbon (Busato et al., 2012), water retention, drainage, permeability, fertility, chemistry, among others (Weil and Brady, 2017). Besides that, it is essential for soil classification (Hristov, 2013) and directly impacts soil erosion processes (Nciizah and Wakindiki, 2015; Reichert et al., 2009). The clay particles have direct physical interaction with electromagnetic radiation (Demattê et al., 2016), mainly due to minerals such as iron oxides, such as hematite and goethite in visible portion (Silva et al., 2020b), and aluminosilicates, gibbsite and carbonates in shortwave-infrared region (>2000 nm) (Chabrillat et al., 2002; Fang et al., 2018).

The prediction of clay content using spectra acquired in the laboratory has been widely reported as the most feasible compared to other soil properties (Soriano-Disla et al., 2014; Viscarra Rossel et al., 2016). Airborne and spaceborne sensors have been successfully studied in predicting topsoil clay content (Gomez et al., 2019, 2018). Nanni and Demattê (2006) and Gomez et al. (2019, 2018) found promising results using Landsat and Sentinel satellite data to predict clay content. Gasmi et al. (2019) used a multiple linear regression (MLR) on ASTER images to predict clay content in an area of 2000 Km^2 in Tunisia and achieved an $R^2val = 0.60$. Odeh and McBratney (2000) used AVHRR images and regression kriging, and found a correlation coefficient of 0.76. Barnes and Baker (2000) in Arizona compared the SPOT and Landsat images to predict clay content and they demonstrated that all bands, except those from the thermal region, have correlation coefficients (r) > 0.4.

The quantification of clay was also performed by hyperspectral sensors onboard aircrafts, such as SpecTIR (Hively et al., 2011), AISA-DUAL (Gomez et al., 2018) and AVIRIS (Dutta et al., 2015). Hyperspectral sensors in satellites, such as Hyperion (Lu et al., 2013) and HyMap (Gerighausen et al., 2012; Nouri et al., 2017) also provided good results. Gomez et al. (2012) used AISA-DUAL, with spatial resolution of 5 m and 359 non-contiguous bands for imaging an area of 300 Km^2 in Tunisia with high soil variability and achieved an $R^2 = 0.8$.

Usually, the prediction of clay content using ultraspectral laboratory sensors has been performed by models created using spectral data collected in the area under study or from global or regional spectral libraries that have or not data from the same area (Cezar et al., 2019; Guerrero et al., 2014). This approach is the most common approach reported in the literature with good results, with RMSE values from 64.2 to 94.4 g kg^{-1} (Araújo et al., 2014; Shepherd and Walsh, 2002; Viscarra Rossel and Behrens, 2010). There is also a growing interest to use models obtained from global, regional or local spectral libraries to map unknown areas without spectral information (Padarian et al., 2019a; Silva et al., 2019; Viscarra Rossel et al., 2016). Even the spectral library of a country can be used to predict soil attributes from spectra data of another country (Briedis et al., 2020; Gomez et al., 2020). Wetterlind and Stenberg (2010) compared prediction models obtained from external datasets (national and reduced

spectral libraries), internals datasets (local spectral library) and both combined. The best results were obtained when local prediction models were used, followed by local and external data combined (spiking) (Guy et al., 2015; Nawar and Mouazen, 2017). Brown (2007) and Sankey et al. (2008) also found improvement in predictions when combining local samples in external databases. However, these different approaches have only been extensively explored in laboratory ultraspectral data, and not tested for hyper and multispectral data.

Demattê et al. (2018b) used the Landsat 7 ETM+ to obtain prediction models from one region, which were then applied to another area. They found that the coefficients of determination between the observed and estimated values were higher than 0.5 and the prediction errors were lower than 30%. Nouri et al. (2017) used a laboratory spectral database to build regression models and then used them to predict soil properties over bare soils of a hyperspectral airborne image. The results are promising results (R^2test > 0.79 and RMSEP < 38 g kg^{-1}).

Although many articles have already indicated the potential of laboratory, airborne and satellite sensors, only a few compared prediction models obtained from these sensors at different acquisition levels, or compared the use of prediction models obtained by external (regional spectral libraries) and internal datasets (local spectral libraries). Thus, we aimed at evaluating prediction models to predict clay content using spectral data acquired from five different sensors at three acquisition levels: laboratory, aircraft, and satellite. In addition, we compared the prediction results obtained using models built with soil samples collected from our study area (local spectral libraries) and those obtained from external (regional spectral libraries) databases. The results may bring light on strategies how to use spectral libraries.

2.2. Material and methods

2.2.1. Location and characterization of the study area

The study area comprises 83 ha and is located in São Paulo State, Brazil (−22.710315°, −47.516506°) (Fig. 1). A humid subtropical mesothermic temperature regime characterizes the climate with dry winters between June and August, and rainy summers between November and February, according to the Köppen climatic classification system (Alvares et al., 2013). The mean annual precipitation is 1275 mm, being the wettest period (December to February) with a mean of 610 mm of rainfall and the driest period (June to August) with a mean of 101 mm of rainfall. The mean annual temperature is 21.4 °C, with a mean annual maximum of 28.2 °C and a mean annual minimum of 14.8 °C (Domínguez-Castillo et al., 2020). The area is mainly cultivated with sugarcane and is geomorphologically located within the Paulista Peripheral Depression. The main parent materials are the sandy siltstone, massive argillaceous siltstones and sandstones from the Tatuí Formation, and sandstones, sandy mudstones, clayey-sandy or sandy-clayey mudstone, and siltstone from the Itararé Formation (Marques et al., 2018). The soils comprise red oxisol, in the center of the study area. As we move away from the center, red ultisol can be found and after that, red-yellow ultisol (Fig. 1d).

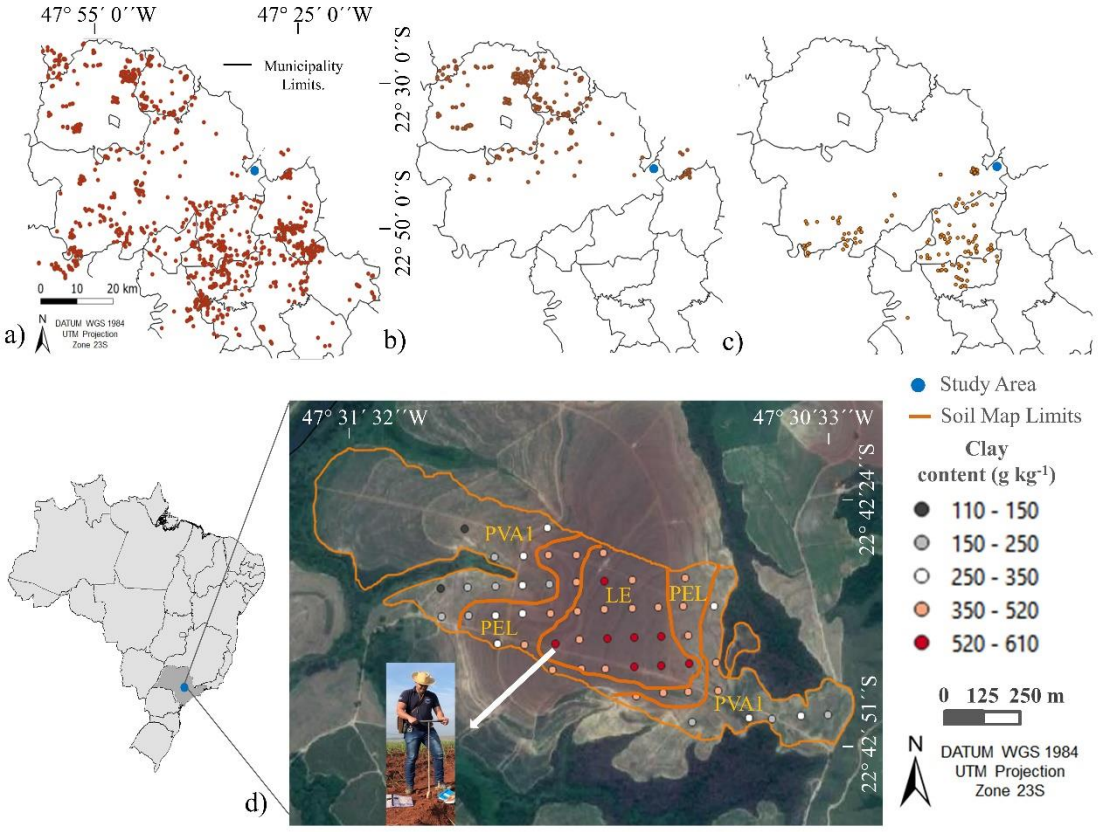

Figure 1. Data location: regional spectral libraries used to develop clay prediction models for Landsat-8 OLI and Sentinel-2 MSI, with 950 samples (a), PlanetScope, with 200 samples (b) and FieldSpec 3 and AISA-FENIX, with 224 samples (c) sensors. Study area (d) with 52 samples locations, clay variability and soil classes. LE - Red Oxisol; PEL - Red Ultisol; PVA1 - Red-yellow Ultisol (adapted from Vidal-Torrado, 1994).

2.2.2. Soil sampling and analysis

On July 25, 2017, soil surface (0–20 cm) samples were collected at 52 locations, recorded by using GNSS (Global Navigation Satellite System) Topcon GPR 3 receiver, with RTK (Real Time Kinematic) corrections obtaining positioning accuracy of 0.3 m. The samples were oven-dried for 48 h at 50 °C, and ground and sieved to 2 mm. Sand, silt and clay contents were determined following the sedimentation method (Teixeira et al., 2017), using 50.0 g of each sample and the sodium hydroxide (0.1 mol L^{-1}) and sodium hexametaphosphate (0.1 mol L^{-1}) as dispersant agents. Soil organic matter was determined by the Walkley-Black method (Teixeira et al., 2017).

2.2.3. Spectral laboratory data acquisition

The spectral data from the soil samples (350-2500 nm) were acquired in the laboratory using the FieldSpec3 spectroradiometer (Analytical Spectral Devices, ASD, Boulder, CO), with spectral resolution of 3 nm, from 350 to 700 nm and 10 nm from 700 to 2500 nm. The output data used in this work, was automatically interpolated to 1 nm, resulting in 2151 bands with 1 nm resolution (Demattê et al., 2019). The samples were placed in petri dishes and were homogeneously distributed over a flat surface for spectral reading. Two halogen lamps (50 W) were used as light sources. The distance between the lamps formed a 90° angle and was located at 0.35 m from the sample with a zenith angle of 30°. These geometric configurations generated a not-collimated light beam towards the target. An optic fiber placed in the vertical position at 0.08 m from the sample surface captured the reflected light from an area

of approximately 2 cm² at the center of the sample (Poppiel et al., 2019). Three replicates from distinct rotations positions for each sample were taken to reduce shadow effects. To maximize the signal-to-noise ratio, 100 readings were performed and the average calculated for each sample. The instrument was calibrated at the beginning and after 20 min, using a white Spectralon® plate with reflectance superior to 99% (Labsphere, North Sutton, NH, USA).

2.2.4. Hyperspectral data acquisition

Hyperspectral data were obtained by imaging the area with the AISA-FENIX sensor onboard the Piper II aircraft (Fig. 2). The AISA-FENIX is a hyperspectral sensor that operates in the visible-near-shortwave-infrared ranges (Vis-NIR-SWIR, 380–2500 nm), with spectral resolutions ranging from 3.5 to 12 nm and 363 spectral bands. The flight altitude was of approximately 660 m, which provided a spatial resolution of 1 m. The field of view (FOV) was 32.3°. After collecting the images, the hypercube was processed in the software Specim CaliGeo PRO® (Spectral Imaging, Specim Ltd., Finland) to convert digital numbers into radiance. Caligeo presents the sensor's factory parameters for the conversion of each spectral band. At the same time the conversion was carried out, a geometric correction was performed in the same software. For that, a GPS/IMU oxford OXTS - RT3050 model collected data related to the plane oscillations in pitch, roll and yaw axis (aircraft principal axes), velocity and geographic coordinates. The correction results in an error lower than 1 m. The image resulting from the correction was converted in ".bsq" format in the ENVI® software and imported to the ATCOR-4® software. Then, in the software, empirical parameters of the AISA-FENIX sensor were created to correct atmospheric influences such as aerosols and water vapor, resulting in a converted image, from radiance to reflectance (Richter and Schläpfer, 2015).

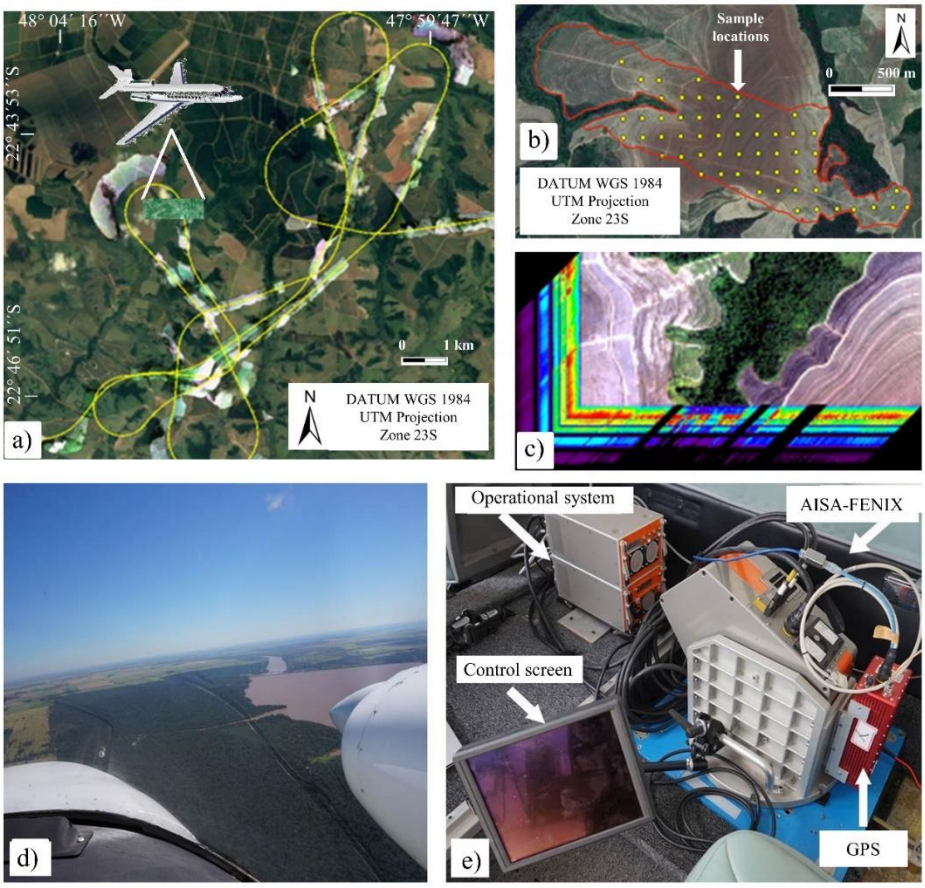

Figure 2. Details of the AISA-FENIX system. a) flight path, b) study area and sampling locations, c) hyperspectral image, d) visualization at 200 feet, e) sensor system. Photos from GALeS group of University of Maringá (http://www.gales.uem.br/.).

2.2.5. Satellite multispectral data acquisition

The multi-temporal images from Landsat8-OLI and Sentinel2-MSI sensors were obtained from Silvero et al. (2021), who applied the GEOS3 method (Dematt̂e et al., 2018a) to a collection of images from both satellites. The GEOS3 method consisted of the use of NDVI (Normalized Difference Vegetation Index), NBR2 (Normalized Burn Ratio 2) and quality mask to exclude from the images areas with vegetation, cloud, shadows, crop residues and burned vegetation. After masking, the images were ordered by date, and the median reflectance was calculated for each pixel. A total of 63 Sentinel2-MSI and 45 Landsat8-OLI images, from 2016 and 2019, were used to obtain the Synthetic Soil Images (SYSI Landsat and SYSI Sentinel) (Fig. 3).

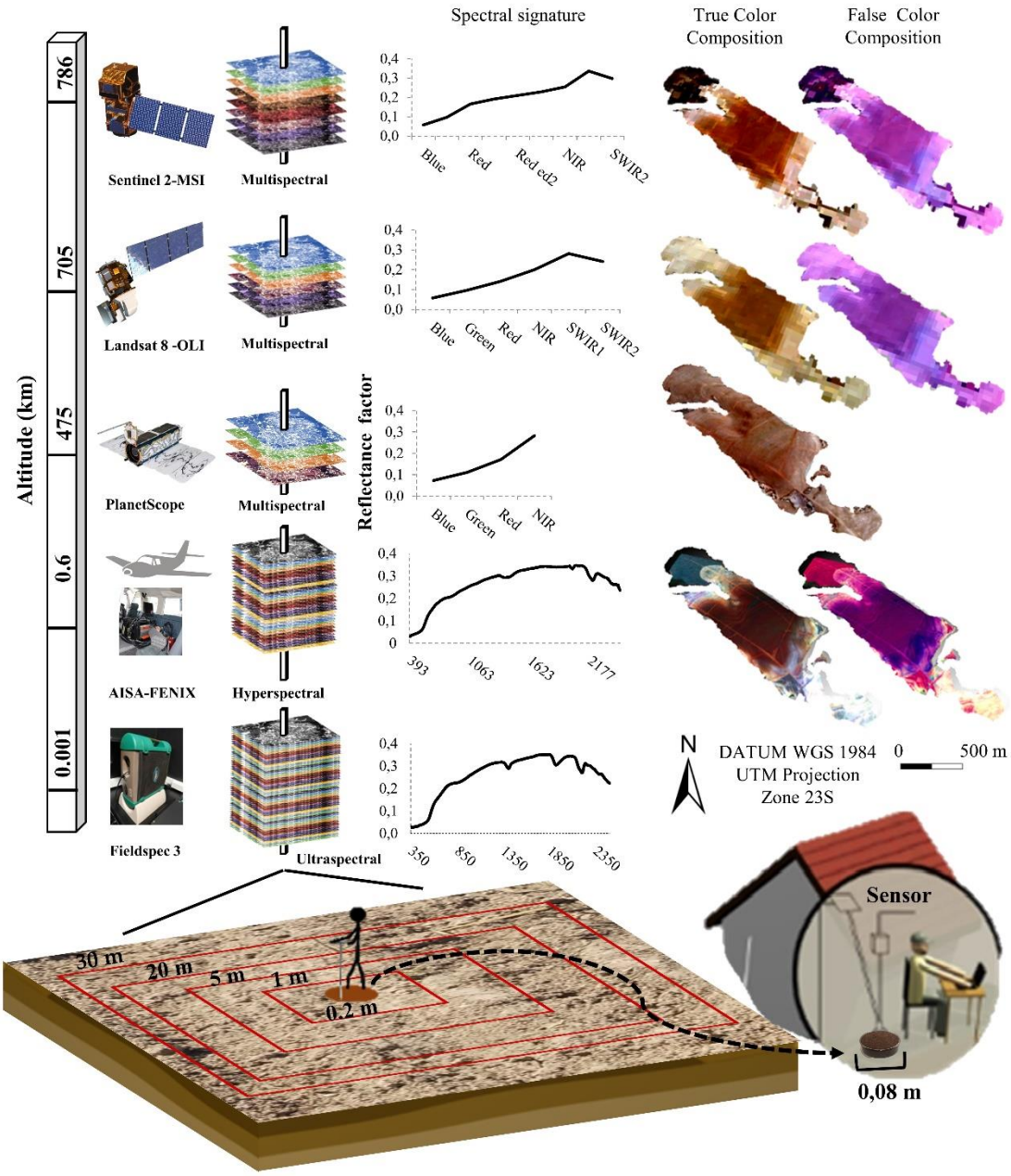

Figure 3. Illustration of the sensors and respective spatial resolution and soil synthetic images (SYSI). True color composition (red, green, blue) and false color (SWIR, NIR, red).

We also used the PlanetScope, which is composed of nanosatellites with a weigh of less than 10 kg to acquire multispectral orbital images with very high spatial and temporal resolution. These nanosatellites are characterized by having four spectral bands, in the visible (Blue: 455-515nm, Green: 500-590nm and Red: 590-670nm) and near-infrared (NIR: 780-860nm) regions. It is a commercial service; however, we obtained the images without charge in this study. Since PlanetScope images do not have bands in the SWIR region, it was not possible to obtain the NBR2 index used in GEOS3 methodology (Demattê et al., 2018) Therefore, a specific methodology was developed to obtain a Synthetic Soil Image from PlanetScope images (SYSI Planet) (Fig. 3).

The SYSI Planet was obtained through a supervised classification using the Random Forest (RF) method. First, twenty surface reflectance images from September and October of 2017 were classified into the following land covers: bare soil, vegetation, cloud, shadows, straw and burned. Training samples of bare soil collected from PlanetScope images were used for the classification procedure.

The RF method is an ensemble learning method (Padarian et al., 2020). It divides training samples into subsets and generates a decision tree for each subset (forest). After the model fitting, the classification is obtained by voting the classes of each tree in the forest. The growing of the decision tree is made by feature vector selection that reduces the impurity of each node of the tree. The RF method estimates the feature importance by computing a mean decrease in impurity (Breiman, 2001; Tian et al., 2016). The number of trees and their maximum depth are adjustable parameters. The number of trees represents the number of Decision Trees created (estimators) and the maximum depth represents the depth of each tree. The deeper the tree, the more divisions are performed, and consequently, bigger is the number of child nodes (Rodriguez-Galiano et al., 2012). The number of trees and maximum depth were evaluated between 10 and 200. Gini index was used as a criterion of division for tree nodes.

The selection of optimal parameters in the classification was performed by cross-validation. The samples were randomly partitioned into 10 sets. These validation samples were used to avoid selecting parameters that that would overfit. To evaluate the performance of the models, the kappa coefficient was used. The modeling was carried out in the Python programming language, with the Scikit-Learn, Numpy and Pandas libraries.

After the classification procedure was finalized, the classified bare soil images were filtered, ordered by date and the median of each pixel calculated. A SYSI Planet with only bare soil pixels was obtained (Fig. 3).

2.2.6 Statistical analysis

2.2.6.1 Descriptive statistics of soil attributes and Pearson's correlation

The first step was to link spectral data at different acquisition levels for the same point (pixel). A soil line analysis, which consists of a linear relationship between reflectance values from two wavebands (NIR and RED portions) (Baret et al., 1993), was carried out to confirm if the reflectance values of each sensor corresponded to bare soil pixels. This analysis removes points that have vegetation or crop residue interference. The lab information was considered as the standard soil spectra.

The next stage was to study the relationship between FieldSpec 3, AISA-FENIX, Sentinel2-MSI, Landsat8-OLI and PlanetScope spectral data by Pearson's correlation analysis. Pearson's correlation was carried out between similar bands of different satellite sensors (i.e. the Landsat8-OLI blue band was correlated with Sentinel2-MSI and PlanetScope blue bands; Landsat8-OLI SWIR1 was correlated Sentinel2-MSI SWIR1 band). The original bands used were for Landsat8-OLI (nm) (blue-452–512; green-533–590; red-636–673; NIR-851–879 nm; SWIR1-1566–1651; SWIR2-2107–2294), Sentinel2-MSI (nm) (blue-458–523; green-543–578; red-650–680; NIR-785–899; SWIR1-1565–1655; SWIR2-2100–2280) and PlanetScope (nm) (blue-455–515; green-500–590; red-590–670; NIR-780–860). Also,

the FieldSpec and AISA-FENIX data were simulated (convoluted) following the spectral range of Landsat8-OLI bands, using the hsdar package (Lehnert et al., 2016) in R software.

A second approach was to relate the original spectral data from different acquisition levels and the clay content by Pearson's correlation. The correlation analysis was performed using R software.

2.2.6.2 Qualitative analysis of spectral signatures

After confirming that the spectra corresponded to bare soil, the clay content was used to assess spectral patterns. The soil samples were classified into five textural classes, usually used for sugarcane soil management in São Paulo State, based on the clay content as follows (g kg^{-1}): sandy (clay content < 150), sandy loam (clay content = 150–250), loam clayey (clay content = 250–350), clayey (clay content = 350–600) and very clayey (clay content > 600) (Lacerda et al., 2016; Demattê et al., 2018). The spectral reflectance of each sensor was averaged for each textural class, and then plotted and compared qualitatively.

2.2.6.3 Prediction of soil attributes - internal and external spectral library approach

Two approaches (Fig. 4) were adopted to predict topsoil in the study area (83 ha field) from spectra collected by various sensors:

a) Internal models, meaning models developed using the local dataset (local spectral library- 52 samples) (Fig 1d)

b) external models, meaning that models were developed using regional spectral libraries (without spectral data from the study area). The regional libraries were obtained from different locations located in the region of the study area (São Paulo) along with measured clay content values (Fig 1a, b, c). The models generated with these external datasets were used to predict clay content on the study area.

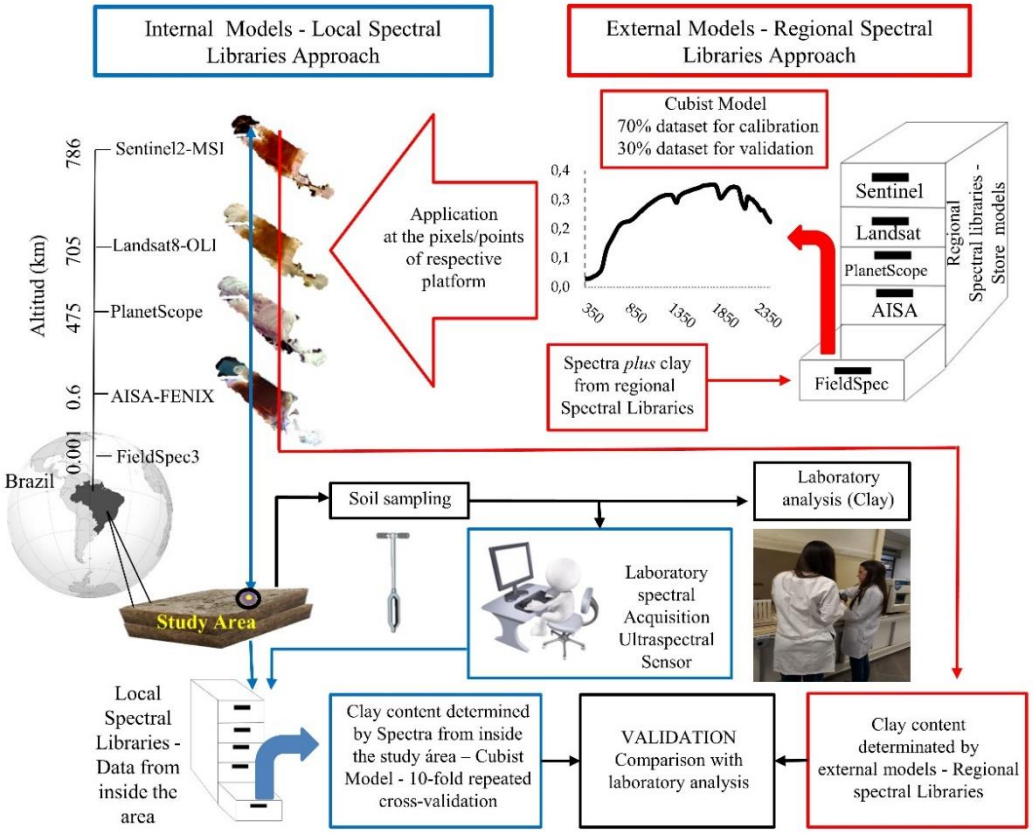

Figure 4. Flowchart of the prediction models development methodology. Red lines and squares indicate the steps followed to obtain prediction models from external datasets (regional spectral libraries) while blue lines correspond to clay content predicted by internal datasets (local spectral libraries). The black color is related to the validation procedure (clay content determined in the laboratory).

The internal (local spectral libraries) dataset was composed of soil samples collected from the study area (n = 52) (Fig. 1d) with their corresponding reflectance values collected using five sensors.

The external datasets (regional spectral libraries) were composed of soil data in the same region of the study site, with similar geology, soil types and climate (Fig 1a, b, c). This regional library was collected from our past works (Demattê et al., 2019; Silvero et al., 2021), except for PlanetScope sensor, and the number of samples of each library was 200 for AISA-FENIX and FieldSpec 3, 222 for PlanetScope and 950 for Sentinel2-MSI and Landsat8-OLI (Fig. 5). The procedure obstianed by SYSI was variable for each sensor. Differences in the number of multitemporal images used to obtain each SYSI created different numbers of bare soil pixels. In the case of hyperspectral sensors, we used the samples that have soil analysis and spectral data collected in the laboratory.

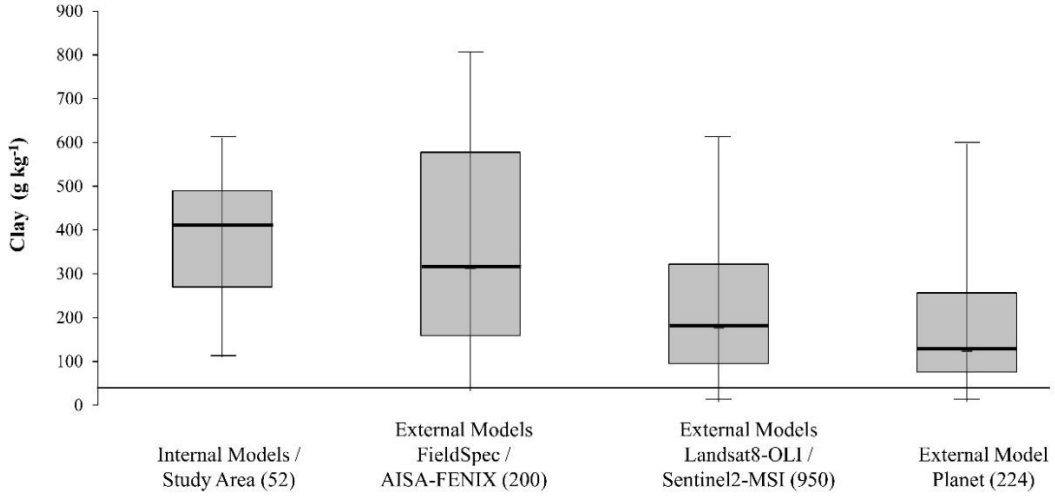

Figure 5. Descriptive statistics of Local and Regional datasets.

All samples from the internal dataset were used to calibrate and validate prediction models, using a 10-fold repeated cross-validation method (Vapnik, 1995). For external models, data of regional spectral libraries (Fig 1abc) were randomly partitioned into training (70%) and validation (30%) sets using the *createDataPartition* function in R software. The generated models were then applied to predict clay content in the study area, and validated using the local data.

For model fitting and prediction accuracy measurements, a bootstrapping method with 100 repetitions and the Cubist algorithm were used for both internal and external datasets. Briefly, the Cubist is a tree-rule-based algorithm in which linear regression models are obtained at each branch of the tree to allow the prediction of the values. It uses a boosting-like procedure named committees and the most common k neighbors to avoid overfitting (Kuhn et al., 2013; Quinlan, 1992). The algorithm has shown high accuracy in predicting soil properties (Coblinski et al., 2020; Fathololoumi et al., 2020; Zhang et al., 2017). Furthermore, the algorithm was also used for clay content prediction in various papers, usually showing better results than other algorithms (Demattê et al., 2019; Silva et al., 2019; Zhao et al., 2018). The bootstrapping method implies that the dataset used represents the population's characteristics and thus, it can be simulated from the dataset by multiple realizations (Padarian et al., 2019b), which was performed by sampling random with replacement. At each realization of the bootstrap routine, the coefficient of determination (R^2), root mean square error (RMSE) and performance to interquartile ratio (RPIQ) were calculated using the goof function from the *ithir* package in R software.

The FieldSpec and AISA-FENIX spectra were reduced by Principal Components Analysis due to their high number of variables and multicollinearity. The first three PCs were used to develop and validate the models. The AISA-FENIX image was also reduced to three PCs and the model obtained were applied to it to obtain the clay content map. For the FieldSpec 3 spectra, since the spectra were not available throughout the field, the predicted clay content values of the 52 points, were interpolated throughout the area by ordinary kriging (Viscarra-Rossel et al., 2010c; Viscarra-Rossel et al., 2011; Knadel et al., 2015), with a regular grid of 5m spacing using the *gstat* package (Pebesma, 2009) in R software. For other sensors, the models and the clay content maps were calibrated and spatialized in R software using the *caret* and *raster* packages.

The uncertainty maps for each sensor were represented by the 90% prediction interval (90% PI) obtained from the bootstrapping routine. The lower and upper limits (5th and 95th) and the mean of the 100 realizations were

calculated. The 90% PI was calculated as the difference between 95th and 5th percentiles (90% PI = 95th - 5th). The mean and the 90% PI were presented and discussed.

2.3 Results

2.3.1. Descriptive analysis of soil attributes and soil line analysis

A wide range of clay contents (110 to 610 g kg^{-1}), with a high CV was observed in the study area (Fig. 5 and S.2). In general, most of the data were concentrated around 400 and 500 g kg^{-1}. For the external datasets, a wide range with a suitable distribution was verified for FieldSpec 3 and AISA-FENIX (Fig. S1). Landsta8-OLI, Sentinel2-MSI and PlanetScope datasets also showed variability, but with more samples with low clay content.

Five spectral datasets were analyzed by the soil line (Fig. 6). Comparing the slope and coefficient of determination (R^2) among them, it can be confirmed that the spectra collected at different acquisition levels corresponded to bare soil, where the best trend was observed for laboratory and AISA-FENIX spectra. The laboratory spectra were very close to the 1:1 line, with coefficient of determination (R^2: 0.97) similar to AISA-FENIX data. The other sensors also had high values of R^2 (Fig. 6).

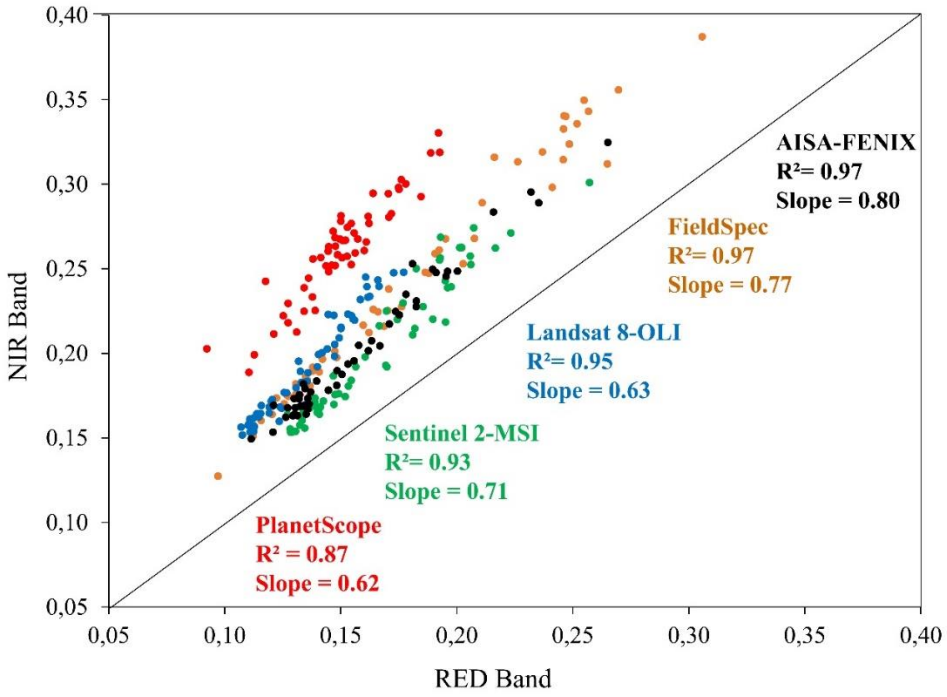

Figure 6. Soil line analysis for each sensor.

2.3.2. Quantitative relationship between sensors

The correlation between the spectra of the sensors is shown in Fig. 7. Strong positive correlations were found for all bands and sensors, except between PlanetScope and the other sensors, where the lowest positive values were observed. The most significant correlations were observed between Landsat8-OLI and Sentinel2-MSI, followed

by FieldSpec and Sentinel2-MSI. Most of the positive correlation values were observed between the blue, green and SWIR bands. In general, the lowest values of positive correlations were observed between the red and NIR bands. Considering the FieldSpec 3 sensor as a standard spectral reference, its correlation with other sensors was in the following order: Sentinel2-MSI, Landsat8-OLI, AISA-FENIX, and PlanetScope.

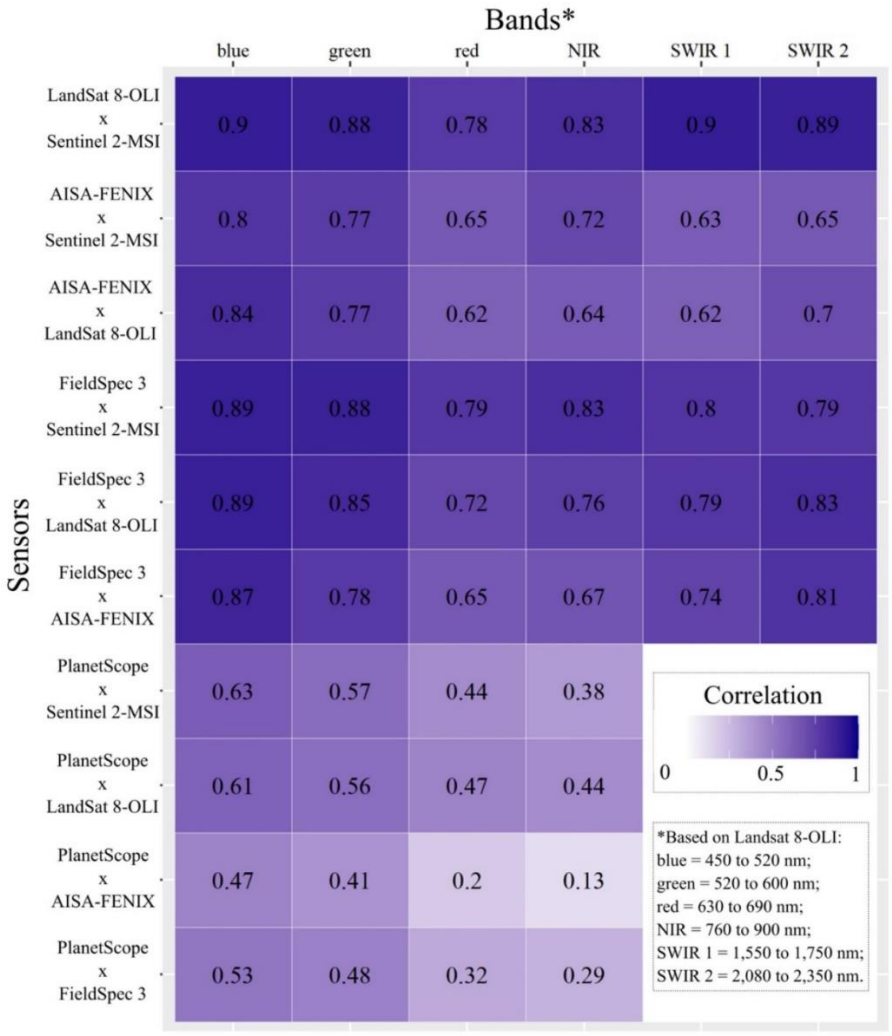

Figure 7. Pearson's correlation between spectra from all sensors.

2.3.3. Spectral signatures in function of the clay content

The spectral signatures of all sensors as function of soil textural classes are presented in Fig. 8. Each sensor gave a specific spectral behavior due to the different number spectral ranges. FieldSpec3, with 2151 bands, has a very detailed signature showing absorption characteristics and reflectance intensities. With 363 bands, AISA-FENIX maintains this trend but loses information at 1400 and 1900 nm due to atmospheric water absorption. Regarding the multispectral sensors, Sentinel2-MSI and Landsat8-OLI, several absorption characteristics have disappeared, but the spectral behavior characteristic of soils remains. In all of these sensors, the trend of reflectance intensity and textural class is maintained. The PlanetScope image has no bands in the SWIR portion, which makes it difficult to assess its spectral patterns.

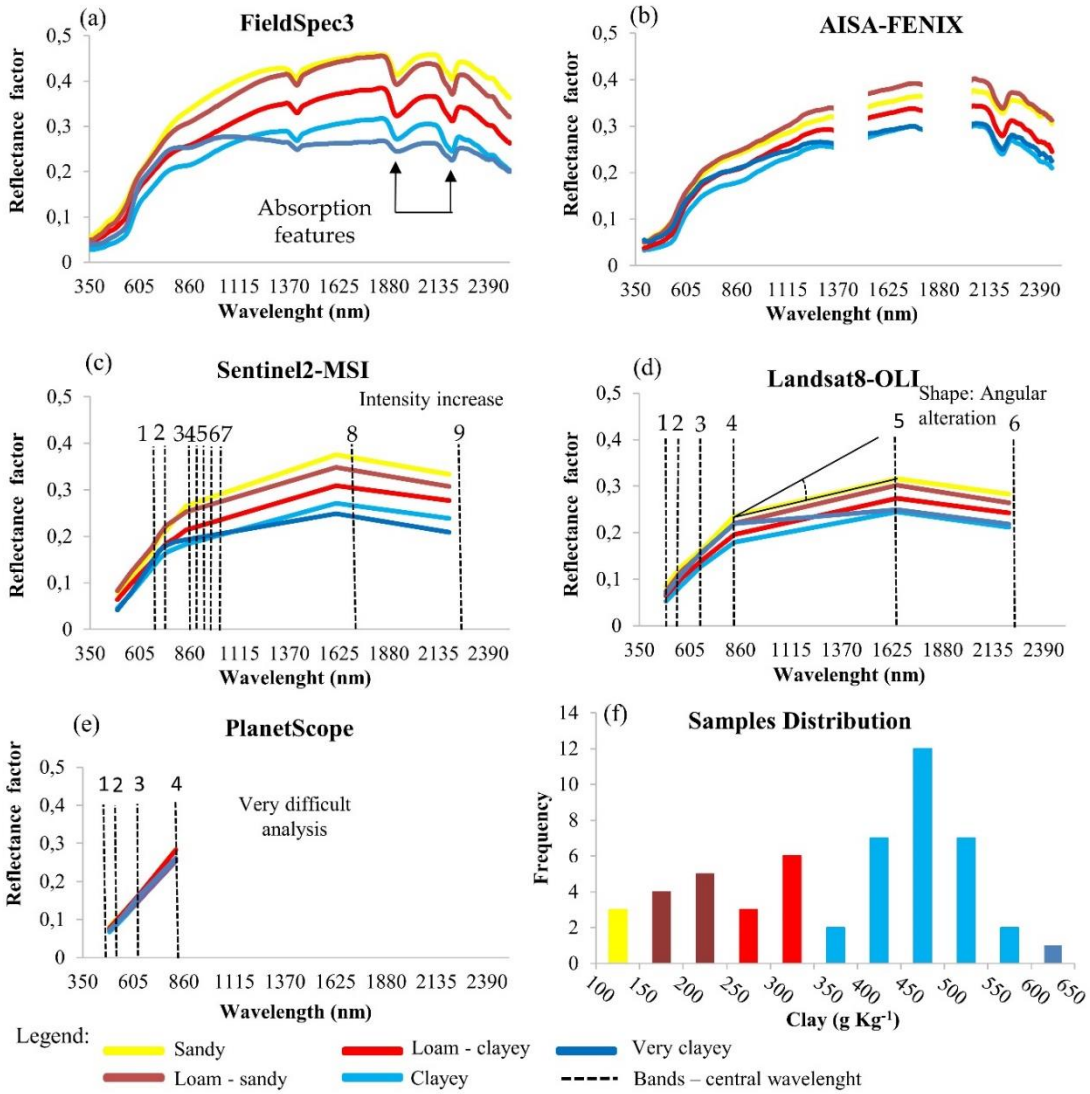

Figure 8. Mean spectral signatures from each sensor classified by textural classes: sandy (<150 g kg^{-1}), loam-sandy (150–250 g kg^{-1}), loam-clayey (250–350 g kg^{-1}), clayey (350–600 g kg^{-1}), and very clayey (>600 g kg^{-1}). a) FieldSpec 3, b) AISA-FENIX, c) Sentinel-2 MSI, d) Landsat-8 OLI, e) PlanetScope, f) sample distribution in each textural class.

2.3.4. Correlation between clay content and spectral data

The relationship between the clay content and the spectral bands of the five sensors is shown in Fig. 9. A strong negative correlation was evidenced for all sensors along the electromagnetic spectrum, with the PlanetScope data being an exception, where the lowest negative correlation values were observed. Generally, most of the negative correlation values were observed in the blue, green, and SWIR bands of the orbital sensors and in the wavelengths: 440 to 550 nm and 2100 to 2350 nm from FieldSpec and AISA-FENIX.

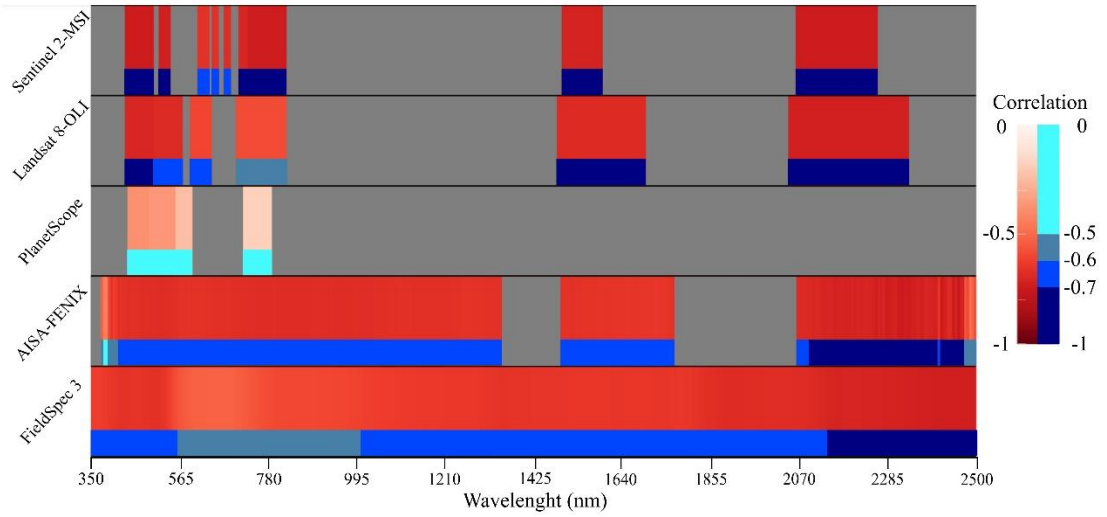

Figure 9. Pearson's correlation analysis between clay content and spectra for each sensors bands. Scale in red tones corresponding to continuous values and scale in blue tones corresponding to classes of correlation values.

2.3.5. Prediction of clay content by models built with internal and external datasets

The results of clay content prediction by internal (local) and external (regional) datasets are presented in Fig. 10 and 11, respectively. For the internal models, we found that the FieldSpec and AISA-FENIX had the best performance ($R^2 > 0.75$), followed by the Sentinel2-MSI and Landsat8-OLI ($R^2 > 0.60$) while the PlanetScope showed the worst result with $R^2 = 0.26$.

The uncertainty maps for each sensor, represented by the 90% prediction interval of 100 realizations (90%PI), are also presented for the internal dataset (Fig. 10). The narrower the prediction interval, the more certain were our predictions. However, considering that the mean value of the clay content measured in our study area was 384.80 g kg^{-1}, we can say that the values predicted by the Sentinel2-MSI showed the lowest uncertainty, confirmed by their narrower prediction interval and the closeness of the values to the measured clay content. Among the other sensors, L8-OLI showed the second lowest uncertainty, with predictions ranging between 60 and 430 g kg^{-1}, but the mean was below 300 g kg^{-1}. The predictions obtained from PlanetScope and AISA FENIX were the more uncertain, as confirmed by their highest prediction intervals and outliers. Although the values predicted by the FieldSpec showed the lowest prediction interval, probably indicating the lowest uncertainty, this is not completely true, because it tends to overestimate clay content values.

For the external models (models developed using regional data), the results are shown in Fig. 11. We observed that, in general, all external models applied to our study area had lower performances than internal (local) models. Only FieldSpec model showed a good resuls ($R^2 = 0.66$ and RPIQ 1.6). The PlanetScope again showed the lowest R^2 (0.14). The AISA-FENIX showed the largest decrease in the performance from the external model validation ($R^2 = 0.78$) to the internal model validation ($R^2 = 0.32$). The mean predicted spatial maps of clay content were quite different among the sensors. Nevertheless, results from Landsat8-OLI and Sentinel2-MSI were very similar, as the difference in their pixel size is not large (30 and 20 m, respectively). Regarding the uncertainty, we showed that the prediction interval width was considerably lower than those observed for the internal dataset (Fig. 11), giving the wrong idea that the uncertainty was low. The true is that the external models tended to underestimate the clay content values of our study area. The exception was the clay content predicted by the FieldSpec, which showed a high PI width but it was more prone to overestimate clay content values.

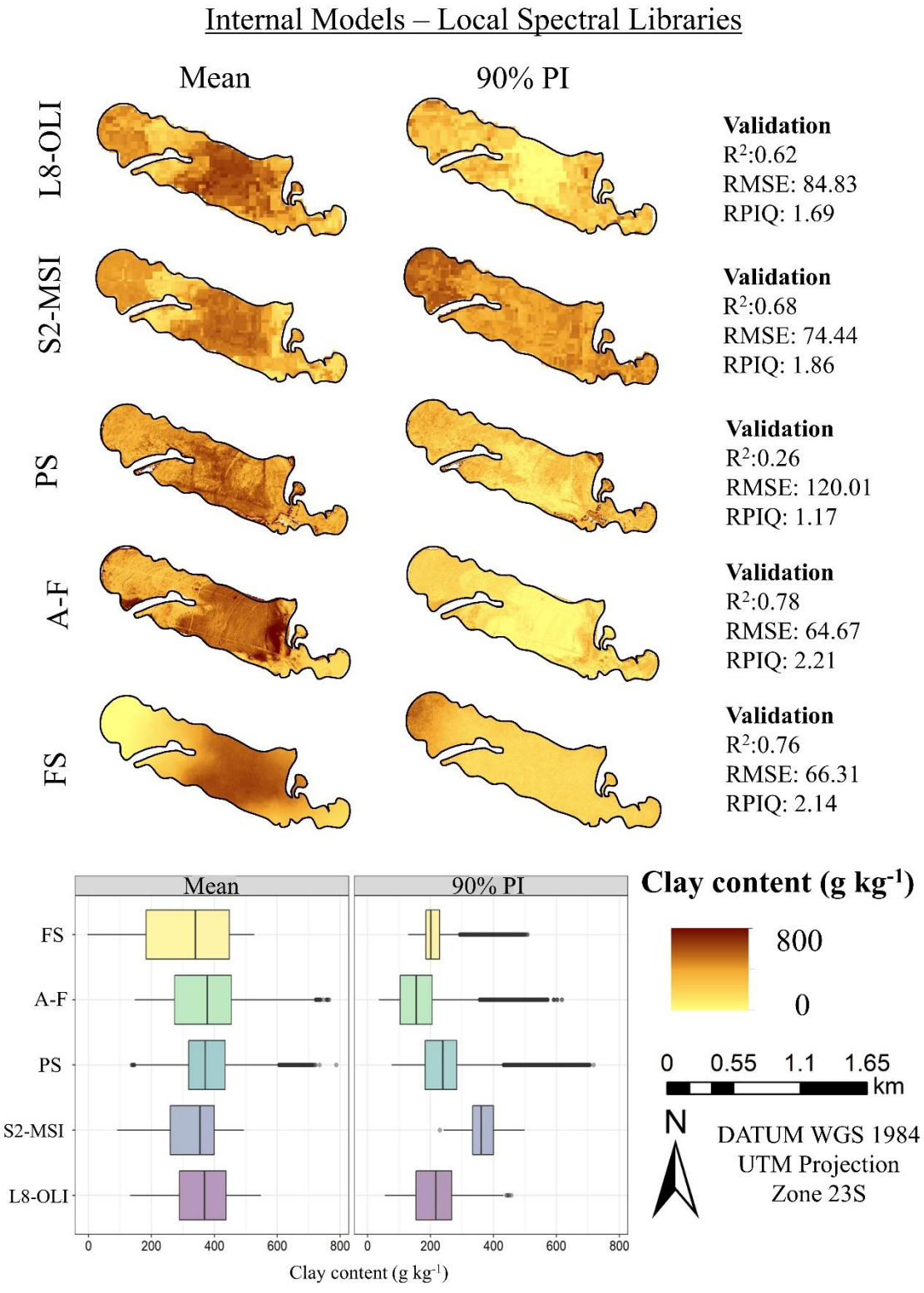

Figure 10. Spatial predictions of clay content and internal (Local) model performances. Mean of 100 realizations (left) and 90% prediction interval (right) for each sensor. FS: FieldSpec 3, A-F: AISA-FENIX, PS: PlanetScope, S2-MSI: Sentinel 2-MultiSpectral Instrument, L8-OLI: Landsat 8-Operational Land Imager, R^2: Coefficient of determination, RMSE: Root Mean Square Error, RPIQ: Performance to Interquartile Ratio.

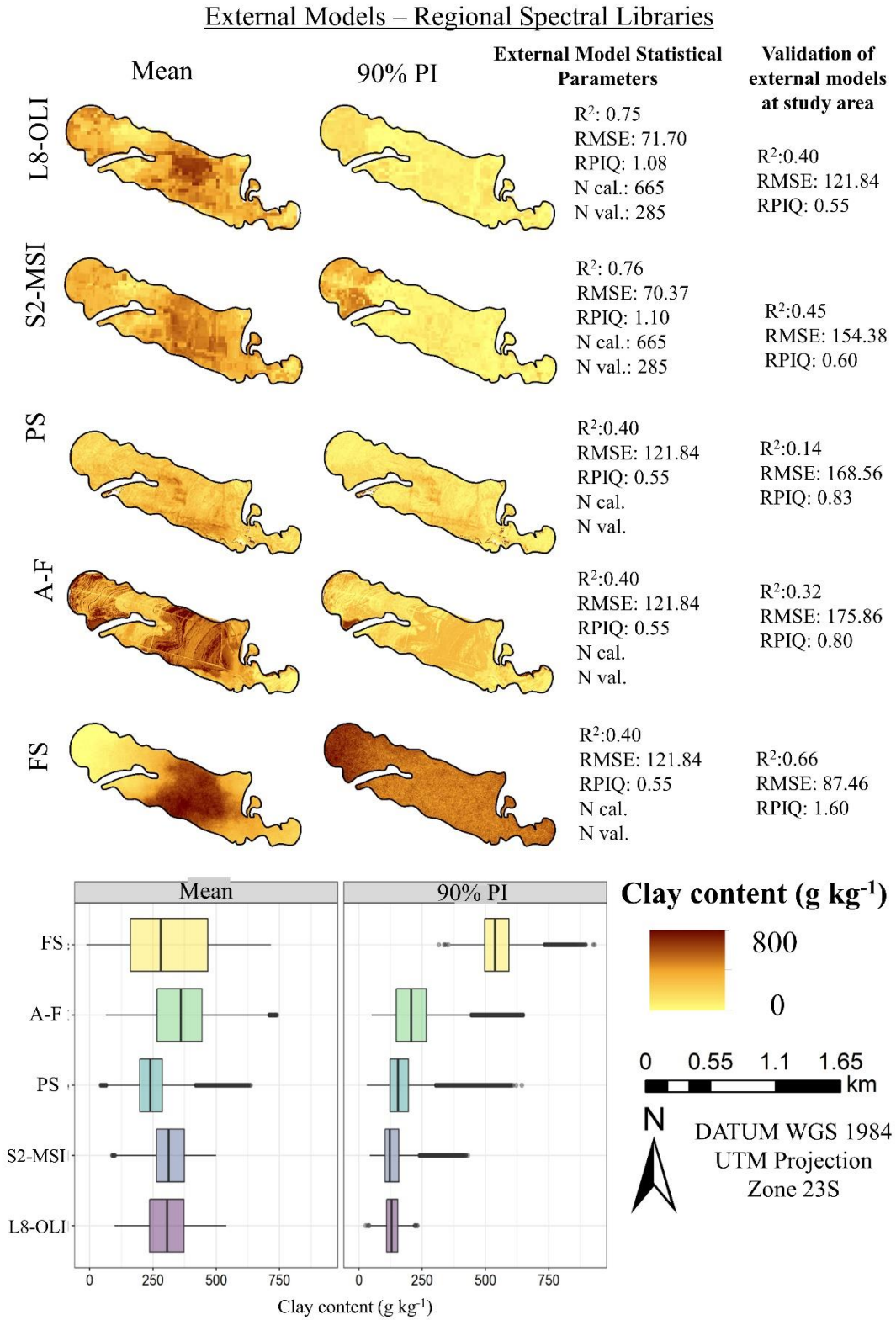

Figure 11. Spatial predictions of clay content and external (regional) model performances. Mean of 100 realizations (left) and 90% prediction interval (right) for each sensor. FS: FieldSpec 3, A-F: AISA-FENIX, PS: PlanetScope, S2-MSI: Sentinel 2-MultiSpectral Instrument, L8-OLI: Landsat 8-Operational Land Imager, R^2: Coefficient of determination, RMSE: Root Mean Square Error, RPIQ: Performance to Interquartile Ratio.

2.4. Discussions

2.4.1. Importance of the soil attribute analysis

Although the study area is small (83 ha), it was possible to observe a high variability in clay content, which provided a wide range of textural classes (from sandy to very clayey) (Fig. 1d). The variability of the clay content observed in the study area is related to the different parent materials (Marques et al., 2018), with sandstone from two different formations, massive argillaceous siltstones, sandy mudstones, clayey-sandy or sandy-clayey mudstone and siltstone. The region presents a highly complex geological domain (Gallo et al., 2018), which also impacts the different predominant soil types described there and their respective textural classes in the soil surface: Oxisols (clayey and very clayey) and Ultisols (sandy and loam sandy) (Fig. 1d).

2.4.2. Is the pixel with bare soil?

We attempted to obtain spectra for all samples corresponding to bare soil. The high variability of soils in the study area explained the high amplitude of distribution of points in the soil line for all sensors (Fig. 6).

The best results shown for the laboratory spectral data can be explained by the low impact of environmental factors in the spectra, especially humidity, which in general decreases the reflectance intensities, mainly in sandy soils (Galvão and Vitorello, 1998; Knadel et al., 2014). Laboratory spectra were not affected by environmental interferences. The spectra from Sentinel2-MSI, Landsat8-OLI and PlanetScope came from synthetic soil images (SYSI) obtained from satellite time-series, and represented only bare soil areas throughout a period.

Recently, bare soil images based on satellite time series, like SYSI images in our work, have been proposed basically calculating mean (Diek et al., 2017; Gasmi et al., 2021; Rogge et al., 2018) or median (Demattê et al., 2020, 2018a; Safanelli et al., 2020) spectral reflectance from the bare soil pixels along the period of the time series, both approaches showing good results. Roberts et al. (2019) proposed another method applying a high-dimensional statistic called a weighted geometric median (WGM). Demattê et al. (2018a) considered that use of median is the key of GEOS3 methodology. However, Safanelli et al. (2020) pointed that in the case of bare soil composite, generated using a shorter historical collection, median could not be a good approach because of the only few bare soil exposures along the time series. Most of these works highlight that the spectral reflectance data obtained from composite image are more robust than spectra obtained from a single image. This is probably due to the mitigation of the impact of some factor that influence the spectral response of the soil surface such as surface roughness, surface residues, soil crust and soil humidity (Demattê et al., 2018a; Diek et al., 2016; Gasmi et al., 2021). New works comparing these different methodologies could be developed for a better comparison between them.

We observed that the SYSIs from Sentinel2-MSI, Landsat8-OLI and PlanetScope well represented the bare soil. Interestingly, the soil line from PlanetScope showed the worst result, which was probably because the NIR region´s reflectance values are generally higher than those observed on other sensors. The differences in the soil line observed among sensors could be related to the differences in sensor characteristics (e.g., differences in sensors spectral and spatial resolutions; geometric distortions; view angle) and environments effects (e.g., differences in atmospheric and surface conditions on acquisition dates and spectral mixture of features) (Richter and Schläpfer, 2002). These effects could be the cause of the difference in the intensity of the reflectance factor values, for the different sensors (Fig. 8). However, it is not possible to state the degree of influence of these differences in clay prediction.

Another aspect that needs to be considered is that the SYSI PlanetScope was obtained from images of only two months from the same year due to financial limitations (the images are commercial). A short historical collection could be a problem for median spectral reflectance data (Safanelli et al., 2020). Meanwhile images from Sentinel2-MSI and Landsat8-OLI were obtained from a four-year period. The greater temporal variation of the images used could be a factor in attenuating interferences in spectral data, caused by soil surface conditions, such as roughness and the presence of vegetation residues (Castaldi et al., 2016; Gasmi et al., 2021; Wulder et al., 2015).

2.4.3. Evaluation of the spectral reflectance data

The distribution of soil surface reflectance points near the 1:1 soil line, in addition to proving the absence (or low influence) of photo synthetically active biomass (Rukhovich et al., 2016), evidenced the correspondence between the spectra of different sensors. This is reiterated by the high correlation coefficients observed between the sensors at all acquisition levels (except PlanetScope) and all spectral regions considered (Fig. 7). These analyses also proved the connection between sensors and consolidated the path for soil attribute predictions with data from various acquisition levels. Similar results were obtained by Rizzo et al. (2020), comparing SYSI Landsat spectra with convoluted laboratory spectra. Differences in the correlation between the sensor bands can be explained by the fact that multispectral and hyperspectral sensors perform direct measurements of the surface, the ultraspectral sensor is performed with standardized parameters (e.g., following sample preparation and environmentally controlled conditions). Besides that, differences are also related to the scale of measurement, satellite-based pixels can show different signal than the laboratory measurement (Rizzo et al., 2020); differences in atmospheric and surface conditions on acquisition dates; structural effects; differences in sensors spectral and spatial resolutions; geometric distortions; view angle and spectral mixture of features (Kriebel, 1978; Anderson et al., 2005; Mulder et al., 2011; Richter and Schläpfer, 2002).

In addition to the aforementioned fact of the possible influence on the data spectral quality due to the fact that SYSI Planet was obtained with images collected in an interval of two months, the poor correlation between all sensors and PlanetScope (0.13 to 0.63), can be explained because PlanetScope images provide high spatial (3 m) and temporal (daily) resolution, composed of a constellation greater than 150 microsatellites, dominated by "Doves" or CubeSat. This microsatellite constellation has a low quality in the radiometric and orbital parameters, causing inconsistencies in the spectral responses of the sensors (Leach et al. 2019).

We observed a common soil spectral pattern for each textural class, in which the reflectance intensities decreased from sandy to very clayey textures, except PlanetScope. A decrease in the mean reflectance intensities was observed for the different sensors following the order: FieldSpec, AISA-FENIX and satellites. This behavior was also observed by Gholizadeh et al. (2018) but diverged from that observed by Gomez et al. (2018). Soil particles' mineral composition could explain the reflectance decrease related to clay content. The presence of quartz (sandy soil) increases the reflectance, while the presence of iron oxides (clayey soil) decreases the reflectance (Demattê et al., 2007). The difference in reflectance intensities was more easily observed for sandy and loam sandy soils, but it also occurred for loam clay and clay. The lower influence of water can explain the higher reflectance values found for the Fieldspec data since the soil samples were dried and sieved (Gholizadeh et al., 2018; Nocita et al., 2013; Nouri et al., 2017). Other factors such as light sources, instrumental noise, spatial resolution, atmospheric condition and purity of the pixels can explain these differences as well (Gomez et al., 2015).

The qualitative analysis of the spectral signatures acquired in the laboratory with the FieldSpec sensor (Fig. 8a), demonstrated a typical kaolinite feature at 2200 nm for all textural classes (Vicente and de Souza Filho, 2011).

Clay soils, can present a smoothed gibbsite feature at 2265 nm (Madeira et al., 1995). Concave features, characteristic of the presence of iron oxides (Demattê et al., 2014), were verified in all textural classes; however, its intensity declined proportionally as the clay content decreased. The spectral signatures obtained by the AISA-FENIX hyperspectral sensor had similar features to those described for the lab spectra, except the gibbsite feature, which was very smoothed as also observed by Galvão et al. (2008).

The spectral data from airborne and spaceborne sensors showed lower reflectance intensities than those observed from the laboratory spectra, caused by differences in moisture conditions and other environmental factors (Gomez et al., 2015). Specifically, for the NIR band, the PlanetScope spectra showed reflectance values closer to the values of the laboratory data than the other sensors. Sentinel2-MSI spectra showed slightly higher reflectance intensities than Landsat8-OLI for the sandy, loam-sandy and loam-clay textural classes, especially in the SWIR region.

The great negative correlation values found between the clay content and the spectral bands of all sensors was observed mainly in the SWIR region and blue, green and red bands (Fig. 9). Similar results were found by Castaldi et al. (2016) for Sentinel2-MSI spectral bands. Sorensen and Dalsgaard (2005) found the best correlations on 400-600 nm, 1350-1600 nm and 1850-2500 nm wavelengths, for laboratory spectral data. Fongaro et al. (2018) working with Landsat multi-temporal images, found greater correlation with clay content for NIR and SWIR, but not for blue, green and red bands. For Sentinel2-MSI, Gholizadeh at al. (2018) found that the red-edge band from 773 to 793 nm provided the highest correlation with clay content, while Vaudour et al. (2019) found the highest importance for SWIR bands. For AISA-FENIX and Sentinel2-MSI sensors, the NIR bands also showed an important correlation. PlanetScope had the worst results about correlation with other sensors, soil line, spectral correlation with clay content and ability to be used in prediction models, possibly due to the issues previously discussed, such as environmental interferences and sensor characteristics.

2.4.4. Prediction of clay content - the internal and external dataset approach

2.4.4.1 Local prediction models - internal dataset approach

Even working with a small number of local data (52), we demonstrated that the use of internal (local) models had better performance to predict topsoil clay content, and better represented its variability than those observed for the external (regional) models (Fig. 10 and 11). Considering the results of the local modeling, the ultraspectral and hyperspectral sensors obtained good results while Landsat8-OLI and Sentinel2-MSI satisfactory results. The similar results obtained for AISA-FENIX and FieldSpec3 for internal model prediction, were in agreement with the results obtained by Castaldi et al. (2016), Adeline et al. (2017) and Gomez et al (2018). Gomez et al (2018) evaluated the effect of spectral degradation of AISA-DUAL hyperspectral data, on clay prediction. The authors found that the clay prediction did not have a marked decrease in accuracy when the spectral degradation was performed until a number of 19 bands (with a 100 nm spectral resolution) was reached. This number is approximately triple the number of bands of the Landsat8-OLI and Sentinel2-MSI satellites, which agree with the lower predictive potential of the multispectral sensors used in our work than FielSpec3 and AISA-FENIZ sensors.

The use of Landsat8-OLI and Sentinel2-MSI to predict clay content have been shown to provide good results in several works either using single or multi-temporal images (Chagas et al., 2016; Demattê et al., 2016; Fongaro et al., 2018; Gasmi et al., 2021; Gholizadeh et al., 2018; Gomez et al., 2019; Loiseau et al., 2019; Vaudour et al., 2019). In our work, satellite data showed satisfactory results, but worse than observed for airborne and laboratory

data. This is probably due to environmental factors that influence the spectra acquired by spaceborne, as atmosphere effects, surface roughness and moisture, and spatial resolution (Ben-Dor et al., 2009; Zhang and Zhou, 2016).

The PlanetScope showed the worst result, it can be attributed to the absence of spectral ranges in the shortwave-infrared region. Usually, in the SWIR region there are differences in reflectance intensities for different soil granulometric classes, especially due to the spectral expression of quartz (from 1900 to 2500 nm) and clay minerals around 2200 nm (Friedel et al., 2018; Gomez et al., 2018; Lacerda et al., 2016).

Better spectral resolution of hyperspectral and ultraspectral sensors allows better detection of the influence of iron oxides, such as goethite and hematite, in visible and NIR range and clay minerals such as illite, vermiculite, kaolinite and gibbsite in SWIR region, especially around 2200 nm. These clay minerals and oxides features detection are important factors that contribute to better prediction performance of clay content by these sensors (Adeline et al., 2017; Fang et al., 2018; Gomez et al., 2015; Mohamed et al., 2018).

Although we have obtained good and satisfactory results, the small local dataset (52 samples) probably could limit the prediction performance. Shepherd & Walsh (2002) stated that the prediction's accuracy using Vis-NIR-SWIR spectra data could be compromised in the number of samples are less than 200 samples.

On the other hand, Wetterlind and Stenberg (2010) obtained suitable results using local datasets with 25 samples to calibrate models for four farm-scale areas (with 97, 78, 69 and 62 ha) with a cross-validation with 25 randomly selected segments to determine the optimum number of PLS factors included in the calibrations by minimization of the root-mean-squared error of the coefficient of variation. Then, the models validation were performed in independent datasets of each areas. Coblinky et al. (2020) ran models with 66 and 197 samples datasets. While a good result can be achieved with 66 samples, the best results were obtained using 197 samples. Despite these, probably the best number of samples depends on the variation of the soils in the area. Spectral libraries spiked with local data, as a more robust approach and with less variation in results (Briedis et al., 2020; Brown, 2007; Gogé et al., 2014; Sankey et al., 2008; Wetterlind and Stenberg, 2010), and needs to be tested for multispectral and hyperspectral sensors.

The internal dataset used varied considerably from very low to high clay content values (Fig. 1d and 5), contribute to increasing RMSE values (Gholizadeh et al., 2018). However, it can also improve R^2 values (Coblinski et al., 2020; Demattê et al., 2016; Wetterlind and Stenberg, 2010). It is important to understand that each statistical parameter used in the evaluation of prediction models has limitations (Bellon-Maurel et al., 2010). Therefore, model evaluation should be performed by analyzing the entire context of the data and results. Golizadeh et al (2018) reinforce that when there are great differences in soil´s spectral characteristics, there are problems in obtainingsuitable predictions. However, robust soil prediction attributesmodels depend on a wide range on the sample population and exhibit a uniform distribution of samples across the range (Niederberger et al., 2015; Gandariasbeitia et al., 2017). In these appointments, we agree with Coblinky et al. (2020) who concluded that the variability of the input data is a key factor affecting prediction results. Therefore, this should be considered when a prediction result is interpreted or when we compare results from different works.

The use of information from ultra and hyperspectral sensors as well as those from multispectral ones has practical application for clay content estimation. The need for more accurate data to support decision making in agricultural and environmental applications could benefit from the information provided by ultra and hyperspectral sensors. When the objective is to obtain information from large areas rapidly with less accuracy, the multispectral sensors gain prominence. Even though the hyperspectral sensor's high spatial resolution is an important factor for modeling, the revisiting time of the multispectral sensors (Immitzer et al., 2016) can compensate, improving the

prediction accuracy. Besides the influence of spectral and spatial resolutions, recent studies have shown that the use of multi-temporal multi-spectral satellite images provided better results than just a single-date image (Bousbih et al., 2019; Gallo et al., 2018; Gasmi et al., 2021).

2.4.4.2 Regional prediction models - external dataset approach

The use of external datasets to develop clay prediction models showed, in general, lower accuracy than those observed for the internal data (Fig. 11). Only FieldSpec 3 presented a satisfactory result, which agrees with past studies (Brown et al., 2005; Chang et al., 2001; Demattê et al., 2016; Shepherd and Walsh, 2002). For ultraspectral sensors, in general, numerous studies found poorly prediction's accuracies when large spectral libraries were used (Brown, 2007; Gogé et al., 2014; Sankey et al., 2008) when compared to local spectral libraries (Briedis et al., 2020; Wetterlind and Stenberg, 2010). Global or regional spectral libraries spiked with local data have been showing the most robust results (Brown, 2007; Gogé et al., 2014; Wetterlind and Stenberg, 2010; Seidel et al., 2019)

The difference in the data distribution characteristics of the datasets used to develop the models and the study area dataset, is probably the best explanation for the low accuracy, in general, obtained (Fig. 5 and S.1). The ultraspectral model, which obtained the best result, was built with a well-distributed sample dataset and with median and mean values close to the values of the study area. Demattê et al. (2018b) pointed out the importance of the amplitude values of the validation samples, which should not be wider than the one found in the training samples. A good result was expected for the airborne hyperspectral data as well. However, the performance of the sensor in this platform dropped considerably. This is probably due to the methodology used in our work, where data was obtained by simulating the airborne spectral responses from ultraspectral laboratory dataset (since we did not have an AISA spectral library) was used to calibrate the model and it was applied for real image.

Despite that, data distribution characteristics of the datasets probably influenced the uncertainty. None of the external models showed prediction intervals close to the measured clay content value from our study area (Fig. 11), all results had the tendency of sub estimate, in fact the regional dataset, in general, have major number of data with lower clay content than local dataset (Fig. S1).

Another important limitation is that this study does not have an independent validation dataset for local validation dataset. The internal models were validated using cross validation which may disadvantage for the external model result.

Regardless of the result, we believe that this study has developed an approach to obtain clay content by hyperspectral and multispectral data for a smallfield scale using regional dataset, similar another ultraspectral sensors studies (Brown, 2007; Sankey et al., 2008; Shepherd and Walsh, 2002). Probably better results when using external models from multitemporal images, where the spectral curve of an exposed soil point will be represented by the median of different images (Demattê et al., 2018a). The use of multispectral and hyperspectral spectral libraries spiked with local data to develop prediction models, could be a interesting approach to be studied, since it is mainly trialled in the literature for ultraspectral data (Briedis et al., 2020; Brown, 2007; Gogé et al., 2014; Wetterlind and Stenberg, 2010; Siedel et al., 2019).

2.5. Conclusions

Spatializing clay content by sensing technologies is challenging. Even more when the sensor is remote such as airborne and spaceborne sensors with different spatial and spectral resolution. In this work, we performed to reach the goal of quantifying the clay content by sensors at several acquisition levels in the same smallholder area.

The first step was to defining the quality of each sensor´s spectra by their spectral signature behavior, essential for the development of good prediction models. Afterwards, we observed that the spectral proxy between different sensors (laboratory, airborne and satellites) reached great correlation coefficients. In this case, PlanetScope was the exception. This directly impacted the correlation of spectra with clay property. For all sensors, negatively correlates with the reflectance, mostly in SWIR which is coherent with literature.

Clayey soil samples presented low intensity and flat spectral signatures. As we go from clayey to sandy samples, reflectance intensities increased mainly in the SWIR region. This analysis gave confidence on the soil spectral data, since we saw the behavior spectral signature.

The internal approach presents better results for clay quantification models, but the external approach is still feasible for ultraspectral data. Statistical information indicated better results, i.e., for internal and external approaches, for ultraspectral sensors, and worst for PlanetScope. Despite that the Planetscope having a greater spatial and temporal resolution, it lacks the SWIR band which is important for clay quantification. Thus, if we focus only on the quantification of clay property, ground to space sensors (with exception of PlanetScope) are important tools.

We emphasize the importance that spectral libraries should have a wide range and a good distribution of the attributes values. These factors should be taken into account in the evaluation and comparison of prediction results. Finally, the strategy, approach and sensor will depend on the users´ requirements and objectives. The most important take-home message is that soil sensing is possible at any level taking into account its advantages and limitations.

Acknowledgments

We thank members of the Geotechnologies in Soil Science group (https://esalqgeocis.wixsite.com/english/team) for the technical support and GALeS group of University of Maringá (http://gales.uem.br/) for using the AISA-FENIX sensor. This research was funded by the Fundação de Amparo à Pesquisa do Estado de São Paulo – FAPESP, grant numbers: 2014/22262-0, 2016/26124-6 and 2016/01597-9. The AISA-FENIX acquisition was founded by the Studies and Projects Financer - FINEP (Financiadora de Estudos e Projetos).

Appendix A. Supplementary data

Supplementary data to this article can be found online at: https://doi.org/10.1016/j.geoderma.2021.115116

References

Adeline, K.R.M., Gomez, C., Gorretta, N., Roger, J.M., 2017. Predictive ability of soil properties to spectral degradation from laboratory Vis-NIR spectroscopy data. Geoderma, 288, 143-153. https://doi.org/10.1016/j.geoderma.2016.11.010

Agyeman, P.C., Ahado, S.K., Borůvka, L., Biney, J.K.M., Sarkodie, V.Y.O., Kebonye, N.M., Kingsley, J., 2020. Trend analysis of global usage of digital soil mapping models in the prediction of potentially toxic elements in soil/sediments: a bibliometric review. Environ. Geochem. Health. https://doi.org/10.1007/s10653-020-00742-9

Anderson, G.P., Wang, J., Hoke, M.L., Kneizys, F.X., Chetwynd, Jr., J.H., Rothman, L.S., Kimball, L.M., McClatchey, R.A., Shettle, E.P., Clough, S., Gallery, W.O., Abreu, L.W., Selby, J.E.A., 2005. History of one

family of atmospheric radiative transfer codes in: Passive Infrared Remote Sensing of Clouds and the Atmosphere II. https://doi.org//10.1117/12.196674.

Alvares, C.A., Stape, J.L., Sentelhas, P.C., de Moraes Gonçalves, J.L., Sparovek, G., 2013. Köppen's climate classification map for Brazil. Meteorol. Zeitschrift 22, 711–728. https://doi.org/10.1127/0941-2948/2013/0507

Araújo, S.R., Wetterlind, J., Demattê, J.A.M., Stenberg, B., 2014. Improving the prediction performance of a large tropical vis-NIR spectroscopic soil library from Brazil by clustering into smaller subsets or use of data mining calibration techniques. Eur. J. Soil Sci. 65, 718–729. https://doi.org/10.1111/ejss.12165

Arrouays, D., Richer-de-Forges, A.C., Chen, S., Saby, N., Martin, M., Libohova, Z., Roudier, P., McBratney, A.B., Minasny, B., Padarian, J., Grundy, M., McKenzie, N., Viscarra Rossel, R., Savin, I.Yu., Leenaars, J.G.B., Hempel, J., 2018. GlobalSoilMap history and main achievements. In: Arrouays, D., Savin, I., Leenaars, J., McBratney, A.B., (Eds.). GlobalSoilMap - Digital Soil Mapping from Country to Globe: Proceedings of the Global Soil Map 2017 Conference, July 4-6, 2017, Moscow, Russia (1st ed.). CRC Press. https://doi.org/10.1201/9781351239707

Arrouays, D., Grundy, M.G., Hartemink, A.E., Hempel, J.W., Heuvelink, G.B.M., Hong, S.Y., Lagacherie, P., Lelyk, G., McBratney, A.B., McKenzie, N.J., Mendonca-Santos, M. d. L., Minasny, B., Montanarella, L., Odeh, I.O.A., Sanchez, P.A., Thompson, J.A., Zhang, G.-L., 2014. Chapter Three - GlobalSoilMap: Toward a Fine-Resolution Global Grid of Soil Properties, in: Sparks, D.L. (Ed.), Advances in Agronomy, 125. Academic Press, San Diego, pp. 93–134. https://doi.org/10.1016/B978-0-12-800137-0.00003-0

Baret, F., Jacquemoud, S., Hanocq, J.F., 1993. About the soil line concept in remote sensing. Adv. Sp. Res. 13, 281–284. https://doi.org/10.1016/0273-1177(93)90560-X

Barnes, E.M., and Baker, M.G., (2000). Multispectral data for mapping soil texture: possibilities and limitations. Appl. Eng. Agric. 16 (6), 731–741.

Bellon-Maurel, V., Fernandez-Ahumada, E., Palagos, B., Roger, J.-M., McBratney, A., 2010. Critical review of chemometric indicators commonly used for assessing the quality of the prediction of soil attributes by {NIR} spectroscopy. TrAC Trends Anal. Chem. 29, 1073–1081. https://doi.org/10.1016/j.trac.2010.05.006

Ben-Dor, E., 2002. Quantitative remote sensing of soil properties. Adv. Agron. 75, 173–243. https://doi.org/10.1016/S0065-2113(02)75005-0

Ben-Dor, E., Chabrillat, S., Demattê, J.A.M., Taylor, G.R., Hill, J., Whiting, M.L., Sommer, S., 2009. Using Imaging Spectroscopy to study soil properties. Remote Sens. Environ. 113, S38–S55. https://doi.org/10.1016/j.rse.2008.09.019

Bouma, J., Broll, G., Crane, T.A., Dewitte, O., Gardi, C., Schulte, R.P.O., Towers, W., 2012. Soil information in support of policy making and awareness raising. Curr. Opin. Environ. Sustain. 4, 552–558. https://doi.org/10.1016/j.cosust.2012.07.001

Bousbih, S., Zribi, M., Pelletier, C., Gorrab, A., Lili-Chabaane, Z., Baghdadi, N., Ben Aissa, N., Mougenot, B., 2019. Soil Texture Estimation Using Radar and Optical Data from Sentinel-1 and Sentinel-2. Remote Sens. 11, 1520. . https://doi.org/10.3390/rs11131520

Breiman, L., 2001. Random Forests. Mach. Learn. 45, 5–32. https://doi.org/10.1023/A:1010933404324

Briedis, C., Baldock, J., de Moraes Sá, J.C., dos Santos, J.B., Milori, D.M.B.P., 2020. Strategies to improve the prediction of bulk soil and fraction organic carbon in Brazilian samples by using an Australian national mid-infrared spectral library. Geoderma 373, 114401. https://doi.org/10.1016/j.geoderma.2020.114401

Brown, D.J., Bricklemyer, R.S., Miller, P.R., 2005. Validation requirements for diffuse reflectance soil characterization models with a case study of VNIR soil C prediction in Montana. Geoderma 129, 251–267. https://doi.org/10.1016/j.geoderma.2005.01.001

Brown, D.J., 2007. Using a global VNIR soil-spectral library for local soil characterization and landscape modeling in a 2nd-order Uganda watershed. Geoderma 140, 444–453. https://doi.org/10.1016/j.geoderma.2007.04.021

Busato, J.G., Leão, T.P., Baldotto, M.A., Canellas, L.P., 2012. Organic matter quality and dynamics in tropical soils amended with sugar industry residue. Rev. Bras. Cienc. Solo, 36, 1179-1188. https://doi.org/10.1590/S0100-06832012000400012

Castaldi, F., Palombo, A., Santini, F., Pascucci, S., Pignatti, S., Casa, R., 2016. Evaluation of the potential of the current and forthcoming multispectral and hyperspectral imagers to estimate soil texture and organic carbon. Remote Sens. Environ. 179, 54–65. https://doi.org/10.1016/j.rse.2016.03.025

Cezar, E., Nanni, M.R., Guerrero, C., da Silva Junior, C.A., Cruciol, L.G.T., Chicati, M.L., Silva, G.F.C., 2019. Organic matter and sand estimates by spectroradiometry: Strategies for the development of models with applicability at a local scale. Geoderma 340, 224–233. https://doi.org/10.1016/j.geoderma.2019.01.021

Chabrillat, S., Goetz, A.F.H., Krosley, L., Olsen, H.W., 2002. Use of hyperspectral images in the identification and mapping of expansive clay soils and the role of spatial resolution. Remote Sens. Environ. 82, 431–445. https://doi.org/https://doi.org/10.1016/S0034-4257(02)00060-3

Chagas, C. da S., de Carvalho Junior, W., Bhering, S.B., Calderano Filho, B., 2016. Spatial prediction of soil surface texture in a semiarid region using random forest and multiple linear regressions. Catena 139, 232–240. https://doi.org/10.1016/j.catena.2016.01.001

Chang, C.-W., Laird, D.A., Mausbach, M.J., Hurburgh, C.R., 2001. Near-infrared reflectance spectroscopy - principal components regression analyses of soil properties. Soil Sci. Soc. Am. J. 65, 480–490. https://doi.org/10.2136/sssaj2001.652480x

Cherubin, M.R., Franco, A.L.C., Cerri, C.E.P., Oliveira, D.M. da S., Davies, C.A., Cerri, C.C., 2015. Sugarcane expansion in Brazilian tropical soils—Effects of land use change on soil chemical attributes. Agric. Ecosyst. Environ. 211, 173–184. https://doi.org/10.1016/j.agee.2015.06.006

Cherubin, M.R., Karlen, D.L., Franco, A.L.C., Tormena, C.A., Cerri, C.E.P., Davies, C.A., Cerri, C.C., 2016. Soil physical quality response to sugarcane expansion in Brazil. Geoderma 267, 156–168. https://doi.org/10.1016/j.geoderma.2016.01.004

Coblinski, J.A., Giasson, É., Demattê, J.A.M., Dotto, A.C., Costa, J.J.F., Vašát, R., 2020. Prediction of soil texture classes through different wavelength regions of reflectance spectroscopy at various soil depths. Catena 189, 104485. https://doi.org/10.1016/j.catena.2020.104485

Coelho, F.F., Giasson, E., Campos, A.R., Tiecher, T., Costa, J.J.F., Coblinski, J.A., 2021. Digital soil class mapping in Brazil: a systematic review. Sci. Agric. 78, n5, e20190227. https://doi.org/10.1590/1678-992X-2019-0227

Demattê, J.A.M., Nanni, M.R., Formaggio, A.R., Epiphanio, J.C.N., 2007. Spectral reflectance for the mineralogical evaluation of Brazilian low clay activity soils. Int. J. Remote Sens. 28, 4537–4559. https://doi.org/10.1080/01431160701250408

Demattê, J.A.M., Bellinaso, H., Romero, D.J., Fongaro, C.T., 2014. Morphological Interpretation of Reflectance Spectrum (MIRS) using libraries looking towards soil classification. Sci. Agric. 71, 509–520. https://doi.org/10.1590/0103-9016-2013-0365

Demattê, J.A.M., Morgan, C.L.S., Chabrillat, S., Rizzo, R., Franceschini, M.H.D., Terra, F. da S., Vasques, G.M., Wetterlind, J., 2015. Spectral sensing from ground to space in soil science: state of the art, applications, potential, and perspectives, in: Thenkabail, P.S. (Ed.), Remote Sensing Handbook. CRC Press, Boca Raton, pp. 661–732.https://doi.org/10.1201/b19355

Demattê, J.A.M., Bellinaso, H., Araújo, S.R., Rizzo, R., Souza, A.B., 2016. Spectral regionalization of tropical soils in the estimation of soil attributes. Rev. Ciênc. Agron. 47, 589-598. https://doi.org/10.5935/1806-6690.20160071

Demattê, J.A.M., Fongaro, C.T., Rizzo, R., Safanelli, J.L., 2018a. Geospatial Soil Sensing System (GEOS3): A powerful data mining procedure to retrieve soil spectral reflectance from satellite images. Remote Sens. Environ. 212, 161–175. https://doi.org/10.1016/j.rse.2018.04.047

Demattê, J.A.M., Guimarães, C.C.B., Fongaro, C.T., Vidoy, E.L.F., Sayão, V.M., Dotto, A.C., Santos, N.V. dos, 2018b. Satellite Spectral Data on the Quantification of Soil Particle Size from Different Geographic Regions. Rev. Bras. Cienc. do Solo 42, e0170392. https://doi.org/10.1590/18069657rbcs20170392

Demattê, J.A.M., Dotto, A.C., Paiva, A.F.S., Sato, M. V., Dalmolin, R.S.D., de Araújo, M. do S.B., da Silva, E.B., Nanni, M.R., ten Caten, A., Noronha, N.C., Lacerda, M.P.C., de Araújo Filho, J.C., Rizzo, R., Bellinaso, H., Francelino, M.R., Schaefer, C.E.G.R., Vicente, L.E., dos Santos, U.J., de Sá Barretto Sampaio, E. V., Menezes, R.S.C., de Souza, J.J.L.L., Abrahão, W.A.P., Coelho, R.M., Grego, C.R., Lani, J.L., Fernandes, A.R., Gonçalves, D.A.M., Silva, S.H.G., de Menezes, M.D., Curi, N., Couto, E.G., dos Anjos, L.H.C., Ceddia, M.B., Pinheiro, É.F.M., Grunwald, S., Vasques, G.M., Marques Júnior, J., da Silva, A.J., Barreto, M.C. de V., Nóbrega, G.N., da Silva, M.Z., de Souza, S.F., Valladares, G.S., Viana, J.H.M., da Silva Terra, F., Horák-Terra, I., Fiorio, P.R., da Silva, R.C., Frade Júnior, E.F., Lima, R.H.C., Alba, J.M.F., de Souza Junior, V.S., Brefin, M.D.L.M.S., Ruivo, M.D.L.P., Ferreira, T.O., Brait, M.A., Caetano, N.R., Bringhenti, I., de Sousa Mendes, W., Safanelli, J.L., Guimarães, C.C.B., Poppiel, R.R., e Souza, A.B., Quesada, C.A., do Couto, H.T.Z., 2019. The Brazilian Soil Spectral Library (BSSL): A general view, application and challenges. Geoderma 354, 113793. https://doi.org/10.1016/j.geoderma.2019.05.043

Demattê, J.A.M., Safanelli, J.L., Poppiel, R.R., Rizzo, R., Silvero, N.E.Q., Mendes, W. de S., Bonfatti, B.R., Dotto, A.C., Salazar, D.F.U., Mello, F.A. de O., Paiva, A.F. da S., Souza, A.B., Santos, N.V. dos, Maria Nascimento, C., Mello, D.C. de, Bellinaso, H., Gonzaga Neto, L., Amorim, M.T.A., Resende, M.E.B. de, Vieira, J. da S., Queiroz, L.G. de, Gallo, B.C., Sayão, V.M., Lisboa, C.J. da S., 2020. Bare Earth's Surface Spectra as a Proxy for Soil Resource Monitoring. Sci. Rep. 10, 4461. https://doi.org/10.1038/s41598-020-61408-1

Diek, S., Fornallaz, F., Schaepman, M.E., de Jong, R., 2017. Barest Pixel Composite for agricultural areas using landsat time series. Remote Sens. 9, 1245. https://doi.org/10.3390/rs9121245

Diek, S., Schaepman, M., de Jong, R., 2016. Creating multi-temporal composites of airborne imaging spectroscopy data in support of digital soil mapping. Remote Sens. 8, 906. https://doi.org/10.3390/rs8110906

Domínguez-Castillo, V., Bovi, R. C., Chartier, M. P., Tomazello Filho, M., Cooper, M. 2020. Using dendrogeomorphology to estimate soil erosion in mixed native species and pine forests on Ultisols in Piracicaba, Brazil. Geoderma Regional 21, e00276, https://doi.org/10.1016/j.geodrs.2020.e00276

Dutta D., Goodwell, A.E., Kumar, P., Garvey, J.E., Darmody, R.G., Berretta, D.P., Jonathan A. Greenberg, J.A. 2015. On the Feasibility of Characterizing Soil Properties from AVIRIS Data. IEEE Transactions on Geoscience and Remote Sensing 53, n.9, 5133-5147. https://doi.org/10.1109/TGRS.2015.2417547.

Fang, Q., Hong, H., Zhao, L., Kukolich, S., Yin, K., Wang, C., 2018. Visible and Near-Infrared Reflectance Spectroscopy for Investigating Soil Mineralogy: A Review. J. Spectrosc. 2018, 3168974. https://doi.org/10.1155/2018/3168974

Fathololoumi, S., Vaezi, A.R., Alavipanah, S.K., Ghorbani, A., Saurette, D., Biswas, A., 2020. Improved digital soil mapping with multitemporal remotely sensed satellite data fusion: A case study in Iran. Sci. Total Environ. 721, 137703. https://doi.org/https://doi.org/10.1016/j.scitotenv.2020.137703

Feizizadeh, B., Blaschke, T., 2013. Land suitability analysis for Tabriz County, Iran: a multi-criteria evaluation approach using GIS. J. Environ. Plan. Manag. 56, 1–23. https://doi.org/10.1080/09640568.2011.646964

Foley, J.A., DeFries, R., Asner, G.P., Barford, C., Bonan, G., Carpenter, S.R., Chapin, F.S., Coe, M.T., Daily, G.C., Gibbs, H.K., Helkowski, J.H., Holloway, T., Howard, E.A., Kucharik, C.J., Monfreda, C., Patz, J.A., Prentice, I.C., Ramankutty, N., Snyder, P.K., 2005. Global Consequences of Land Use. Science 309, 570–574. https://doi.org/10.1126/science.1111772

Fongaro, C.T., Demattê, J.A.M., Rizzo, R., Safanelli, J.L., Mendes, W. de S., Dotto, A.C., Vicente, L.E., Franceschini, M.H.D., Ustin, S.L., 2018. Improvement of clay and sand quantification based on a novel approach with a focus on multispectral satellite images. Remote Sens. 10, 1555. https://doi.org/10.3390/rs10101555

Friedel, M.J., Buscema, M., Vicente, L.E., Iwashita, F., Koga-Vicente, A., 2018. Mapping fractional landscape soils and vegetation components from Hyperion satellite imagery using an unsupervised machine-learning workflow. Int. J. Digit. Earth 11, 670–690. https://doi.org/10.1080/17538947.2017.1349841

Gallo, B.C., Demattê, J.A.M., Rizzo, R., Safanelli, J.L., Mendes, W.D.S., Lepsch, I.F., Sato, M. V, Romero, D.J., Lacerda, M.P.C., 2018. Multi-Temporal Satellite Images on Topsoil Attribute Quantification and the Relationship with Soil Classes and Geology. Remote Sens. 10, 1571. https://doi.org/10.3390/rs10101571

Galvão, L.S., Formaggio, A.R., Couto, E.G., Roberts, D.A., 2008. Relationships between the mineralogical and chemical composition of tropical soils and topography from hyperspectral remote sensing data. ISPRS J. Photogramm. Remote Sens. 63, 259–271. https://doi.org/https://doi.org/10.1016/j.isprsjprs.2007.09.006

Galvão, L.S., Vitorello, Í., 1998. Variability of Laboratory Measured Soil Lines of Soils from Southeastern Brazil. Remote Sens. Environ. 63, 166–181. https://doi.org/10.1016/S0034-4257(97)00135-1

Gandariasbeitia, M., Besga, G., Albizu, I., Larregla, S., Mendarte, S., 2017. Prediction of chemical and biological variables of soil in grazing areas with visible- and near-infrared spectroscopy. Geoderma 305, 228–235. http://dx.doi.org/10.1016/j.geoderma.2017.05.045

Gasmi, A., Gomez, C., Lagacherie P., Zouari H., 2019. Surface soil clay content mapping at large scales using multispectral (VNIR–SWIR) ASTER data, International Journal of Remote Sensing, 40(4), 1506-1533.

Gasmi, A., Gomez, C., Lagacherie, P., Zouari, H., Laamrani, A., Chehbouni, A., 2021. Mean spectral reflectance from bare soil pixels along a Landsat-TM time series to increase both the prediction accuracy of soil clay content and mapping coverage. Geoderma 388, 114864. https://doi.org/https://doi.org/10.1016/j.geoderma.2020.114864

Gerighausen, H., Menz, G., Kaufmann, H., 2012. Spatially explicit estimation of clay and organic carbon content in agricultural soils using multi-annual imaging spectroscopy data. Appl. Environ. Soil Sci. 2012, 868090. https://doi.org/10.1155/2012/868090

Gholizadeh, A., Žižala, D., Saberioon, M., Borůvka, L., 2018. Soil organic carbon and texture retrieving and mapping using proximal, airborne and Sentinel-2 spectral imaging. Remote Sens. Environ. 218, 89–103. https://doi.org/10.1016/j.rse.2018.09.015

Goetz, A.F.H., 2009. Three decades of hyperspectral remote sensing of the Earth: A personal view. Remote Sens. Environ. 113, S5–S16. https://doi.org/10.1016/j.rse.2007.12.014

Gogé, F., Gomez, C., Jolivet, C., Joffre, R., 2014. Which strategy is best to predict soil properties of a local site from a national Vis-NIR database? Geoderma 213, 1–9. https://doi.org/10.1016/j.geoderma.2013.07.016

Gomez, C., Lagacherie, P., Bacha. S., 2012. Using Vis-NIR Hyperspectral Data to Map Topsoil Properties over Bare Soils in the Cap-Bon Region, Tunisia. Digital Soil Assessments and Beyond: Proceedings of the 5th Global Workshop on Digital Soil Mapping 2012, Sydney, Australia, 387– 392.

Gomez, C., Adeline, K., Bacha, S., Driessen, B., Gorretta, N., Lagacherie, P., Roger, J.M., Briottet, X., 2018. Sensitivity of clay content prediction to spectral configuration of VNIR/SWIR imaging data, from multispectral to hyperspectral scenarios. Remote Sens. Environ. 204, 18–30. https://doi.org/10.1016/j.rse.2017.10.047

Gomez, C., Dharumarajan, S., Féret, J.-B., Lagacherie, P., Ruiz, L., Sekhar, M., 2019. Use of Sentinel-2 Time-Series Images for Classification and Uncertainty Analysis of Inherent Biophysical Property: Case of Soil Texture Mapping. Remote Sens. 11, 595. https://doi.org/10.3390/rs11050565

Gomez, C., Chevallier, T., Moulin, P., Bouferra, I., Hmaidi, K., Arrouays, D., Jolivet, C., Barthèsc, B.G., 2020. Prediction of soil organic and inorganic carbon concentrations in Tunisian samples by mid-infrared reflectance spectroscopy using a French national library. Geoderma 375, 114469. https://doi.org/10.1016/j.geoderma.2020.114469

Gomez, C., Oltra-Carrió, R., Bacha, S., Lagacherie, P., Briottet, X., 2015. Evaluating the sensitivity of clay content prediction to atmospheric effects and degradation of image spatial resolution using Hyperspectral VNIR/SWIR imagery. Remote Sens. Environ. 164, 1–15. https://doi.org/10.1016/j.rse.2015.02.019

Guerrero, C., Stenberg, B., Wetterlind, J., Viscarra Rossel, R.A., Maestre, F.T., Mouazen, A.M., Zornoza, R., Ruiz-Sinoga, J.D., Kuang, B., 2014. Assessment of soil organic carbon at local scale with spiked NIR calibrations: effects of selection and extra-weighting on the spiking subset. Eur. J. Soil Sci. 65, 248–263. https://doi.org/10.1111/ejss.12129

Guevara, M., Olmedo, G.F., Stell, E., Yigini, Y., Aguilar Duarte, Y., Arellano Hernández, C., Arévalo, G.E., Arroyo-Cruz, C.E., Bolivar, A., Bunning, S., Bustamante Cañas, N., Cruz-Gaistardo, C.O., Davila, F., Dell Acqua, M., Encina, A., Figueredo Tacona, H., Fontes, F., Hernández Herrera, J.A., Ibelles Navarro, A.R., Loayza, V., Manueles, A.M., Mendoza Jara, F., Olivera, C., Osorio Hermosilla, R., Pereira, G., Prieto, P., Ramos, I.A., Rey Brina, J.C., Rivera, R., Rodríguez-Rodríguez, J., Roopnarine, R., Rosales Ibarra, A., Rosales Riveiro, K.A., Schulz, G.A., Spence, A., Vasques, G.M., Vargas, R.R., Vargas, R., 2018. No silver bullet for digital soil mapping: country-specific soil organic carbon estimates across Latin America. SOIL 4, 173–193. https://doi.org/10.5194/soil-4-173-2018

Guy, A. L., Siciliano, S. D. and Lamb, E. G. 2015. Spiking regional vis-NIR calibration models with local samples to predict soil organic carbon in two High Arctic polar deserts using a vis-NIR probe. Can. J. Soil Sci. 95, 237–249. https://doi.org/10.4141/cjss-2015-004

Hively, W.D., McCarty, G.W., Reeves, J.B., Lang, M.W., Oesterling, R.A., Delwiche, S.R., 2011. Use of Airborne Hyperspectral Imagery to Map Soil Properties in Tilled Agricultural Fields. Appl. Environ. Soil Sci. 2011, 1–13. https://doi.org/10.1155/2011/358193

Hristov, B., 2013. The importance of soil texture in soil classification systems. J. Balk. Ecol. 16, 137–139.

Huete, A.R., 1996. Extension of soil spectra to the satellite: atmosphere, geometric, and sensor considerations. Photo Interpret. Images Aeriennes Spat. 34, 101–118.

Immitzer, M., Vuolo, F., Atzberger, C., 2016. First Experience with Sentinel-2 Data for Crop and Tree Species Classifications in Central Europe. Remote Sens. 8, 166. https://doi.org/10.3390/rs8030166

Khaledian, Y., Kiani, F., Ebrahimi, S., Brevik, E.C., Aitkenhead-Peterson, J., 2017. Assessment and Monitoring of Soil Degradation during Land Use Change Using Multivariate Analysis. L. Degrad. Dev. 28, 128–141. https://doi.org/10.1002/ldr.2541

Knadel, M., Deng, F., Alinejadian, A., Wollesen de Jonge, L., Moldrup, P., Greve, M.H., 2014. The Effects of Moisture Conditions—From Wet to Hyper dry—On Visible Near-Infrared Spectra of Danish Reference Soils. Soil Sci. Soc. Am. J. 78, 422–433. https://doi.org/10.2136/sssaj2012.0401

Knadel, M., Thomsen, A., Schelde, K., Greve, M.H., 2015. Soil organic carbon and particle sizes mapping using vis–NIR, EC and temperature mobile sensor platform. Comput. Electron. Agric. 114, 134–144. https://doi.org/10.1016/j.compag.2015.03.013

Kriebel, K.T., 1978. Average variability of the radiation reflected by vegetated surfaces due to differing irradiations. Remote Sens. Environ. https://doi.org//10.1016/0034-4257(78)90010-X.

Kuhn, M., Weston, S., Keefer, C., Coulter, N., Quinlan, R., 2013. Cubist: Rule-and instance-based regression modeling, R package version 0.0. 18. https://topepo.github.io/Cubist (accessed 05 April 2020).

Lacerda, M.P.C., Demattê, J.A.M., Sato, M.V., Fongaro, C.T., Gallo, B.C., Souza, A.B., 2016. Tropical Texture Determination by Proximal Sensing Using a Regional Spectral Library and Its Relationship with Soil Classification. Remote Sens., 8(9), 701. https://doi.org/10.3390/rs8090701

Ladoni, M., Bahrami, H.A., Alavipanah, S.K., Norouzi, A.A., 2010. Estimating soil organic carbon from soil reflectance: a review. Precis. Agric. 11, 82–99. https://doi.org/10.1007/s11119-009-9123-3

Lagacherie, P., Arrouays, D., Bourennane, H., Gomez, C., Nkuba-Kasanda, L., 2020. Analysing the impact of soil spatial sampling on the performances of Digital Soil Mapping models and their evaluation: A numerical experiment on Quantile Random Forest using clay contents obtained from Vis-NIR-SWIR hyperspectral imagery. Geoderma 375, 114503. https://doi.org/10.1016/j.geoderma.2020.114503

Lausch, A., Baade, J., Bannehr, L., Borg, E., Bumberger, J., Chabrilliat, S., Dietrich, P., Gerighausen, H., Glässer, C., Hacker, J.M., Haase, D., Jagdhuber, T., Jany, S., Jung, A., Karnieli, A., Kraemer, R., Makki, M., Mielke, C., Möller, M., Mollenhauer, H., Montzka, C., Pause, M., Rogass, C., Rozenstein, O., Schmullius, C., Schrodt, F., Schrön, M., Schulz, K., Schütze, C., Schweitzer, C., Selsam, P., Skidmore, A.K., Spengler, D., Thiel, C., Truckenbrodt, S.C., Vohland, M., Wagner, R., Weber, U., Werban, U., Wollschläger, U., Zacharias, S., Schaepman, M.E., 2019. Linking Remote Sensing and Geodiversity and Their Traits Relevant to Biodiversity—Part I: Soil Characteristics. Remote Sens. 11, 2356. https://doi.org/10.3390/rs11202356

Leach, N., Coops, N.C., Obrknezev, N., 2019. Normalization method for multi-sensor high spatial and temporal resolution satellite imagery with radiometric inconsistencies. Comput. Electron. Agric. 164, 104893.

Lepsch, I.F., 2013. Status of Soil Surveys and Demand for Soil Series Descriptions in Brazil. Soil Horizons 54, sh2013-54-2-gc. https://doi.org/https://doi.org/10.2136/sh2013-54-2-gc

Loiseau, T., Chen, S., Mulder, V.L., Román Dobarco, M., Richer-de-Forges, A.C., Lehmann, S., Bourennane, H., Saby, N.P.A., Martin, M.P., Vaudour, E., Gomez, C., Lagacherie, P., Arrouays, D., 2019. Satellite data integration for soil clay content modelling at a national scale. Int. J. Appl. Earth Obs. Geoinf. 82, 101905. https://doi.org/10.1016/j.jag.2019.101905

Lu, P., Wang, L., Niu, Z., Li, L., Zhang, W., 2013. Prediction of soil properties using laboratory VIS–NIR spectroscopy and Hyperion imagery. J. Geochemical Explor. 132, 26–33.https://doi.org/10.1016/j.gexplo.2013.04.003

Madeira, J., Bedidi, A., Pouget, M., Cervelle, B., Flay, N., 1995. Spectral (MIR) determination of kaolinite and gibbsite contents in lateritic soils. Comptes Rendus de l 'Academie Bulg. des Sci. PARIS, Ser. 2 Sci. La Terre Des Planetes Fasc. 321, 119–127.

Mallavan, B., Minasny, B., McBratney A., 2010. Homosoil, a Methodology for Quantitative Extrapolation of Soil Information Across the Globe. In: Boettinger, J.L., Howell, D.W., Moore, A.C., Hartemink, A.E., Kienast-Brown, S. (eds) Digital Soil Mapping. Progress in Soil Science, vol 2. Springer, Dordrecht. https://doi.org/10.1007/978-90-481-8863-5_12

Marques, K.P.P., Demattê, J.A.M., Miller, B.A., Lepsch, I.F., 2018. Geomorphometric segmentation of complex slope elements for detailed digital soil mapping in southeast Brazil. Geoderma Reg. 14, e00175./https://doi.org/10.1016/j.geodrs.2018.e00175

Minasny, B., Hartemink, A.E., 2011. Predicting soil properties in the tropics. Earth-Science Rev. 106, 52–62. https://doi.org/https://doi.org/10.1016/j.earscirev.2011.01.005

Mohamed, E.S., Saleh, A.M., Belal, A.B., Gad, A.A., 2018. Application of near-infrared reflectance for quantitative assessment of soil properties. Egypt. J. Remote Sens. Sp. Sci. 21, 1–14. https://doi.org/10.1016/j.ejrs.2017.02.001

Mulder, V.L., de Bruin, S., Schaepman, M.E., Mayr, T.R., 2011. The use of remote sensing in soil and terrain mapping – a review. Geoderma. https://doi.org/10.1016/j.geoderma.2010.12.018.

Nanni, M.R., Demattê, J.A.M., 2006. Spectral Reflectance Methodology in Comparison to Traditional Soil Analysis. Soil Sci. Soc. Am. J. 70, 393–407. https://doi.org/10.2136/SSSAJ2003.0285

Nawar, S., Mouazen, A. M. 2017. Predictive performance of mobile vis-near infrared spectroscopy for key soil properties at different geographical scales by using spiking and data mining techniques. CATENA 151, 118-129. https://doi.org/10.1016/j.catena.2016.12.014

Niederberger, J., Todt, B., Boča, A., Nitschke, R., Kohler, M., Kühn, P., Bauhus, J., 2015. Use of near-infrared spectroscopy to assess phosphorus fractions of different plant availability in forest soils. Biogeosciences 12, 3415–3428.

Nciizah, A.D., Wakindiki, I.I.C., 2015. Physical indicators of soil erosion, aggregate stability and erodibility. Arch. Agron. Soil Sci. 61, 827–842. https://doi.org/10.1080/03650340.2014.956660

Nocita, M., Stevens, A., Noon, C., van Wesemael, B., 2013. Prediction of soil organic carbon for different levels of soil moisture using Vis-NIR spectroscopy. Geoderma 199, 37–42. https://doi.org/10.1016/j.geoderma.2012.07.020

Nolasco de Carvalho, C.C., Nunes, F.C., Homem Antunes, M.A., Nolasco, M.C., 2015. Soil surveys in Brazil and perspectives in digital soil mapping. Soil Horizons 56. https://doi.org/10.2136/sh14-01-0002

Nouri, M., Gomez, C., Gorretta, N., Roger, J.M.M., 2017. Clay content mapping from airborne hyperspectral Vis-NIR data by transferring a laboratory regression model. Geoderma 298, 54–66. https://doi.org/10.1016/j.geoderma.2017.03.011

Odeh, I.O.A., and McBratney, A.B., (2000). Using AVHRR images for spatial prediction of clay content in the lower Namoi Valley of eastern Australia. Geoderma 97 (3-4), 237-254.

Onyango, C.M., Nyaga, J.M., Wetterlind, J., Söderström, M., Piikki, K., 2021. Precision Agriculture for Resource Use Efficiency in Smallholder Farming Systems in Sub-Saharan Africa: A Systematic Review. Sustain. . https://doi.org/10.3390/su13031158

Padarian, J, Minasny, B., McBratney, A.B., 2019a. Transfer learning to localise a continental soil vis-NIR calibration model. Geoderma 340, 279–288. https://doi.org/10.1016/j.geoderma.2019.01.009

Padarian, J., Minasny, B., McBratney, A.B., 2019b. Using deep learning to predict soil properties from regional spectral data. Geoderma Reg. 16, e00198. https://doi.org/10.1016/j.geodrs.2018.e00198

Padarian, J., Minasny, B., McBratney, A.B., 2020. Machine learning and soil sciences: a review aided by machine learning tools. SOIL 6, 35–52, https://doi.org/10.5194/soil-6-35-2020

Panagos, P., Van Liedekerke, M., Jones, A., Montanarella, L., 2012. European Soil Data Centre: Response to European policy support and public data requirements. Land use policy 29, 329–338. https://doi.org/10.1016/j.landusepol.2011.07.003

Pebesma, E.J., 2009. The meuse data set: a tutorial for the gstat R package. https://cran.r-project.org/web/packages/gstat/vignettes/gstat.pdf (accessed 30 April 2020).

Poppiel, R.R. , Lacerda, M.P.C., Demattê, J.A.M., Oliveira Jr., M.P., Gallo, B.C., Safanelli, J.L. 2019. Pedology and soil class mapping from proximal and remote sensed data, Geoderma 348, 189-206. https://doi.org/10.1016/j.geoderma.2019.04.028

Quinlan, J., 1992. Learning with continuous classes, in: Adams, A., Sterling, L. (Eds.), Proceedings AI'92, 5th Australian Conference on Artificial Intelligence.World Scientific. Singapure, pp. 343–348.

Reichert, J.M., Norton, L.D., Favaretto, N., Huang, C., Blume, E., 2009. Settling Velocity, Aggregate Stability, and Interrill Erodibility of Soils Varying in Clay Mineralogy. Soil Sci. Soc. Am. J. 73, 1369–1377. https://doi.org/10.2136/sssaj2007.0067

Richter, R., Schläpfer, D., 2002. Geo-atmospheric processing of airborne imaging spectrometry data. Part 2: Atmospheric/topographic correction. Int. J. Remote Sens. https://doi.org/10.1080/01431160110115834.

Richter, R., Schläpfer, D., 2015. Atmospheric / Topographic Correction for Airborne Imagery - ATCOR-4 User Guide version 7.0.0, DLR report DLR-IB 565-02/15, Wessling, Germany, pp 252.

Richter, R., Schläpfer, D., 2002. Geo-atmospheric processing of airborne imaging spectrometry data. Part 2: Atmospheric/topographic correction. Int. J. Remote Sens. 23, 2631–2649. https://doi.org/10.1080/01431160110115834

Roberts, D., Wilford, J., Ghattas, O., 2019. Exposed soil and mineral map of the Australian continent revealing the land at its barest. Nat. Commun. 10, 5297. https://doi.org/10.1038/s41467-019-13276-1

Rodriguez-Galiano, V.F., Ghimire, B., Rogan, J., Chica-Olmo, M., Rigol-Sanchez, J.P., 2012. An assessment of the effectiveness of a random forest classifier for land-cover classification. ISPRS J. Photogramm. Remote Sens. 67, 93–104. https://doi.org/https://doi.org/10.1016/j.isprsjprs.2011.11.002

Rogge, D., Bauer, A., Zeidler, J., Mueller, A., Esch, T., Heiden, U., 2018. Building an exposed soil composite processor (SCMaP) for mapping spatial and temporal characteristics of soils with Landsat imagery (1984–2014). Remote Sens. Environ. 205, 1–17. https://doi.org/10.1016/J.RSE.2017.11.004

Rukhovich, D.I., Rukhovich, A.D., Rukhovich, D.D., Simakova, M.S., Kulyanitsa, A.L., Bryzzhev, A. V, Koroleva, P. V, 2016. The informativeness of coefficients a and b of the soil line for the analysis of remote sensing materials. Eurasian Soil Sci. 49, 831–845. https://doi.org/10.1134/S1064229316080123

Safanelli, J.L., Chabrillat, S., Ben-Dor, E., Demattê, J.A.M., 2020. Multispectral Models from Bare Soil Composites for Mapping Topsoil Properties over Europe. Remote Sens. https://doi.org/10.3390/rs12091369

Samuel-Rosa, A., Dalmolin, R.S.D., Moura-Bueno, J.M., Teixeira, W.G., Alba, J.M.F., 2020. Open legacy soil survey data in Brazil: geospatial data quality and how to improve it . Sci. Agric. 77, n1, e20170430. http://dx.doi.org/10.1590/1678-992X-2017-0430

Sanchez, P.A., 2019. Properties and Management of Soils in the Tropics, 2nd ed. Cambridge University Press, Cambridge. https://doi.org/DOI: 10.1017/9781316809785

Sankey, J.B., Brown, D.J., Bernard, M.L., Lawrence, R.L., 2008. Comparing local vs. global visible and near-infrared (VisNIR) diffuse reflectance spectroscopy (DRS) calibrations for the prediction of soil clay, organic C and inorganic C. Geoderma 148, 149–158.https://doi.org/10.1016/j.geoderma.2008.09.019

Santra, P., Kumar, M., Panwar, N.R., Yadav, R.S., 2021. Digital Soil Mapping: The Future Need of Sustainable Soil Management. In: Mitran, T., Meena, R.S., Chakraborty, A., (eds) Geospatial Technologies for Crops and Soils. Springer, Singapore. https://doi.org/10.1007/978-981-15-6864-0_9

Seidel, M., Huten, C., Ludwig, B., Thiele-Bruhn, S., Vohland, M., 2019. Strategies for the efficient estimation of soil organic carbon at the field scale with vis-NIR spectroscopy: Spectral libraries and spiking vs. local calibrations. Geoderma 354, 113856. https://doi.org/10.1016/j.geoderma.2019.07.014

Shepherd, K.D., Walsh, M.G., 2002. Development of Reflectance Spectral Libraries for Characterization of Soil Properties. Soil Sci. Soc. Am. J. 66, 988. https://doi.org/10.2136/sssaj2002.0988

Silatsa, F.B.T., Tabi, F.O., Yemefack, M., Wilczok, C., Heuvelink, G.B.M., Hengl, T., Leenaars, J.G.B., 2018. Digital soil mapping using soilgrids and national soil data in Cameroon. In: Arrouays, D., Savin, I., Leenaars, J., McBratney, A.B., (Eds.). GlobalSoilMap - Digital Soil Mapping from Country to Globe: Proceedings of the Global Soil Map 2017 Conference, July 4-6, 2017, Moscow, Russia (1st ed.). CRC Press. https://doi.org/10.1201/9781351239707

Silva, E.B., Giasson, É., Dotto, A.C., Caten, A. ten, Demattê, J.A.M., Bacic, I.L.Z., Veiga, M. da, 2019. A Regional Legacy Soil Dataset for Prediction of Sand and Clay Content with Vis-Nir-Swir, in Southern Brazil. Rev. Bras. Cienc. Solo 43, e0180174. https://doi.org/10.1590/18069657rbcs20180174

Silva, S.H.G., Weindorf, D.C., Pinto, L.C., Faria, W.M., Acerbi Junior, F.W., Gomide, L.R., de Mello, J.M., de Pádua Junior, A.L., de Souza, I.A., Teixeira, A.F. dos S., Guilherme, L.R.G., Curi, N., 2020a. Soil texture prediction in tropical soils: A portable X-ray fluorescence spectrometry approach. Geoderma 362, 114136. https://doi.org/https://doi.org/10.1016/j.geoderma.2019.114136

Silva, L.S., Marques Júnior, J., Barrón, V., Gomes, R.P., Teixeira, D.D.B., Siqueira, D.S., Vasconcelos, V., 2020b. Spatial variability of iron oxides in soils from Brazilian sandstone and basalt. Catena 185, 104258. https://doi.org/10.1016/j.catena.2019.104258

Silvero, N.E.Q., Demattê, J.A.M., Amorim, M.T.A., Santos, N.V. dos, Rizzo, R., Safanelli, J.L., Poppiel, R.R., Mendes, W.S., Bonfatti, B.R., 2021. Soil variability and quantification based on Sentinel-2 and Landsat-8 bare soil images: A comparison. Remote Sens. Environ., 252, 112117. https://doi.org/10.1016/j.rse.2020.112117

Sørensen, L.K., Dalsgaard, S., 2005. Determination of Clay and Other Soil Properties by Near Infrared Spectroscopy. Soil Sci. Soc. Am. J. 69, 159–167. https://doi.org/10.2136/sssaj2005.0159

Soriano-Disla, J.M., Janik, L.J., Viscarra Rossel, R., MacDonald, L.M., McLaughlin, M.J., 2014. The Performance of Visible, Near-, and Mid-Infrared Reflectance Spectroscopy for Prediction of Soil Physical, Chemical, and Biological Properties. Appl. Spectrosc. Rev. 49, 139–186. https://doi.org/10.1080/05704928.2013.811081

Steinmetz, A.A., Cassalho, F., Caldeira, T.L., Oliveira, V.A. de, Beskow, S., Timm, L.C., 2018. Assessment of soil loss vulnerability in data-scarce watersheds in southern Brazil. Ciência e Agrotecnologia.

Stenberg, B., Viscarra Rossel, R.A., Mouazen, A.M., Wetterlind, J., 2010. Visible and Near Infrared Spectroscopy in Soil Science, in: Sparks, D.L. (Ed.), Advances in Agronomy. Academic Press, San Diego, pp. 163–215. https://doi.org/10.1016/S0065-2113(10)07005-7

Teixeira, P.C., Donagemma, G.K., Fontana, A., Teixeira, W.G., 2017. Manual de métodos de análise de solo. Embrapa, Rio Janeiro, 573p.

Tian, S., Zhang, X., Tian, J., Sun, Q., 2016. Random Forest Classification of Wetland Land covers from Multi-Sensor Data in the Arid Region of Xinjiang, China. Remote Sens. 8, 954. https://doi.org/10.3390/rs8110954

Vapnik, V., 1995. The Nature of Statistical Learning Theory. Springer-Verlag.

Vaudour, E., Gomez, C., Fouad, Y., Lagacherie, P., 2019. Sentinel-2 image capacities to predict common topsoil properties of temperate and Mediterranean agroecosystems. Remote Sens. Environ. 223, 21–33. https://doi.org/10.1016/j.rse.2019.01.006

Vicente, L.E., de Souza Filho, C.R., 2011. Identification of mineral components in tropical soils using reflectance spectroscopy and advanced spaceborne thermal emission and reflection radiometer (ASTER) data. Remote Sens. Environ. 115, 1824–1836. https://doi.org/10.1016/j.rse.2011.02.023

Viscarra Rossel, R.A.V., Behrens, T., 2010a. Using data mining to model and interpret soil diffuse reflectance spectra. Geoderma, Diffuse reflectance spectroscopy in soil science and land resource assessment 158, 46–54. https://doi.org/10.1016/j.geoderma.2009.12.025

Viscarra Rossel, R.A., McBratney, A.B., Minasny, B. (Eds.), 2010b. Proximal Soil Sensing. Springer, Dordrecht, 446p. https://doi.org/10.1007/978-90-481-8859-8

Viscarra Rossel, R.A., Rizzo, R., Demattê, J. and Behrens, T. (2010c), Spatial Modeling of a Soil Fertility Index using Visible–Near-Infrared Spectra and Terrain Attributes. Soil Sci. Soc. Am. J., 74: 1293-1300. https://doi.org/10.2136/sssaj2009.0130

Viscarra Rossel, R.A., Chappell, A., De Caritat, P. and McKenzie, N.J. (2011), On the soil information content of visible–near infrared reflectance spectra. European Journal of Soil Science, 62: 442-453. https://doi.org/10.1111/j.1365-2389.2011.01372.x

Viscarra Rossel, R.A., Behrens, T., Ben-Dor, E., Brown, D.J., Demattê, J.A.M., Shepherd, K.D., Shi, Z., Stenberg, B., Stevens, A., Adamchuk, V., Aïchi, H., Barthès, B.G., Bartholomeus, H.M., Bayer, A.D., Bernoux, M., Böttcher, K., Brodský, L., Du, C.W., Chappell, A., Fouad, Y., Genot, V., Gomez, C., Grunwald, S., Gubler, A., Guerrero, C., Hedley, C.B., Knadel, M., Morrás, H.J.M., Nocita, M., Ramirez-Lopez, L., Roudier, P., Campos, E.M.R., Sanborn, P., Sellitto, V.M., Sudduth, K.A., Rawlins, B.G., Walter, C., Winowiecki, L.A., Hong, S.Y., Ji, W., 2016. A global spectral library to characterize the world's soil. Earth-Science Rev. 155, 198–230. https://doi.org/10.1016/j.earscirev.2016.01.012

Vidal-Torrado, P., 1994. Pedogênese e Morfogênese no distrito de Tupi (Piracicaba, SP). Tese, Escola Superior de Agricultura "Luiz de Queiroz", Universidade de São Paulo, Brasil.

Weil, R.R., Brady, N.C., 2017. The nature and properties of soils, 15th ed. Pearson Press, Upper Saddle River, 1104p.

Wetterlind, J., Stenberg, B., 2010. Near-infrared spectroscopy for within-field soil characterization: small local calibrations compared with national libraries spiked with local samples. Eur. J. Soil Sci. 61, 823–843. https://doi.org/10.1111/j.1365-2389.2010.01283.x

Wulder, M.A., Hilker, T., White, J.C., Coops, N.C., Masek, J.G., Pflugmacher, D., Crevier, Y., 2015. Virtual constellations for global terrestrial monitoring. Remote Sens. Environ. 170, 62–76. https://doi.org/10.1016/j.rse.2015.09.001

Yoshioka, H., Miura, T., Demattê, J.A.M., Batchily, K., Huete, A.R., 2010. Soil Line Influences on Two-Band Vegetation Indices and Vegetation Isolines: A Numerical Study. Remote Sens. 2, 545–561. https://doi.org/10.3390/rs2020545

Zhang, D., Zhou, G., 2016. Estimation of Soil Moisture from Optical and Thermal Remote Sensing: A Review. Sensors (Basel). 16, 1308. https://doi.org/10.3390/s16081308

Zhang, Y., Biswas, A., Ji, W., Adamchuk, V.I., 2017. Depth-Specific Prediction of Soil Properties In Situ using vis-NIR Spectroscopy. Soil Sci. Soc. Am. J. 81, 993–1004. https://doi.org/10.2136/sssaj2016.08.0253

Zhao, D., Zhao, X., Khongnawang, T., Arshad, M., Triantafilis, J., 2018. A Vis-NIR Spectral Library to Predict Clay in Australian Cotton Growing Soil. Soil Sci. Soc. Am. J. 82, 1347–1357. https://doi.org/10.2136/sssaj2018.03.0100

van Zijl, G., 2019. Digital soil mapping approaches to address real world problems in southern Africa. Geoderma 337, 1301–1308. https://doi.org/https://doi.org/10.1016/j.geoderma.2018.07.052

3. KRIGING AND COVARIATE-BASED METHOD FOR MAPPING SOIL ERODIBILITY: ALTERNATIVES FOR DATA-SCARCITY AREAS.

Abstract

The Universal Soil Loss Equation and its derivations (USLE-based) are the most applied soil erosion models globally. One of the factors used in these equations is the soil erodibility (K), which indicates the soil's inherent susceptibility to erosion. Although important for modeling soil erosion, there is a lack of adequate K factor maps, especially for research covering watershed or farm extensions. To address this challenge, the objective of this work was to use remote and proximal sensed data for soil erodibility mapping. Our hypothesis was that digital soil erodibility maps estimated from remote sensing or vis-NIR-SWIR spectroscopy (350 -2500nm) have strong spatial agreement with detailed soil maps and are an alternative for areas where data is scarce. In a tropical area with 2,574 km², we developed prediction models (cubist algorithm) by a covariate-based method approach (CBMA) using a multi-temporal bare soil image called Synthetic Soil Image (SYSI) and topographic parameters as predictors, and a ordinary kriging approach (OKA) using 215 spectral bands in the 350-2500nm range as predictors. The dataset comprised 3210 soil observations for CBMA (0-20 cm depth) and 3644 for OKA (0-20, 40-60, 80-100 cm depth). The Erosion Productivity Impact Calculator (EPIC) methodology, which uses the contents of clay, sand and SOC, was used to calculate the erodibility (K factor). We nominate as Kpred the values obtained with the model developed using Kfactor as the dependent variable and environmental covariates or 350-2500nm bands, as independent variables. We also performed models of soil sand, clay, and SOC contents, and inputs the results in EPIC K equation to obtain another erodibility values nominated as "Kcalc". Two areas were used to conduct a case study where we assessed the performance of erodibility digital maps. For OKA, kriging was used to spatialize the Kfactor, Kpred and Kcalc values obtained. A watershed and a farm scale area were used as case studies. Kpred, clay, sand and SOC model validation performances were R^2 = 0.47, 0.80, 0.67, 0.47 respectively for CBMA and 0.58, 0.83, 0.69, 0.44 for OKA. The results obtained from the two approaches, better represent the spatial variation of erodibility than information obtained from low-scale soil maps (1: 100,000).

Keywords: USLE/RUSLE, K factor, Erosion, Remote Sensing, Proximal sensing

3.1. Introduction

The Universal Soil Loss Equation and its derivations (USLE-based) are the most applied soil erosion models globally ((Borrelli et al., 2021). The application of these models has been increasing since 1980 all of the world. The United States of America, China, Brazil, Italy, India, Spain, Australia, and Turkey are reported as the main countries that used these models (Alewell et al., 2019; Kumar et al., 2022). USLE-based models are normally simple, easy to use, and require a few input data, which makes their use more accessible in regions where data is scarce ((Borrelli et al., 2021). They also require relatively low computational processing power when compared to other models (Bahrami et al., 2017; Efthimiou, 2018; Gelagay and Minale, 2016; Kumar et al., 2022).

Erosional models consider several factors: the rainfall-runoff erosivity (R), the soil erodibility (K), the slope length (L), the slope steepness (S), the land cover and management (C), and the soil conservation practices (P) (Wischmeier & Smith, 1965, 1978; Renard et al., 1991). The K factor indicates the soil's inherent susceptibility to erosion, which is obtained by calculating the rate of soil loss per rainfall erosivity index measured in unit-plot conditions (Weil and Brady, 2017). It must be obtained from data collected for at least two years (ideal five years) from erosion plots (Wischmeier and Smith, 1965, 1978). However, due to the high cost and time required by traditional methods, other methodologies were also developed over time, as the pedotransfer functions (PTFs) that consider different soil attributes as inputs (Sharpley and Williams, 1990; Römkens et al. 1997; Ostovari et al., 2016; Vaezi et al., 2016; Zhang et al., 2019).

Usually, erodibility data for USLE-based models is obtained from legacy soil maps, in which a K value is attributed to each soil class (Briak et al., 2016; Kumar et al., 2022; Marques et al., 2019). Geostatistical methods are

also used to obtain maps of K-factor (Avalos et al., 2018; Vaezi et al., 2016; Zhu et al., 2021). Majhi et al. (2021) analyzed the results of 100 studies that used USLE-based models in India and found that i) 74% of them used soil maps to derive K factor maps, ii) 25% estimated the soil erodibility from soil samples, and iii) just one measured K values from plot-scale experiments. However, obtaining erodibility maps from soil maps can be compromised in regions with data scarcity, either by the lack of soil maps at adequate scale or by insufficient number of soil samples needed for geostatistical approaches. This situation is common in developing countries (Bellinaso et al., 2021; Minasny and Hartemink, 2011), especially in small farms or watersheds, where this problem is more pronounced (Benavidez et al., 2018; Gonçalves et al., 2021; Lepsch, 2013; Steinmetz et al., 2018). Often the consequence of this is the use of maps with inadequate scales (Majhi et al. 2021), but the use of input data with high uncertainty contributes to the higher prediction uncertainty in USLE-based models (Kumar et al., 2022; Schürz et al., 2020). Avalos et al. (2018) concluded that uncertainty in model outputs could be decreased as an effect of the reduction of estimation variance in the soil erodibility parameter.

Digital soil mapping (DSM), remote and proximal soil sensing, spatial statistics, geographic information systems, and PTFs provide tools to easily and accurately obtain information regarding soil erodibility (Minasny and Hartemink, 2011; Nolasco de Carvalho et al., 2015). Numerous works have demonstrated the potential of using visible, near infrared, and short wave infrared (Vis-NIR-SWIR) data to predict soil attributes related to soil erodibility, such as clay, sand, and soil organic carbon (SOC) contents (Angelopoulou et al., 2020; Nocita et al., 2015; Stenberg et al., 2010), as well as remote sensing techniques (Chagas et al., 2016; Nanni and Demattê, 2006), which recently have been enhanced through the use of multi-temporal images (Bellinaso et al., 2021; Castaldi, 2021; Gasmi et al., 2021; Loiseau et al., 2019). Similarly, recent literature reviews on USLE-based models highlights the importance of remote sensing techniques integrated with GIS to improve the performance of these models (Alewell et al., 2019; Kumar et al., 2022; Mello et al., 2016). However, Phinzi and Ngetar (2019), in an extensive literature review, found that among all RUSLE factors, the K factor has the lowest number of studies that use remote sensing for its estimation. According to the authors, only 2% of the reviewed papers proposed to determine the K factor through information obtained by remote sensing.

Despite this, recent research has shown promising results from the use of these techniques to obtain soil erodibility information. Ostovari et al. (2018) and Salehi-Varnousfaderani et al. (2022), evaluating soils from Iran, obtained good performances in predicting erodibility values using Vis-NIR-SWIR data as independent variables. The same approach, with soils of a watershed in a subtropical monsoon region in China, was used by Jiang et al. (2020). Teng et al. (2016), developed a digital soil erodibility map of Australia from terrain, climate and soil variables, obtained by remote and proximal sensing. Godoi et al. (2021) and Tian et al. (2022) obtained digital erodibility maps, with 250 m resolution based on SoilGrids for an entire country, similar approaches were carried out by Panagos et al. (2014) and Efthimiou (2020) using Land Use/Cover Area frame Survey (LUCAS) data to obtain digital maps with 500 m resolution for Europe and Greece. However, there is still a need for studies evaluating the potential of these techniques to generate information to be used on smaller scales, especially using multi-temporal images, as well as the comparison of these results with traditional mapping methods.

The objective of this work was to use remote and proximal sensing variables for spatial erodibility predictions by a covariate-based method approach (CBMA) (multi-temporal bare soil images and terrain variables) and ordinary kriging approach (OKA) (predicting erodibility values of soil samples from 350-2500nm variables). The hypotheses are: digital soil erodibility maps estimated using variables obtained from remote sensing or spectroscopy data have greater spatial agreement with reference K map (obtained from detailed soil maps) than K map obtained

from low-scale soil legacy maps; digital soil erodibility maps obtained are a alternative for scarce-data areas, especially for farm and watershed scale. To evaluate the results obtained, two case studies were carried out in different areas, aiming to evaluate the potential of the approaches carried out to represent the spatial variability of erodibility. For this, traditional methodologies for obtaining erodibility maps were used as a reference.

3.2. Material and methods

3.2.1. Study area

The study area has 2,574 km² and is located in the municipalities of Piracicaba, Charqueada, Iracemápolis, Saltinho, Rio das Pedras, Mombuca, Rafard, and Capivari, in São Paulo State, Brazil (Fig. 1). The region's climate, according to the Köppen system, is classified as Cwa, a Humid Subtropical with dry winter and hot rainy summer (Alvares et al., 2013). The mean annual precipitation is 1274 mm and the annual average temperature between 20.1 and 22.5 °C. The relief consists of undulating hills and rolling uplands and the altitude varies between 450 to 900 m. The vegetation is characterized as a transitional zone between savanna and tropical forest (Barreto et al., 2006). It is geomorphologically located mainly within the Paulista Peripheral Depression, with only the northern part located in a transition zone with the Paulista Western Plateau. The region has a great diversity of parent materials (Mendes et al., 2021), predominant soils being Lixisols/Acrisols (~58%), Ferralsols (~19%), Leptosols (~13%) and Arenosols (~6%) (Oliveira et al., 1989).

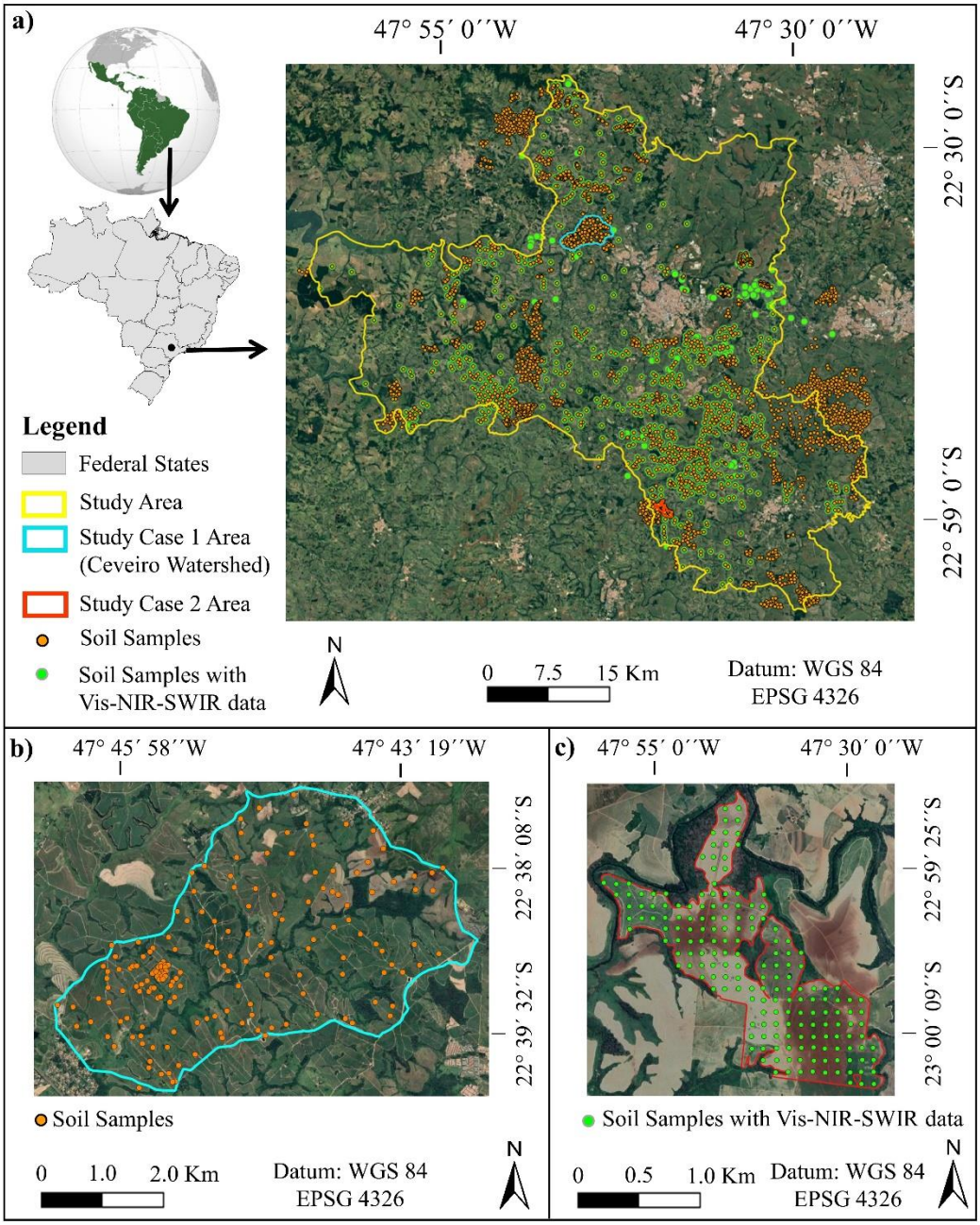

Figure 1. Study area and soil datasets used in modeling (a), Ceveiro watershed area used as case study 1 (b) and farm extend area used as case study 2.

3.2.2. Case Studies Area

Two sites within the study area were chosen as case studies (Fig. 1b,c). The Ceveiro watershed for the CBMA and a farm scale area at Rafard municipality for the OKA. The main reason for choosing these areas was that both have detailed soil maps available at 1:10,000 scale and also a legacy soil map at 1:100,000 scale. The Ceveiro watershed had soil routine analyses information, but not 350 - 2500nm laboratory spectral data, whereas the farm extent area had routine laboratory information and 350 - 2500nm laboratory spectral data spatially distributed over a 100 x 100 m regular grid. The Ceveiro watershed comprised 1990 ha in the municipality of Piracicaba (Fig. 1b), with central coordinates of 22°38’53"S and 47°44’48"W. The local relief is gently undulating, with altitude ranging from 460 to 580 m. The geology consists of sandstones from the Pirambóia Formation, basic intrusive rocks from the

Serra Geral Formation, siltstones, claystones, and shales from the Corumbataí Formation (IPT, 1981). The predominant soils are Lixisols/Acrisols, Leptosols and Cambisols originated from different parent materials, Nitisols and Gleysols (Oliveira et al. 1989). Further details on the characterization of the Ceveiro Watershed can be obtained from Sparovek and Schnug (2001) and Weill and Sparovek (2008). The farm scale area (Fig 1c) has 182 ha and is located in Rafard city, with central coordinates of 22°59'58"S and 47°38'42"W. The local relief is gently undulating, with altitude ranging from 460 to 580 m. The soil classes of the area are Acrisols/Lixisols, Chernozems, Nitisols, Leptosols, and Cambisols, developed from a diversified parent material as diabase, siltite, metamorphosed siltite and alluvial deposits. Further details on the characterization of the area can be obtained from Nanni and Demattê (2006) and Bazaglia Filho et al. (2013).

3.2.3. Soil data

The soil information was obtained from the database of the Geotechnologies in Soil Science Group (GeoCiS) of the University of São Paulo, Brazil, which comprises a series of soil surveys conducted in the region of Piracicaba (Demattê et al., 2019). This dataset contains more than 9000 locations with soil data of physical and chemical attributes at 0–20, 40–60 and 80–100 cm depth (Fig. 2a).

This soil dataset was separated to be used in the CBMA and OKA approaches. First, we selected 3210 samples (Fig. 1a) containing laboratory analysis of clay, sand, silt, and soil organic carbon (SOC) (Fig. 2e). These analyses were used to calculate the erodibility (we nominate as Kfactor value) for each location according to the equation proposed by Sharply & Williams (1990) (see item 2.4) (Fig. 2c). These samples were also used to perform the CBMA, by combining the soil data with multiple environmental variables and calibrating a prediction model for the study area (Fig. 2e,f).

The OKA used different samples from the general GeoCiS database, since it required Vis-NIR-SWIR (350–2500 nm) spectral analysis (Fig. 2d). We used 3644 soil samples that contained this information (Fig. 1a) and used it to calibrate a second prediction models of the Kfactor, clay, sand and SOC for the study area (Fig. 2m).

The two case study areas used for external validation also had soil datasets, which were used to interact with the models from CBMA and OKA and perform statistical analysis. The Ceveiro watershed (Fig. 1b) had 174 soil samples collected at 0-20 cm depth with physicochemical laboratory analysis of clay, sand, silt, and SOC. This soil dataset was provided from the work of Weill and Sparovek (2008). The farm scale site located in the Rafard municipality (Fig. 1c) contained a soil dataset with 124 soil samples at 0-20 cm depth displaced in a 100 x 100 m grid across the area. The samples also contained the physicochemical analysis from laboratory (Silvero et al., 2021a).

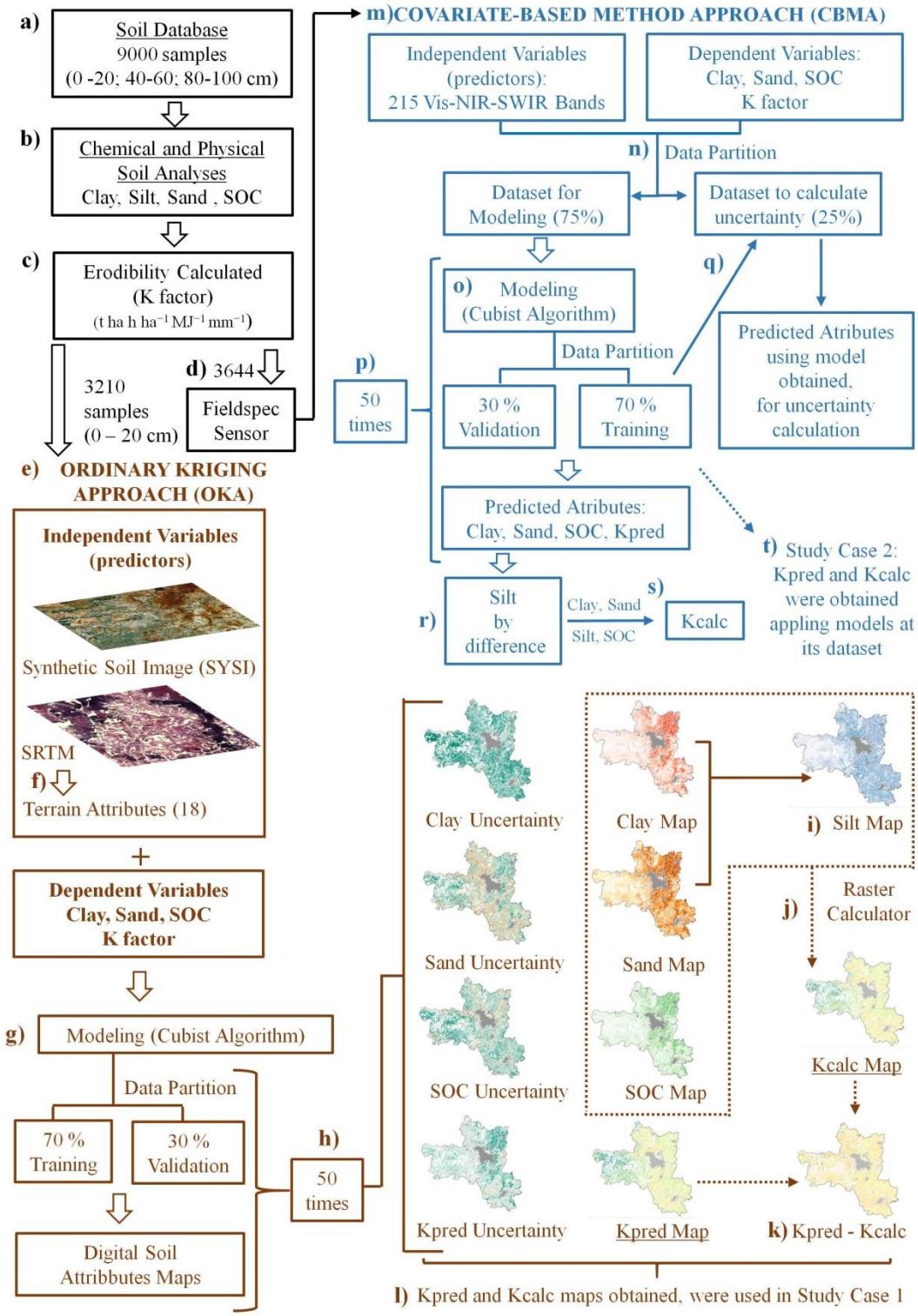

Figure 2. Flowchart containing all the steps developed in the methodology.

3.2.4. Laboratory analysis and spectral data acquisition 350-2500nm (Vis-NIR-SWIR)

The soil samples were air dried, ground, and sieved in a 2 mm mesh for physical and chemical determinations in the laboratory according to the methods proposed by (Teixeira et al., 2017). The clay and sand contents were determined by the analysis, while the silt fraction was obtained by difference between clay and sand.

The soil organic carbon (SOC) was determined by the Walkley-Black oxidation method (Walkley and Black, 1934) (Fig. 2b).

For the 3644 soil samples of OKA (Fig. 1a) and farm scale case study area (Fig. 1c), the Vis-NIR-SWIR spectral data (350–2500 nm) was collected from the GeoCiS database (Fig. 2d). The spectroscopic analysis was conducted with the FieldSpec 3 spectroradiometer (Analytical Spectral Devices, ASD, Boulder, CO), with spectral resolution of 3 nm, from 350 to 700 nm and 10 nm from 700 to 2500 nm. The output data was automatically interpolated to 1 nm, resulting in 2151 bands with 1 nm resolution (Demattê et al., 2019). The samples were placed in petri dishes and were homogeneously distributed over a flat surface for spectral reading. Two halogen lamps (50 W) were used as light sources. The distance between the lamps formed a 90° angle and was located at 0.35 m from the sample with a zenith angle of 30°. These geometric configurations generated a not-collimated light beam towards the target. An optic fiber placed in the vertical position at 0.08 m from the sample surface captured the reflected light from an area of approximately 2 cm2 at the center of the sample (Poppiel et al. 2019a). Three replicates from distinct rotations positions for each sample were taken to reduce shadow effects. To maximize the signal-to-noise ratio, 100 readings were performed and the average calculated for each sample. The instrument was calibrated at the beginning and after 20 min, using a white Spectralon® plate with reflectance superior to 99% (Labsphere, North Sutton, NH, USA). Using the binning function from the prospectr package in R software, all data were resampled by 10 nm width, totalizing 215 bands.

3.2.5. Erodibility Estimation

We used the soil databases to calculate the erodibility (Kfactor) through the EPIC - Erosion Productivity Impact Calculator (EPIC) equation (Sharply & Williams 1990):

$$Kfactor = (0.2 + 0.3exp(-0.0256SAN(1 - SIL/100))) \times (SIL/SIL + CLA)^{0.3} \times (1 - (0.25SOC/(SOC + exp(3.72 - 2.95SOC)))) \times (1 - (0.7SN/(SN + exp(-5.51 + 22.9SN)))) \times 0.1317$$

where Kfactor is the soil erodibility (t ha h ha^{-1} MJ^{-1} mm^{-1}); SAN is the sand content (%); SIL is the silt content (%); CLA is the clay content (%); SOC is the soil organic carbon content (%); SN = 1 – SAN/100 and 0.1317 is the SI metric unit conversion factor (Fig. 2c).

The calculated values, obtained in this step, were established as reference values and named in the text as "Kfactor" values. These values were later used as a dependent variable in the prediction models, together with the clay, sand and SOC values obtained by routine laboratory analyses.

3.2.6. Environmental information

3.2.6.1. Soil Synthetic Image (SYSI)

We acquired a time-series of surface reflectance images from satellites Landsat 4 to 8 between 1985 to 2019 and applied the Geospatial Soil Sensing System (GEOS3) algorithm (Demattê et al., 2018; Poppiel et al., 2019) to obtain a bare soil image called Synthetic Soil Image (SYSI) using the Google Earth Engine platform (GEE) (Gorelick et al., 2017). SYSI is a single image obtained by computing the median values from the bare soil images. Several works have demonstrated the potential the image in the prediction of soil attributes (Mendes et al., 2021; Raúl R Poppiel et al., 2019a; Safanelli et al., 2020). To classify the pixels of the time series images as bare soil, a set of

rules based on spectral indices were applied. These rules were coupled with quality assessment bands to remove clouds, shadows, inland water, photosynthetic vegetation, and non-photosynthetic vegetation (crop residues) (Safanelli et al., 2020). For the Normalized Difference Vegetation Index (NDVI), a threshold between −0.15 and 0.25 was used to mask out green vegetation, Normalized Burning Ratio (NBR2), with a − 0.15 and 0.15 to mask out crop residues (Demattê et al., 2020, 2018). Afterwards, the bare soil pixels were used to calculate, pixel-by-pixel, the median values of topsoil reflectance for single bands and obtain the final reflectance value (Demattê et al., 2020, 2018). SYSI had 30 m spatial resolution and six spectral bands harmonized as blue (0.45 - 0.52 μm), green (0.52 - 0.60 μm), red (0.63 - 0.69 μm), near-infrared (0.76 - 0.90 μm), short-wave infrared 1 (1.55 - 1.75 μm), short-wave infrared 2 (2.08 - 2.35 μm) and thermal infrared (10.4 - 12.5 μm). The thermal band was resampled for 30 m resolution.

3.2.6.2. Terrain Attributes

The s.c.o.r.p.a.n model presented by McBratney et al. (2003) defined soil as the product of multiple formin factors such as soil (s), climate (c), vegetation (o), relief (r), parent material (p), age of surface (a) and spatial position (n). Thus, we used topographic information as covariates in the prediction models based on spatial association, the covariate-based method approacha. We acquired the 30 m Shuttle Radar Topography Mission digital elevation model (DEM) and we used it as input to calculate 18 terrain attributes with the Terrain Analysis Library in SAGA GIS 2.3.2 software (Conrad et al., 2015) (Table 1) (Fig. 2f).

Table 1: Environmental variables used as soil predictors for CBMA. The relief/drainage class were calculated using a DEM obtained from SRTM with 30 m resolution. SYSI was obtained from Landsat Images collection from 1985 to 2019.

Class	Attribute	Description	Unit	Reference
Relief/	LS	LS Factor - slope length	non-dimensional	Conrad et al. (2015)
Drainage	TRI	Terrain Ruggedness Index - measures terrain heterogeneity related to elevation	non-dimensional	Riley et al. (1999)
	SLOPE	Slope - a space curve defined for the set of nonspecial points on the surface	Degree	Florinsky (2012)
	TWI	Topographic Wetness Index - indicator of soil moisture distribution at different landscape positions	non-dimensional	Pei et al. (2010)
	CNBL	Channel Network Base Level	m	Bock and Köthe, (2008)
	VDCN	Vertical Distance to Channel Network	m	Rennó et al. (2008)
	Elevation	Elevation grid representing altitude	m	(Zhang and Montgomery, 1994)
	AH	Analytical Hillshading	Radians	Tayebi et al. (2021)
	Aspect	Aspect	Degree	Mendes et al (2022)
	VD	Valley Depth	m	Mendes et al (2022)
	CS	Catchment Slope	Degree	Tayebi et al. (2021)
	GC	General Curvature	Degree	SAGA 2.3.2
	LC	Longitudinal Curvature	Degree	SAGA 2.3.2
	MSP	Mid-slope Position	non-dimensional	SAGA 2.3.2
	NH	Normalized Height	non-dimensional	Tayebi et al. (2021)
	RSP	Relative Slope Position	non-dimensional	SAGA 2.3.2
	SH	Slope Height	non-dimensional	Tayebi et al. (2021)
	SHe	Standardized Height	non-dimensional	Tayebi et al. (2021)
SYSI	Band 1	Blue	Reflectance factor	Demattê et al., (2018)
	Band 2	Green	Reflectance factor	Demattê et al., (2018)
	Band 3	Red	Reflectance factor	Demattê et al., (2018)
	Band 4	Near Infrared	Reflectance factor	Demattê et al., (2018)
	Band 5	Short Wave Infrared - 1	Reflectance factor	Demattê et al., (2018)
	Band 6	Short Wave Infrared - 2	Reflectance factor	Demattê et al., (2018)
	Band 7	Thermal Infrared	LST	Poppiel et al. (2019)

3.2.7. Soil erodibility (K) prediction

3.2.7.1. Cubist algorithm

We used the cubist algorithm to make spatial predictions of soil attributes (clay, sand, and SOC) and the K factor in the study area. The cubist is a common machine learning algorithm often used for DSM works, having good results for the prediction of soil texture (Chagas et al., 2016; Lagacherie et al., 2019; Mello et al., 2022) and SOC (John et al., 2020; Li et al., 2021; Moura-Bueno et al., 2021).

Cubist is a tree-rule-based algorithm in which linear regression models are obtained at each branch of the tree to allow the prediction of the values. It uses a boosting-like procedure named committees and the most common k neighbors to avoid overfitting (Kuhn et al., 2013; Quinlan, 1992). The default the number of committees (1, 10 and 20) and neighbors (0, 5 and 9) were used to build the prediction models using the function train of caret package, totalizing nine models, the model with the minor root mean square error (RMSE) was chosen and applied to the validation dataset.

The coefficient of determination (R^2) and the root mean square error (RMSE) were used to evaluate the performance of the training and validation set's prediction.

3.2.7.2. Covariate-based method approach (CBMA)

The CBMA follows the established DSM framework to predict topsoil properties (Clay, Sand, SOC, and K) for the study area. We created a 60 m buffer for the 3210 soil points locations in the study area and use the circular areas to calculate the mean value of all the environmental variables (Table 1) through zonal statistics, producing a dataset with soil and environmental information. The resulting dataset was randomly partitioned into training (70%) and validation/test (30%) using the createDataPartition function from the caret package in R software (Kuhn, 2008). The training dataset was used to calibrate the prediction model (Fig. 2g). K factor was used as dependent variable and environmental covariates as independent variables (Table 1), to fit a cubist prediction model. The result was a 30 x 30 m soil erodibility predicted map for the study area. The erodibility map obtained was nominated as "Kpred" map (Fig 2).

The random sampling and subsequent modeling were repeated 50 times for each setting to get a distribution of the performance of prediction (Fig. 2h). The 50 realizations mean represents overall model performance (Heil et al., 2022; Tang et al., 2020). The uncertainty map was constructed by 50 realizations of the previously described routine. They represent the 90% prediction interval (90% PI) obtained in the 50 realizations (Fig. 2h). The lower and upper limits (5th and 95th percentiles) were obtained and the 90% PI was calculated as the difference between 95th and 5th percentiles (90% PI = 95th − 5th). The mean value considered as the final attribute map.

We also performed digital maps of soil sand, clay, and SOC contents, using the same machine learning algorithm. The digital map of silt was obtained by the difference between the digital maps of clay and sand (Fig. 2i). These maps were used as inputs to calculate a different digital soil erodibility map for the study area. We applied the EPIC equation in the predicted maps (clay, sand, silt and SOC) using the raster calculator function in QGIS 3.16 software, resulting in another K map, nominated as "Kcalc" map (Fig. 2j).

In order to compare the two digital soil erodibility maps obtained (Kpred and Kcal), a difference map was obtained (Kpred - Kcalc) (Fig. 2k).

3.2.7.3. Ordinary kriging approach (OKA)

3.2.7.3.1 Obtaining point values

Cubist prediction models were fit using the Kfactor of each sample as dependent variables and the 215 bands of the Vis-NIR-SWIR as predictors. For this, 2733 samples of the dataset (Fig. 2o) were randomly partitioned into training (70%) and validation/test (30%), using the createDataPartition function from the caret package in R software. The remaining samples (911, denominated "uncertainty dataset") were later used to calculate the uncertainty of the models (Fig 2n,q). The random sampling and subsequent modeling were repeated 50 times for each setting to get a distribution of the performance of prediction. The 50 realizations mean represents overall model performance (Heil et al., 2022; Tang et al., 2020) (Fig. 2p). Results of the erodibility model obtained was nominated as "Kpred". We also performed models of soil sand, clay, and SOC contents, using the same machine learning algorithm.

The uncertainty of each model was constructed by 50 realizations of the previously described routine (Fig. 2q). For each realization the model obtained was applied in the "uncertainty dataset", resulting in 50 predicted values for each sample. Then, the lower and upper limits (5th and 95th percentiles) were obtained and the 90% PI was calculated. In addition, the models built in each of the realizations.

The models were also applied to the 124 samples of the farm extent area in order to be kriging for the OKA case study. The mean value was considered the predicted value of each farm scale area sample. The silt values were obtained by the difference using clay and sand predicted (Fig. 2r). These information (clay, sand, silt and SOC) was used as inputs in EPIC K equation, to calculate a different erodibility value for the study area, nominated as "Kcalc" (Fig. 2s).

3.2.7.3.2 Digital soil erodibility maps by interpolation for case studies

In other to compare erodibility maps in the farm extent study case area, obtained from different methodologies, the Kfactor, Kpred and Kcalc values were interpolated throughout the area by ordinary kriging (Knadel et al., 2015; Rossel and Chen, 2011; Viscarra Rossel et al., 2010), with a regular grid of 30 m. For this we first calculated the semivariance following the equation:

$$\gamma(h) = \frac{1}{2n(h)} \sum_{i=1}^{N(h)} [z(x_i) - z(x_i + h)]^2$$

where, γ(h) is the semivariance; n(h) is the number of pairs of points separated by the distance h; z(xi) is the value of z in the position, and z (xi + h) is the value of z in the position xi + h.

Exponential, gaussian and spherical theoretical models were tested to fit the experimental variograms, and the model with minor RMSE in the kriging cross-validation was selected. Then, the kriging estimate was performed following the equation:

$$\hat{z}(x_0) = \sum_{i=1}^{N} \lambda_i \, z(x_i)$$

where $\hat{z}$(x0) is the kriging estimator at the x0 point; z(xi) represents the measured erodibility value at the xi point; and λi is the kriging weight attributed to closest z(xi) values to estimate $\hat{z}$(x0). The estimated values then represented the average values of erodibility at each pixel. For this step the gstat package (Pebesma, 2009) in R software was used.

Of the three therethical models tested, the Exponential model presented the lowest RMSE for spatial estimates of soil erodibility. For the Kfactor, the parameters of the final fitted model were 0.000038 for sill, 80 m for

range and 0.000005 for nugget. For the Kpred, 0.000005 for sill, 154 m for range and 0.000006 for nugget. For The Kcalc, 0.000007 for sill, 186 m for range and 0.000007. For a better presentation of the results, the erodibility maps were multiplied by 1000.

3.2.7.3.3 Digital soil erodibility map by interpolation for Ceveiro watershed

In order to have one more erodibility map for comparison, a digital map using Kfactor values (obtained by soil laboratory routine analyses of the 174 soil samples from Ceveiro dataset) and kriging was also created for the Ceveiro watershed. The same methodology described above (item 2.6.3.2) was used. The parameters of the final fitted model were 0.000047 for sill, 400 m for range and 0.000006 for nugget. The resulting erodibility map was multiplied per 1000 an was nominated as "Kkriging" map. Although the main objective of the Ceveiro watershed case study area is the assessment of CBMA, this map was also created with the objective of being another traditional way of obtaining erodibility maps.

3.2.8. Study cases

The Ceveiro watershed was chosen as the case study area for the covariate-based method approach (Fig. 2l). In the same area, several works related to soil conservation and erosion prediction models were carried out (Sparovek et al., 1997; Sparovek and Schnug, 2001; Weill and Sparovek, 2008). Local conservation planning usually adopts the watershed as the unit of work. Kumar et al. (2022) emphasizes that the USLE-based models were created at their origin in order to assist soil conservation actions at the local level and that the models present better estimation results at this scale of work. To evaluate the agreement of modeled erodibility maps (Kpred and Kcalc), two soil maps were used as a traditional approach for obtaining reference erodibility maps. The first was a soil legacy map produced by Oliveira et al. (1989), with 1:100,000 scale. The second is a detailed soil map obtained from Silva (2001), with 1:10,000 scale. For these traditional approaches, each mapping unit received a unique erodibility value (average value of soil samples within the respective units), a methodology usually used in USLE-based models works. The rasterize tool of Qgis 3.16 was used to create a raster with spatial resolution of 30 m. Difference maps were obtained to evaluate areas with under and over estimation. The kriging map (item 2.6.3.2) was also used as a traditional approach, and it was developed by ordinary kriging o Kfactor values from samples within the Ceveiro watershed.

For the farm extent area (Fig. 2t), the same approach was adopted. The soil legacy map from Oliveira et al. (1989) and the detailed soil map obtained from Bazaglia et al. (2013), with a scale of 1:10,000 as reference. And the Kfactor ordinary kriging map as another traditional approach. Difference maps were obtained to evaluate areas with under and over estimation.

3.3. Results

3.3.1. Descriptive statistics of soil properties

The distribution and descriptive statistics of the soil datasets used are shown in Fig. 3. For the covariate-based method approach, the clay content showed a skewed distribution, with a mean value of 23% and several regions with less than 35%. The mean value of sand content was 57%, with a distribution tending to be bimodal. The SOC content showed a skewed distribution, with a mean value of 0.88 %. The Kfactor presented an average

value of 24.9 (10^{-3} t ha h ha^{-1} MJ^{-1} mm^{-1}), and a wide range with values ranging from 4 to 60.4. The distribution of properties was similar between the training and validation (Test) datasets.

The kriging approach showed a distribution similar to the dataset of the covariate-based method approach. Few differences were observed, a slightly higher mean clay value (32%) and a slightly lower sand (55%). The distribution of sand contents showed a characteristic bimodal distribution.

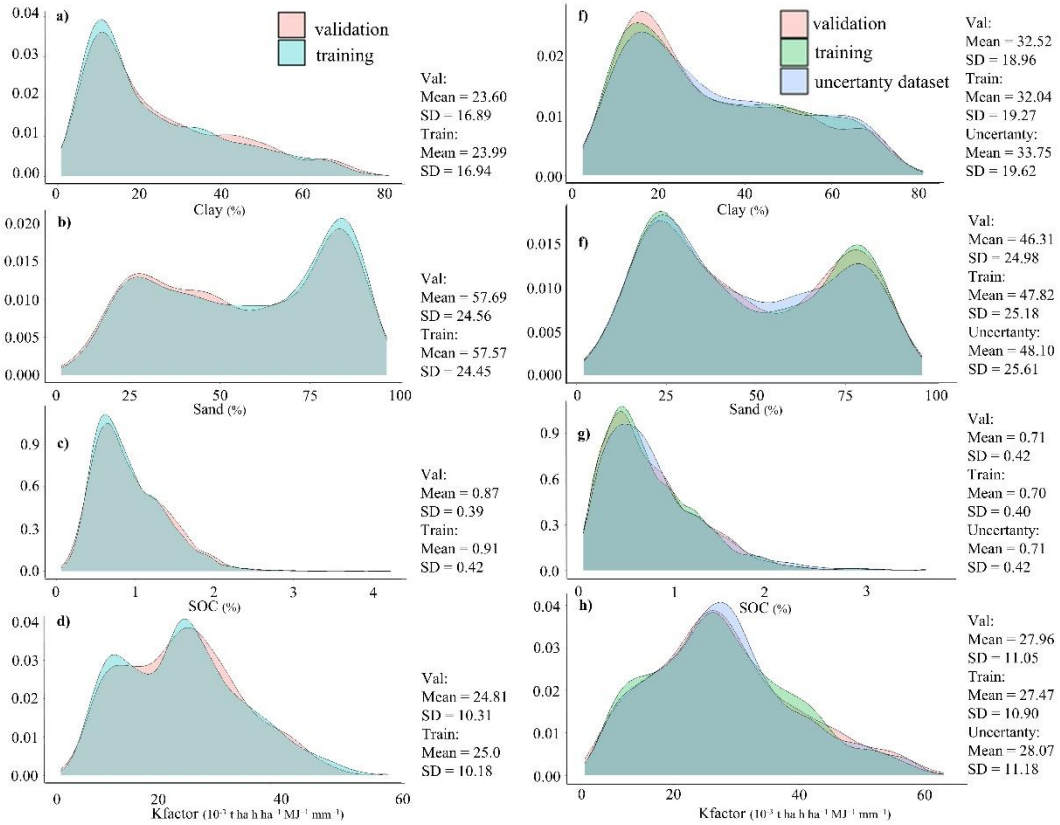

Figure 3. Density plots of soil attributes of covariate-based method (a, b, c, d) and kriging approach (e, f, g, h) datasets.

3.3.2. Prediction performances

3.3.2.1 Mapping soil K by covariate-based method approach

The performance of prediction models and spatial maps of clay, sand and SOC contents and Kpred using the CBMA are presented in Fig. 4 (a,b,c,d). The values of R^2 and RMSE correspond to the average of 50 realizations. Clay´s prediction model had the best performance (R^2val of 0.80 and RMSEval of 7.57%), followed by sand (R^2val of 0.67 and RMSEval of 14.18 %). SOC and K factor models showed the worst results, with R^2val of 0.47 and RMSEval of 0.3 % and 7.43 10^{-3} t ha h ha^{-1} MJ−1 mm^{-1} respectively. For all attributes, the training and validation R^2 and RMSE were very similar

The uncertainty maps for each soil attribute, represented by the 90% prediction interval of 50 realizations (90% PI), are also presented in Fig. 4 (e,f,g,h). For the Kpred, the northwest part of the study area showed the lowest predicted values and also the lowest uncertainty. More to the center, from north to south, areas with higher Kpred values and high uncertainty can be found. In contrast, in the northeast region, intermediate values of Kpred and low uncertainty were observed. For sand, clay and SOC, the northwest region presented low uncertainties, and the same region, in general, presented low levels of clay and SOC and high levels of sand. The northeast region presented the

highest clay and SOC values and the lowest sand values. The same region presented the highest uncertainties for clay and variable uncertainties for sand and clay. The entire central area showed a tendency of intermediate to high uncertainty for sand prediction.

The erodibility map obtained from the soil attribute maps (Kcalc) in general showed slightly lower values than Kpred. Figure 5 presents the Kpred (Fig. 5a) and Kcalc maps (Fig. 5b), as well as the difference map (Kpred - Kcalc) and its distributions. The difference values showed a normal distribution (Fig. 5c), with average values close to zero, an indication that both methodologies had very similar results. it is also possible to observe that the regions with the highest values of Kpred and Kcalc coincide with those with the highest percentage of silt (Fig. 5d).

3.3.2.2 Point base prediction with 350-2500 nm spectral data for the kriging approach

In Fig. 6, the boxplot of R^2 (Fig. 6a), RMSE (Fig. 6b) and the 90% PI (Fig. 6c) values for all soil properties, from both, the training and validation sets are presented. The prediction models using the 215 bands of the Vis-NIR-SWIR spectrum as predictors variables showed satisfactory performance for clay (median R^2val of 0.83), good for sand (median R^2val of 0.69) and reasonable for the Kpred (median R^2val of 0.58). The SOC model presented the worst result (median R^2val of 0.44). The training and validation set coefficients were similar, with a greater range for the validation set.

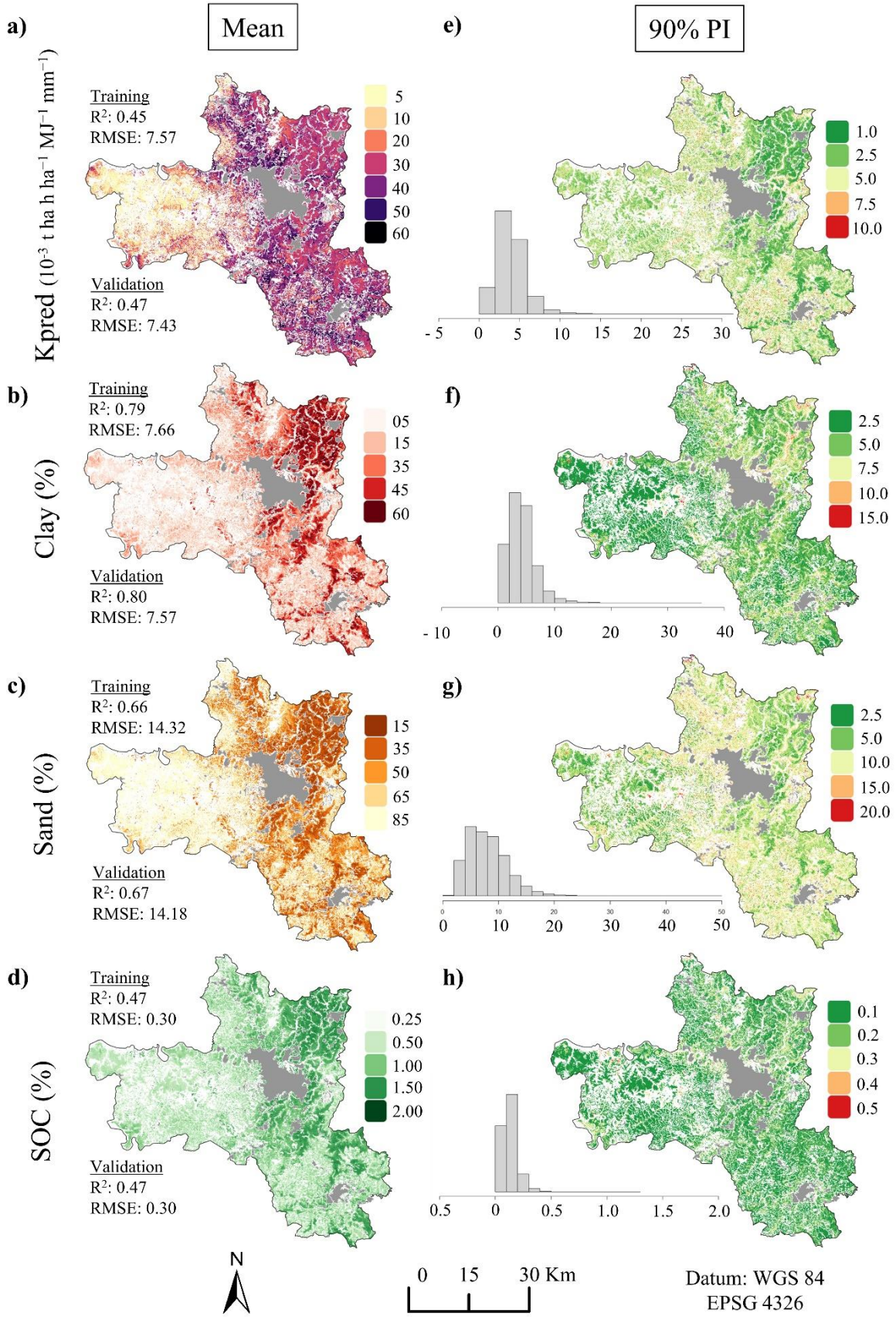

Figure 4. Digital maps of attributes generated in CBMA. Mean values maps for all attributes and the prediction performance of models (a,b,c,d). Uncertainty maps obtained by the 50 realizations and their respective histogram (e,f,g,h).

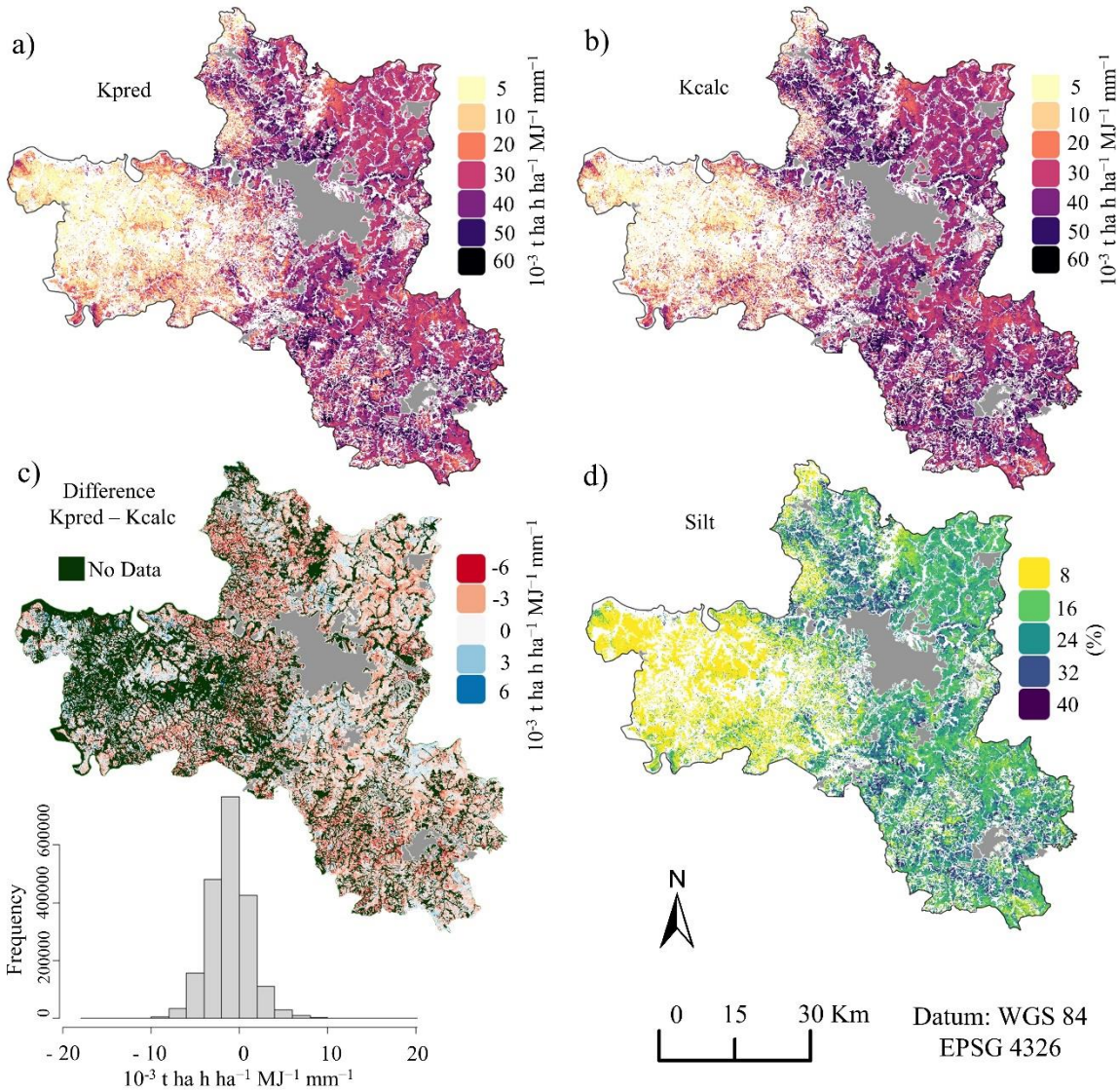

Figure 5. The digital soil erodibility maps for the study area obtained from two different approaches, Kpred (a) and Kcalc (b). The difference map between the two approaches (Kpred - Kcal) and their respective histogran (c). Silt map obtained by difference (100% - Sand + Clay) (d).

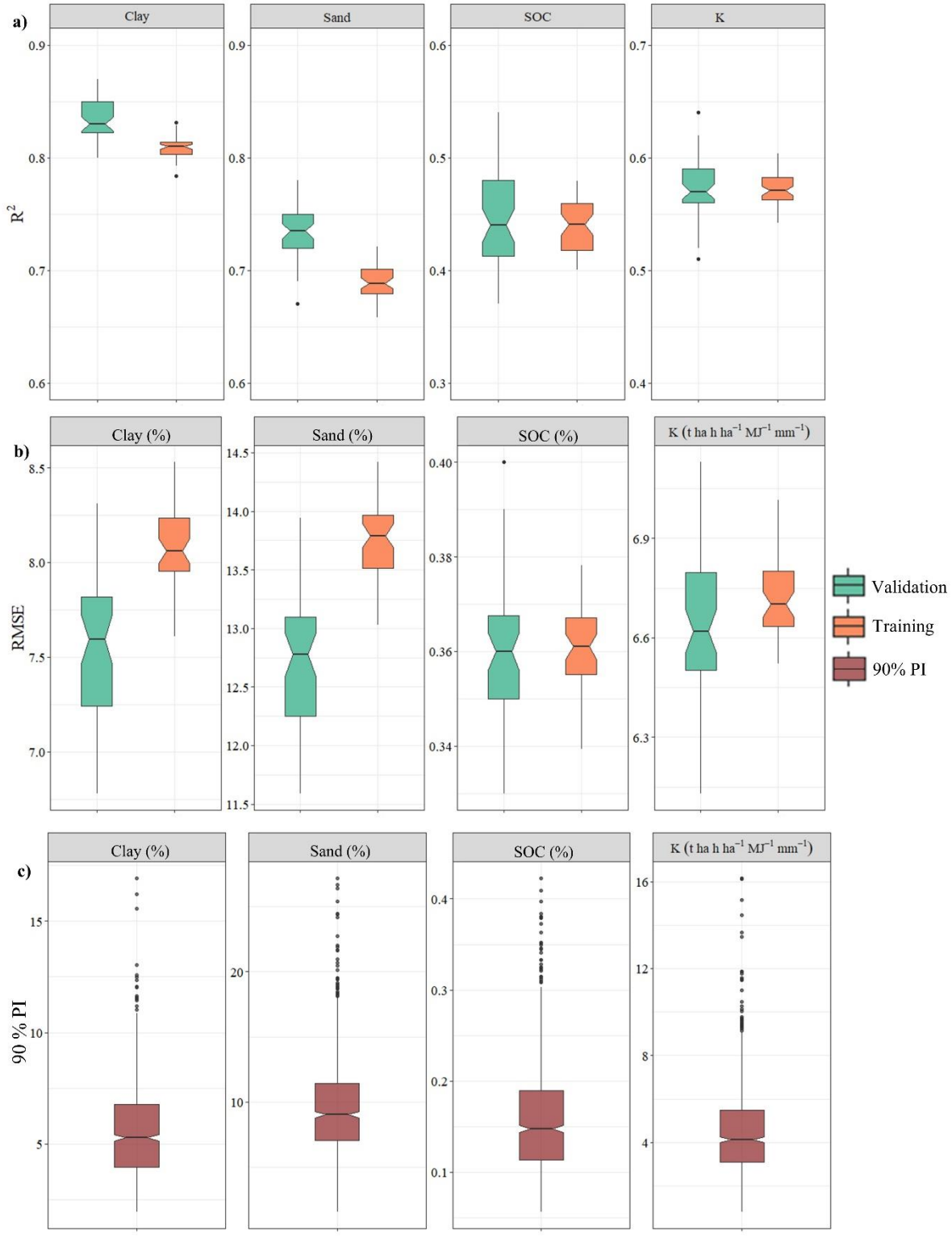

Figure 6. Boxplots showing the distribution of the R2 values (a) and the RMSE (b) for clay, sand, SOC and Kpred. The values were obtained for both the calibration/training (70%) and validation/test (30%) sets, from the 50 realizations. The 90% prediction interval (90% PI) (c) of each model was obtained applying models at the "uncertainty dataset" (50 realizations).

3.3.3. Case studies of the approaches developed

3.3.3.1 Ceveiro watershed - covariate-based method approach

Fig. 7a presents the soil erodibility maps obtained by different methodologies. In general, for all maps, the central area of the watershed presented the highest erodibility values, followed by the eastern region. The lowest values were found in the north west limits. The map generated from the legacy soil map 1: 100,000 presented only six K values, from 18 to 35 (10^{-3} t ha h ha^{-1} MJ^{-1} mm^{-1}). The map obtained from the detailed soil map, the K ranged from 15 to 42. For the kriging Kfactor (Kkriging) map the range was 2 to 47, the Kpred map from 7 to 55 and the Kcalc map from 2 to 46. All other approaches found values higher and lower than the threshold values obtained by the legacy map.

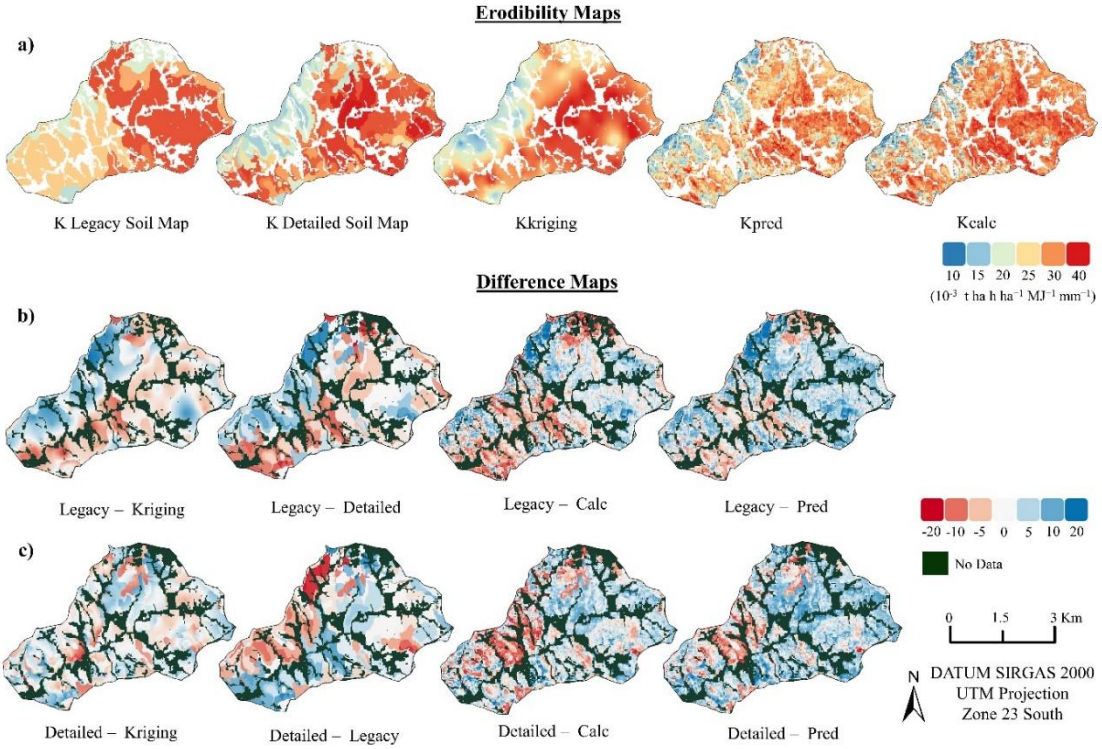

Figure 7. Ceveiro Watershed Soil Erodibility Maps obtained by different methodologies, from a legacy soil map (1:100,000 scale), from a detailed soil map (1:10,000 scale), from a model (Kpred) and calculated from soil attribute maps (Kcalc) and by ordinary kriging (Kkriging) (a); Difference maps between legacy soil map at 1:100,000 scale and other methodologies (b). Difference maps between detailed soil map at 1:10,000 scale and other methodologies (c).

When the legacy map (1:100,000) was chosen as a reference (Fig. 7b), in general, the other methodologies underestimated the values in the northwest limits of the watershed and overestimated in the southwest region. Comparing the difference maps obtained, there was a great agreement between the K legacy minus Kkriging map, K legacy minus K detailed and K legacy minus Kcalc. In the central-east region, however, the K legacy minus Kcalc presents positive values while the other two negative values.

Fig. 7c shows the difference maps obtained using the K detailed map as reference. The K detailed minus Kkriging map showed more areas with slight overestimation of values. Both K detailed minus Kkriging, K detailed minus Kpred and K detailed minus Kcalc maps overestimated the erodibility values (negative values) in the central-west region and in a small part in the north of the watershed.

3.3.3.2 Ceveiro watershed - ordinary kriging approach

Fig. 8a presents the soil erodibility maps obtained by different methodologies in the farm extent area. The highest erodibility values are found in the limits of the area, close to the natural drainage channels of the terrain. All other methodologies showed lower erodibility values, for a large part of the area, than the values obtained by the legacy soil map. The map obtained by kriging the erodibility values calculated from the results of routine soil analysis (Kfactor), showed hotspots with high values. The legacy map presented only three K values, from 31.8, 35.6 and 36.4 (10^{-3} t ha h ha^{-1} MJ^{-1} mm^{-1}). The values of K obtained from the detailed map ranged from 22 to 39. For the Kfactor map, the range was 15 to 50, the Kpred map from 24 to 38 and the Kcalc map from 26.5 to 38.5. All approaches found values higher and lower than the threshold values obtained by the legacy map.

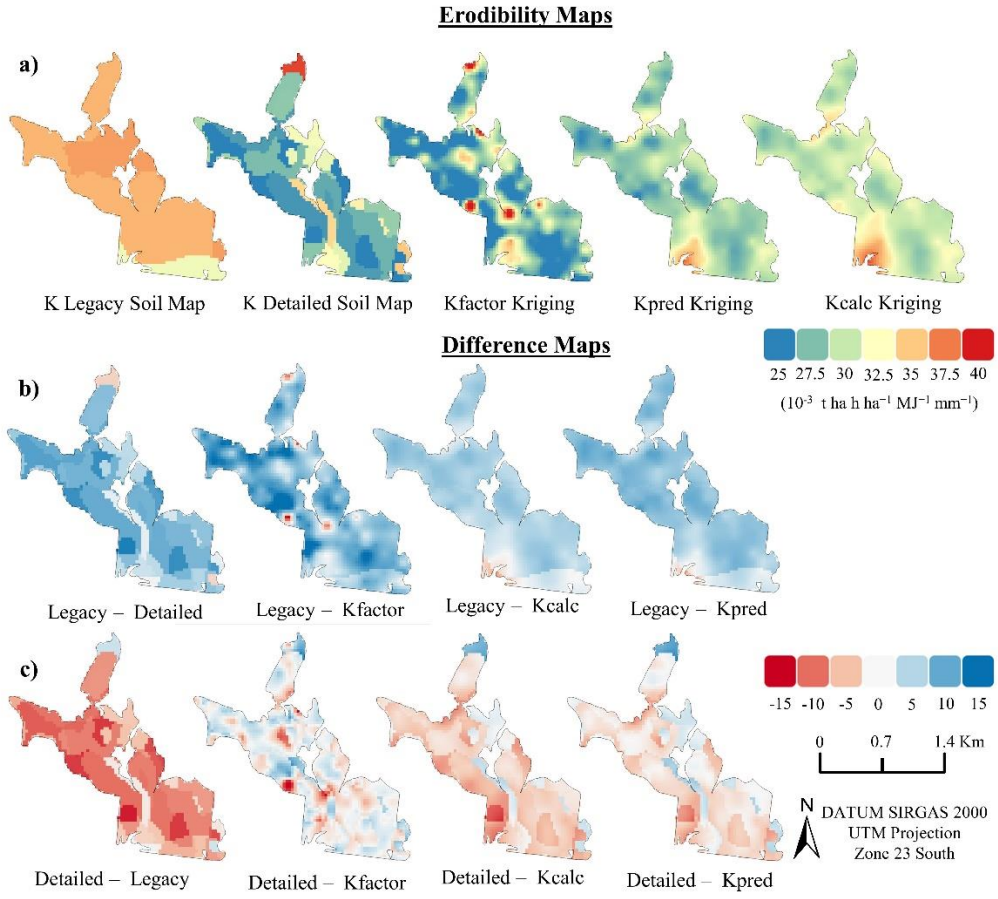

Figure 8. Rafard farm scale area soil erodibility maps obtained by different methodologies, from a legacy soil map (1:100,000 scale), from a detailed soil map (1:10,000 scale), from ordinary kriging of Kfactor, Kpred and Kcalc values (a); Difference maps between legacy soil map at 1:100,000 scale and other methodologies (b). Difference maps between detailed soil map at 1:10,000 scale and other methodologies (c).

Regarding difference maps, when the legacy map was considered as a reference (Fig. 8b), there was greater agreement between the Legacy minus Detailed and Legacy minus Kpred maps, than the Legacy minus Detailed and Legacy minus Kcalc maps. On the other hand, the Legacy minus Kfactor map presented areas with more intense colors, both underestimating and overestimating, and also presented hotspots. When the reference was the detailed map, the Detailed minus Kfactor and Detailed minus Kpred maps presented softer colors in relation to the Detailed minus Kcalc map, indicating greater agreement. However, while Kpred had a general tendency to slightly overestimate erodibility (negative values) for almost the entire area, Kfactor did not show a tendency to either overestimate or underestimate.

3.4. Discussions

3.4.1. Soil properties and erodibility values

The study area is highly variable in parent materials, resulting in a great variability of soil types and spatial variability of soil properties (Gallo et al., 2018; Mendes et al., 2022, 2021). Despite the number of samples showed high variability in clay and sand contents, the database showed a skewed distribution for clay (Fig. 3a). In part this can be explained by the absence of samples in the northeast region of the study area (Fig. 1a). This region has predominantly clayey and very clayey Ferralsols, sandy soils (with clay content < 15%) are found in the northwest region, while in the central region there is a tendency towards medium textured soils, where areas with soils with higher silt content also occur (Campos et al., 2022; Oliveira et al. 1989). The greater representation of samples with clay contents lower than 35% (Fig. 3a) partly explains the predominance of low SOC values (Fig. 3d) (Weil and Brady, 2017). Another explanation is the fact that the region is frequently cultivated with sugarcane, where soil preparation is still predominantly conventional and it favors the oxidation of soil organic matter (Campos et al., 2022).

The K-factor values, calculated from soil properties, ranged between 4 and 60 (10^{-3} t ha h ha^{-1} MJ^{-1} mm^{-1}), with an average of 25.03. In the classification proposed by (Rosewell and Loch, 2002), values below 10 are considered extremely low and values above 60 are considered extremely high. Working with soil data from all over Brazil, Godoi et al. (2021) compared erodibility values using the nomograph (Wischmeier and Smith, 1978) and the EPIC model (Sharpley and Willians, 1990), and observed that EPIC predicts higher values than the nomograph. The authors found values ranging from 0.2 to 63.3, with a mean value of 18.1 using the Nomograph and ranging from 2.09 to 57.6 with a mean value of 30.7 using EPIC. Medeiros et al. (2016) applying the USLE model for the entire state of São Paulo, Brazil, estimated erodibility values between 9.7 and 59.2. Majhi et al. (2021) point out that the universal application of these methodologies needs to be questioned since they were developed for soils of temperate climate with predominance of medium texture. Despite that, Weill and Sparovek (2008), methodology for Brazilian soils proposed by Denardim (1990), in the same Cevereiro watershed, found values between 22 and 48, similar range obtained in our work. Anache et al. (2015), evaluating different methodologies for soils of a subwatershed in the Mato Grosso do Sul State, Brazil, found the EPIC model as the most suitable. Therefore, the approach used in our work can be considered effective to represent the variability of soil erodibility in the study area.

3.4.2. Relationship of soil properties with bare soil images

The best prediction performances were for clay and sand, similar results were obtained by different authors for the same region (Bellinaso et al., 2021; Mello et al., 2022; Nélida Elizabet Quiñonez Silvero et al., 2021). Silvero et al. (2021) obtained slightly lower results, but the authors used just six bands of a Landsat bare soil image. Mello et al. (2022) obtained slightly lower results for clay and higher for sand, using, in addition to a satellite image, terrain and drainage variables. The results demonstrate the importance of using multi-temporal images of bare soil to predict soil properties, wich was also confirmed in other regions (Gasmi et al., 2021; Rogge et al., 2018; Shabou et al., 2015). The highest prediction uncertainties for clay were found in the northeast and northern parts of the study area, as previously pointed out, the absence of samples in the northeast region possibly contributed to the greater uncertainty in this region.

The low performance obtained by the SOC prediction model can be partly explained by the higher SOC dynamics in the soil over time (Ramesh et al., 2019). As SYSI considers the median reflectance value of each band

among all images that had soils exposed in that pixel (Demattê et al., 2018; Safanelli et al., 2020), it ends up portraying the spectral condition of a single day, which does not necessarily is the same period when the samples were collected. Despite this, the use of terrain variables allowed an increase in performance in relation to the results obtained by Silvero et al (2021) and Mello et al. (2022). Regarding the spatial distribution of SOC, even with the low performance of the model, the result found was within the expected, with the lowest values obtained in the northwest region where the sandy soils are found and the highest values in the northeast region where there is a predominance of soils with high clay content (Campos et al., 2022).

The methodology used (EPIC) to calculate the erodibility uses clay, sand, silt and SOC as input data. In this sense, although the independent variables used, were effective for obtaining clay and sand prediction models with a good performance, they were insufficient to provide subsidies for the creation of a good SOC prediction model, consequently affecting the K prediction. This is confirmed by the fact that the Kpred values obtained are very similar to the Kcalc values (Fig. 5a,b). This is noticeable in the difference map of the two methodologies (Fig. 5c), which shows a predominance of colors with low intensity. Fig. 5d also reinforces the importance of silt values to calculate the erodibility, being possible to verify that the areas with the highest silt values present the highest K values, corroborating the conclusions of Bonilla and Johnson (2012). This is due to the fact that the methodology was basically developed with data from temperate areas with predominance of medium textured soils (Majhi et al., 2021).

3.4.3. Spatial kriging approach - prediction performances

The good performance of clay and sand content using Vis-NIR-SWIR data is reported in the literature by different works (Bellinaso et al., 2021; Demattê et al., 2016). For SOC, however, the performance was the lower than those obtained by other works (Heil et al., 2022; Tang et al., 2020). For Kpred, the performance was similar to that obtained by Ostovari et al. (2018) for soils in Iran. However, it should be noted that the authors used erodibility data measured directly from erosion plots as the dependent variable. Jiang et al. (2020) obtained different models for each soil class, with better and worse performance than our work. This difference indicates a possible influence on the results depending on the methodology used to calculate the erodibility reference value.

Regarding the two approaches for obtaining K through the predicted values, Kcalc presented values slightly higher than Kpred (on average 5 more). With Kpred values closer to those obtained when using data from routine laboratory analysis (Kfactor).

3.4.4. Case study of the Ceveiro watershed - covariate-based method approach

The erodibility prediction approaches (Kpred and Kcalc) were able to represent the spatial distribution of this attribute for the area when compared to traditionally methodologies (based in soil maps and interpolation) (Fig. 7a). Even with the limitation of the performance of each model, there was a better agreement of the digital maps with the map obtained through the 1:10,000 scale soil map and by kriging than with the map obtained through the legacy soil map. This fact can be better observed through the similarity of the difference maps obtained using the legacy soil map as a reference. Majhi et al (2021) in an extensive review of the application of USLE-based models in India, pointed out that in a total of 100 works evaluated, 91 studies had generated spatially-discrete K factor maps. In addition, when analyzing the representativeness of samples used to obtain the erodibility maps, they judged that 60 out of 77 studies failed to adequately capture the spatial variability of soil erodibility. The same authors and Kumar et al (2022) reinforce that the best validation results of USLE-based models in predicting soil loss were found when

these models are applied at watershed or smaller areas. Therefore, the use of erodibility maps consistent with these scales of work is necessary for a better identification of the spatial variation of soil loss, since the quality of the result of a model depends on the quality of its inputs (Miller, 2017).

Another issue that must be considered is that even adopting the methodology for obtaining soil erodibility through a soil map at an adequate working scale (in our case the map at a scale of 1:10,000), its also presents errors inherent to the soil mapping process itself (Bazaglia Filho et al., 2013) and the uncertainties from the use of an average erodibility value for each soil mapping unit (Majhi et al., 2021).

3.4.5. Case study of the farm extend area - kriging approach

For this case study, the agreement of the digital erodibility maps obtained through the proposed methodologies with the map obtained from the detailed soil map was higher than with the map obtained from the legacy soil map (Fig. 8). Although the prediction of soil erodibility through Vis-NIR-SWIR data has a point value as a product, this approach can be used to build more detailed grids of information to be used in digital mappings based on spatial autocorrelation, the kriging approach, being faster and less polluting than routine laboratory analysis (Bahia et al., 2015; de Santana et al., 2019).

Another fact that must be discussed is that even though the erodibility map obtained from the detailed soil map was considered the most adequate for the area, it does not necessarily best represent the spatial distribution of erodibility in the area. As previously mentioned, Majhi et al. (2021), point out that the use of average values for a mapping unit can lead to variation smoothing, or even overestimates or underestimates caused by outliers within the same mapping unit. In the study area it is possible to verify this when comparing the map obtained through the detailed soil map and the one obtained by Kfactor ordinary kriging (Fig 8a). It is clear the presence of hotspots with high erodibility values in the Kfactor kriging map, which are smoothed in the detailed map. If there is no error in the routine analysis of these samples that generated the hotspots, even the detailed map would not adequately represent the erodibility of these areas.

3.4.6. Advantages, limitations and future research

In this work, we demonstrated the potential of using DSM and proximal and remote sensing techniques in order to obtain better erodibility maps than those obtained from coarse legacy soil maps, thus contributing to minimize one of the problems of applying USLE-based models (Majhi et al., 2021). For the prediction of the erodibility of the agricultural areas, 3600 soil samples were used), which corresponds to approximately 1 sample per 0.715 Km2. Considering that it is not possible to obtain the SYSI for the entire area and excluding urban areas, it would be around 1 sample per 0.4 km². The potential use of the technique with a relatively low number of samples for model calibration makes the approach even more attractive for countries with scarce data.

Despite this, some limitations are evident, such as the fact that it is not possible to obtain the SYSI of the entire area, which can be an even more limiting factor in regions with a high presence of native vegetation or pastures. An alternative proposed by Silvero et al. (2021) and Poppiel et al. (2019) is the interpolation of information as a way to obtain data for these areas not captured by SYSI. Obtaining Vis-NIR-SWIR data from these areas can potentially contribute to this task.

Another limitation is the relatively low performance of the prediction model obtained in the covariate-based method approach. The use of variables that can contribute to a better SOC prediction performance can be a path to be pursued. Furthermore, considering future research, the following are suggestions to be worked on: the modeling

of soil erodibility calculated through other methodologies (Wishmeier and Smith, 1978; Auerswald et al., 2014; Zhang et al., 2019) or even measured through erosion plots (Ostovari et al., 2018); use of other proximal sensing approaches in point estimates of erodibility, for example Mid-infrared spectroscopy; use of exposed soil images obtained by other sensors (eg Sentinel) as predictors of erodibility, as well as the use of hyperspectral images.

3.5. Conclusions

The work demonstrated the potential of using the SYSI obtained from multi-temporal Landsat images to be an important source of predictor variables for soil attributes modeling, including erodibility. As well as the potential of using proximal sensing in the point prediction of these attributes, as an alternative of information to compose grids to be used especially in spatial prediction autocorrelation approaches, as kriging.

The results obtained better represent the spatial variation of erodibility than information obtained from low-scale soil maps, especially when dealing with working areas at watershed or farm scale. These approaches, to obtain spatial information on soil erodibility, are even more relevant to be applied in regions with scarcity of data, mainly in developing countries.

New researches are necessary to improve the performance of the models, as well as using other calculation methodologies.

References

Alewell, C., Borrelli, P., Meusburger, K., Panagos, P., 2019. Using the USLE: Chances, challenges and limitations of soil erosion modelling. Int. Soil Water Conserv. Res. 7, 203–225. https://doi.org/https://doi.org/10.1016/j.iswcr.2019.05.004

Alvares, C.A., Stape, J.L., Sentelhas, P.C., de Moraes Gonçalves, J.L., Sparovek, G., 2013. Köppen's climate classification map for Brazil. Meteorol. Zeitschrift 22, 711–728. https://doi.org/10.1127/0941-2948/2013/0507

Anache, J.A.A., Bacchi, C.G.V., Panachuki, E., Alves Sobrinho, T., 2015. Assessment of methods for predicting soil erodibility in soil loss modeling. Geosciences 34, n1, 32-40 https://www.periodicos.rc.biblioteca.unesp.br/index.php/geociencias/article/view/9733

Angelopoulou, T., Balafoutis, A., Zalidis, G., Bochtis, D., 2020. From Laboratory to Proximal Sensing Spectroscopy for Soil Organic Carbon Estimation—A Review. Sustain. . https://doi.org/10.3390/su12020443

Auerswald, K., Fiener, P., Martin, W., Elhaus, D., 2014. Use and misuse of the K factor equation in soil erosion modeling: An alternative equation for determining USLE nomograph soil erodibility values. CATENA 118, 220–225. https://doi.org/https://doi.org/10.1016/j.catena.2014.01.008

Avalos, F.A.P., Silva, M.L.N., Batista, P.V.G., Pontes, L.M., de Oliveira, M.S., 2018. Digital soil erodibility mapping by soilscape trending and kriging. L. Degrad. Dev. 29, 3021–3028. https://doi.org/https://doi.org/10.1002/ldr.3057

Bahia, A.S.R. de S., Marques, J., Siqueira, D.S., 2015. Procedures using diffuse reflectance spectroscopy for estimating hematite and goethite in Oxisols of São Paulo, Brazil. Geoderma Reg. 5, 150–156. https://doi.org/https://doi.org/10.1016/j.geodrs.2015.04.006

Bahrami, H.-A., Ghorbani-Dashtaki, S., Naderi, M., Ostovari, Y., Dematte, J.A.M., 2017. Soil loss estimation using RUSLE model, GIS and remote sensing techniques: A case study from the Dembecha Watershed, Northwestern Ethiopia. Geoderma Reg. 11, 28–36. https://doi.org/10.1016/j.geodrs.2017.06.003

Bazaglia Filho, O., Rizzo, R., Lepsch, I.F., Prado, H. do, Gomes, F.H., Mazza, J.A., Demattê, J.A.M., 2013. Comparison between detailed digital and conventional soil maps of an area with complex geology. Rev. Bras. Ciência do Solo 37, 1136–1148. https://doi.org/10.1590/S0100-06832013000500003

Bellinaso, H., Silvero, N.E.Q., Ruiz, L.F.C., Accorsi Amorim, M.T., Rosin, N.A., Mendes, W. de S., Sousa, G.P.B. de Sepulveda, L.M.A., Queiroz, L.G. de, Nanni, M.R., Demattê, J.A.M., 2021. Clay content prediction using spectra data collected from the ground to space platforms in a smallholder tropical area. Geoderma 399, 115116. https://doi.org/https://doi.org/10.1016/j.geoderma.2021.115116

Benavidez, R., Jackson, B., Maxwell, D., Norton, K., 2018. A review of the (Revised) Universal Soil Loss Equation ((R)USLE): with a view to increasing its global applicability and improving soil loss estimates. Hydrol. Earth Syst. Sci. 22, 6059–6086. https://doi.org/10.5194/hess-22-6059-2018

Bonilla, C.A., Johnson, O.I., 2012. Soil erodibility mapping and its correlation with soil properties in Central Chile. Geoderma 189–190, 116–123. https://doi.org/https://doi.org/10.1016/j.geoderma.2012.05.005

Borrelli, P., Alewell, C., Alvarez, P., Anache, J.A.A., Baartman, J., Ballabio, C., Bezak, N., Biddoccu, M., Cerdà, A., Chalise, D., Chen, S., Chen, W., De Girolamo, A.M., Gessesse, G.D., Deumlich, D., Diodato, N., Efthimiou, N., Erpul, G., Fiener, P., Freppaz, M., Gentile, F., Gericke, A., Haregeweyn, N., Hu, B., Jeanneau, A., Kaffas, K., Kiani-Harchegani, M., Villuendas, I.L., Li, C., Lombardo, L., López-Vicente, M., Lucas-Borja, M.E., Märker, M., Matthews, F., Miao, C., Mikoš, M., Modugno, S., Möller, M., Naipal, V., Nearing, M., Owusu, S., Panday, D., Patault, E., Patriche, C.V., Poggio, L., Portes, R., Quijano, L., Rahdari, M.R., Renima, M., Ricci, G.F., Rodrigo-Comino, J., Saia, S., Samani, A.N., Schillaci, C., Syrris, V., Kim, H.S., Spinola, D.N., Oliveira, P.T., Teng, H., Thapa, R., Vantas, K., Vieira, D., Yang, J.E., Yin, S., Zema, D.A., Zhao, G., Panagos, P., 2021. Soil erosion modelling: A global review and statistical analysis. Sci. Total Environ. 780, 146494. https://doi.org/https://doi.org/10.1016/j.scitotenv.2021.146494

Briak, H., Moussadek, R., Aboumaria, K., Mrabet, R., 2016. Assessing sediment yield in Kalaya gauged watershed (Northern Morocco) using GIS and SWAT model. Int. Soil Water Conserv. Res. 4, 177–185. https://doi.org/https://doi.org/10.1016/j.iswcr.2016.08.002

Campos, L.R., Demattê, J.A.M., Bellinaso, H., Poppiel, R.R., Greschuk, L.T., Rizzo, R., Rosin, N.A., Rosas, J.T.F., 2022. Detection of bare soils in sugarcane areas by temporal satellite images: A monitoring technique for soil security. Soil Secur. 7, 100057. https://doi.org/https://doi.org/10.1016/j.soisec.2022.100057

Castaldi, F., 2021. Sentinel-2 and Landsat-8 Multi-Temporal Series to Estimate Topsoil Properties on Croplands. Remote Sens. . https://doi.org/10.3390/rs13173345

Chagas, C. da S., de Carvalho Junior, W., Bhering, S.B., Calderano Filho, B., 2016. Spatial prediction of soil surface texture in a semiarid region using random forest and multiple linear regressions. CATENA 139, 232–240. https://doi.org/10.1016/j.catena.2016.01.001

Conrad, O., Bechtel, B., Bock, M., Dietrich, H., Fischer, E., Gerlitz, L., Wehberg, J., Wichmann, V., Böhner, J., 2015. System for Automated Geoscientific Analyses (SAGA) v. 2.1.4. Geosci. Model Dev. 8, 1991–2007. https://doi.org/10.5194/gmd-8-1991-2015

de Santana, F.B., de Souza, A.M., Poppi, R.J., 2019. Green methodology for soil organic matter analysis using a national near infrared spectral library in tandem with learning machine. Sci. Total Environ. 658, 895–900. https://doi.org/https://doi.org/10.1016/j.scitotenv.2018.12.263

Demattê, J.A.M., Bellinaso, H., Araújo, S.R., Rizzo, R., Souza, A.B., Demattê, J.A.M., Bellinaso, H., Araújo, S.R., Rizzo, R., Souza, A.B., 2016. Spectral regionalization of tropical soils in the estimation of soil attributes. Rev. CIÊNCIA AGRONÔMICA 47, 589–598. https://doi.org/10.5935/1806-6690.20160071

Demattê, J.A.M., Dotto, A.C., Paiva, A.F.S., Sato, M. V., Dalmolin, R.S.D., de Araújo, M. do S.B., da Silva, E.B., Nanni, M.R., ten Caten, A., Noronha, N.C., Lacerda, M.P.C., de Araújo Filho, J.C., Rizzo, R., Bellinaso, H., Francelino, M.R., Schaefer, C.E.G.R., Vicente, L.E., dos Santos, U.J., de Sá Barretto Sampaio, E. V., Menezes, R.S.C., de Souza, J.J.L.L., Abrahão, W.A.P., Coelho, R.M., Grego, C.R., Lani, J.L., Fernandes, A.R., Gonçalves, D.A.M., Silva, S.H.G., de Menezes, M.D., Curi, N., Couto, E.G., dos Anjos, L.H.C., Ceddia, M.B., Pinheiro, É.F.M., Grunwald, S., Vasques, G.M., Marques Júnior, J., da Silva, A.J., Barreto, M.C. de V., Nóbrega, G.N., da Silva, M.Z., de Souza, S.F., Valladares, G.S., Viana, J.H.M., da Silva Terra, F., Horák-Terra, I., Fiorio, P.R., da Silva, R.C., Frade Júnior, E.F., Lima, R.H.C., Alba, J.M.F., de Souza Junior, V.S., Brefin, M.D.L.M.S., Ruivo, M.D.L.P., Ferreira, T.O., Brait, M.A., Caetano, N.R., Bringhenti, I., de Sousa Mendes, W., Safanelli, J.L., Guimarães, C.C.B., Poppiel, R.R., e Souza, A.B., Quesada, C.A., do Couto, H.T.Z., 2019. The Brazilian Soil Spectral Library (BSSL): A general view, application and challenges. Geoderma 354, 113793. https://doi.org/10.1016/j.geoderma.2019.05.043

Demattê, J.A.M., Fongaro, C.T., Rizzo, R., Safanelli, J.L., 2018. Geospatial Soil Sensing System (GEOS3): A powerful data mining procedure to retrieve soil spectral reflectance from satellite images. Remote Sens. Environ. 212, 161–175. https://doi.org/https://doi.org/10.1016/j.rse.2018.04.047

Demattê, J.A.M., Safanelli, J.L., Poppiel, R.R., Rizzo, R., Silvero, N.E.Q., Mendes, W. de S., Bonfatti, B.R., Dotto, A.C., Salazar, D.F.U., Mello, F.A. de O., Paiva, A.F. da S., Souza, A.B., Santos, N.V. dos, Maria Nascimento, C., Mello, D.C. de, Bellinaso, H., Gonzaga Neto, L., Amorim, M.T.A., Resende, M.E.B. de, Vieira, J. da S., Queiroz, L.G. de, Gallo, B.C., Sayão, V.M., Lisboa, C.J. da S., 2020. Bare Earth's Surface Spectra as a Proxy for Soil Resource Monitoring. Sci. Rep. 10, 4461. https://doi.org/10.1038/s41598-020-61408-1

Denardin, J.E. Erodibilidade do solo estimada por meio de parâmetros físicos e químicos. Piracicaba, Escola Superior de Agricultura Luiz de Queiroz, 1990. 114p. (Thesis)

Efthimiou, N., 2020. The new assessment of soil erodibility in Greece. Soil Tillage Res. 204, 104720. https://doi.org/https://doi.org/10.1016/j.still.2020.104720

Efthimiou, N., 2018. The importance of soil data availability on erosion modeling. CATENA 165, 551–566. https://doi.org/https://doi.org/10.1016/j.catena.2018.03.002

Gallo, B.C., Demattê, J.A.M., Rizzo, R., Safanelli, J.L., Mendes, W.D.S., Lepsch, I.F., Sato, M. V, Romero, D.J., Lacerda, M.P.C., 2018. Multi-Temporal Satellite Images on Topsoil Attribute Quantification and the Relationship with Soil Classes and Geology. Remote Sens. https://doi.org/10.3390/rs10101571

Gasmi, A., Gomez, C., Lagacherie, P., Zouari, H., Laamrani, A., Chehbouni, A., 2021. Mean spectral reflectance from bare soil pixels along a Landsat-TM time series to increase both the prediction accuracy of soil clay content and mapping coverage. Geoderma 388, 114864. https://doi.org/https://doi.org/10.1016/j.geoderma.2020.114864

Gelagay, H.S., Minale, A.S., 2016. Soil loss estimation using GIS and Remote sensing techniques: A case of Koga watershed, Northwestern Ethiopia. Int. Soil Water Conserv. Res. 4, 126–136. https://doi.org/https://doi.org/10.1016/j.iswcr.2016.01.002

Godoi, R. de F., Rodrigues, D.B.B., Borrelli, P., Oliveira, P.T.S., 2021. High-resolution soil erodibility map of Brazil. Sci. Total Environ. 781, 146673. https://doi.org/https://doi.org/10.1016/j.scitotenv.2021.146673

Gonçalves, T.G., Pons, N.A.D., Melloni, E.G.P., Mancini, M., Curi, N., 2021. Digital soil mapping: Predicting soil classes distribution in large areas based on existing soil maps from similar small areas. Ciência e Agrotecnologia 45. https://doi.org/10.1590/1413-7054202145007921

Gorelick, N., Hancher, M., Dixon, M., Ilyushchenko, S., Thau, D., Moore, R., 2017. Google Earth Engine: Planetary-scale geospatial analysis for everyone. Remote Sens. Environ. 202, 18–27. https://doi.org/https://doi.org/10.1016/j.rse.2017.06.031

Heil, J., Jörges, C., Stumpe, B., 2022. Evaluation of using digital photography as a cost-effective tool for the rapid assessment of soil organic carbon at a regional scale. Soil Secur. 6, 100023. https://doi.org/https://doi.org/10.1016/j.soisec.2021.100023

Instituto de Pesquisas Tecnológicas – IPT. Mapa geológico do Estado de São Paulo. Escala 1:500.000. São Paulo, 1981. 2v. escala 1: 500.000 (Monografias, 6)

Jiang, Q., Chen, Y., Hu, J., Liu, F., 2020. Use of Visible and Near-Infrared Reflectance Spectroscopy Models to Determine Soil Erodibility Factor (K) in an Ecologically Restored Watershed. Remote Sens. https://doi.org/10.3390/rs12183103

John, K., Abraham Isong, I., Michael Kebonye, N., Okon Ayito, E., Chapman Agyeman, P., Marcus Afu, S., 2020. Using Machine Learning Algorithms to Estimate Soil Organic Carbon Variability with Environmental Variables and Soil Nutrient Indicators in an Alluvial Soil. L. https://doi.org/10.3390/land9120487

Knadel, M., Thomsen, A., Schelde, K., Greve, M.H., 2015. Soil organic carbon and particle sizes mapping using vis–NIR, EC and temperature mobile sensor platform. Comput. Electron. Agric. 114, 134–144. https://doi.org/10.1016/j.compag.2015.03.013

Kuhn, M., 2008. Building Predictive Models in R Using the caret Package. J. Stat. Softw. 28, 1–26. https://doi.org/10.18637/jss.v028.i05

Kuhn, M., Weston, S., Keefer, C., Coulter, N., Quinlan, R., 2013. Cubist: Rule-and instance-based regression modeling, R package version 0.0. 18.

Kumar, M., Sahu, A.P., Sahoo, N., Dash, S.S., Raul, S.K., Panigrahi, B., 2022. Global-scale application of the RUSLE model: a comprehensive review. Hydrol. Sci. J. 1–25. https://doi.org/10.1080/02626667.2021.2020277

Lagacherie, P., Arrouays, D., Bourennane, H., Gomez, C., Martin, M., Saby, N.P.A., 2019. How far can the uncertainty on a Digital Soil Map be known? A numerical experiment using pseudo values of clay content obtained from Vis-SWIR hyperspectral imagery. Geoderma 337, 1320–1328. https://doi.org/https://doi.org/10.1016/j.geoderma.2018.08.024

Lepsch, I.F., 2013. Status of Soil Surveys and Demand for Soil Series Descriptions in Brazil. Soil Horizons 54, sh2013-54-2-gc. https://doi.org/https://doi.org/10.2136/sh2013-54-2-gc

Li, X., Ding, J., Liu, J., Ge, X., Zhang, J., 2021. Digital Mapping of Soil Organic Carbon Using Sentinel Series Data: A Case Study of the Ebinur Lake Watershed in Xinjiang. Remote Sens. https://doi.org/10.3390/rs13040769

Loiseau, T., Chen, S., Mulder, V.L., Román Dobarco, M., Richer-de-Forges, A.C., Lehmann, S., Bourennane, H., Saby, N.P.A., Martin, M.P., Vaudour, E., Gomez, C., Lagacherie, P., Arrouays, D., 2019. Satellite data integration for soil clay content modelling at a national scale. Int. J. Appl. Earth Obs. Geoinf. 82, 101905. https://doi.org/https://doi.org/10.1016/j.jag.2019.101905

Majhi, A., Shaw, R., Mallick, K., Patel, P.P., 2021. Towards improved USLE-based soil erosion modelling in India: A review of prevalent pitfalls and implementation of exemplar methods. Earth-Science Rev. 221, 103786. https://doi.org/https://doi.org/10.1016/j.earscirev.2021.103786

Marques, V.S., Ceddia, M.B., Antunes, M.A.H., Carvalho, D.F., Anache, J.A.A., Rodrigues, D.B.B., Oliveira, P.T.S., 2019. USLE K-Factor Method Selection for a Tropical Catchment. Sustain. . https://doi.org/10.3390/su11071840

McBratney, A.B., Mendonça Santos, M.L., Minasny, B., 2003. On digital soil mapping. Geoderma 117, 3–52. https://doi.org/https://doi.org/10.1016/S0016-7061(03)00223-4

Medeiros, G. de O.R., Giarolla, A., Sampaio, G., Marinho, M. de A., 2016. Estimates of Annual Soil Loss Rates in the State of São Paulo, Brazil. Rev. Bras. Ciência do Solo 40. https://doi.org/10.1590/18069657rbcs20150497

Mello, C.R. de, Norton, L.D., Pinto, L.C., Beskow, S., Curi, N., 2016. Agricultural watershed modeling: a review for hydrology and soil erosion processes. Ciência e Agrotecnologia 40, 7–25. https://doi.org/10.1590/S1413-70542016000100001

Mello, F.A.O., Demattê, J.A.M., Rizzo, R., Mello, D.C. de, Poppiel, R.R., Silvero, N.E.Q., Safanelli, J.L., Bellinaso, H., Bonfatti, B.R., Gomez, A.M.R., Sousa, G.P.B., 2022. Complex hydrological knowledge to support digital soil mapping. Geoderma 409, 115638. https://doi.org/https://doi.org/10.1016/j.geoderma.2021.115638

Mendes, W. de S., Demattê, J.A.M., Minasny, B., Silvero, N.E.Q., Bonfatti, B.R., Safanelli, J.L., Rizzo, R., Costa, A.C.S. da, 2022. Free iron oxide content in tropical soils predicted by integrative digital mapping. Soil Tillage Res. 219, 105346. https://doi.org/https://doi.org/10.1016/j.still.2022.105346

Mendes, W. de S., Demattê, J.A.M., Silvero, N.E.Q., Rabelo Campos, L., 2021. Integration of multispectral and hyperspectral data to map magnetic susceptibility and soil attributes at depth: A novel framework. Geoderma 385, 114885. https://doi.org/https://doi.org/10.1016/j.geoderma.2020.114885

Miller, B.A., 2017. Chapter 5 - Geographic Information Systems and Spatial Statistics Applied for Soil Mapping: A Contribution to Land Use Management, in: Pereira, P., Brevik, E.C., Muñoz-Rojas, M., Miller, B.A.B.T.-S.M. and P.M. for S.L.U.M. (Eds.), . Elsevier, pp. 127–149. https://doi.org/https://doi.org/10.1016/B978-0-12-805200-6.00005-0

Minasny, B., Hartemink, A.E., 2011. Predicting soil properties in the tropics. Earth-Science Rev. 106, 52–62. https://doi.org/https://doi.org/10.1016/j.earscirev.2011.01.005

Moura-Bueno, J.M., Dalmolin, R.S.D., Horst-Heinen, T.Z., Grunwald, S., ten Caten, A., 2021. Environmental covariates improve the spectral predictions of organic carbon in subtropical soils in southern Brazil. Geoderma 393, 114981. https://doi.org/https://doi.org/10.1016/j.geoderma.2021.114981

Nanni, M.R., Demattê, J.A.M., 2006. Spectral Reflectance Methodology in Comparison to Traditional Soil Analysis. Soil Sci. Soc. Am. J. 70, 393–407. https://doi.org/10.2136/SSSAJ2003.0285

Nocita, M., Stevens, A., van Wesemael, B., Aitkenhead, M., Bachmann, M., Barthès, B., Ben Dor, E., Brown, D.J., Clairotte, M., Csorba, A., Dardenne, P., Demattê, J.A.M., Genot, V., Guerrero, C., Knadel, M., Montanarella, L., Noon, C., Ramirez-Lopez, L., Robertson, J., Sakai, H., Soriano-Disla, J.M., Shepherd, K.D., Stenberg, B., Towett, E.K., Vargas, R., Wetterlind, J., 2015. Chapter Four - Soil Spectroscopy: An Alternative to Wet Chemistry for Soil Monitoring, in: Sparks, D.L.B.T.-A. in A. (Ed.), Academic Press, pp. 139–159. https://doi.org/https://doi.org/10.1016/bs.agron.2015.02.002

Nolasco de Carvalho, C.C., Nunes, F.C., Homem Antunes, M.A., Nolasco, M.C., 2015. Soil surveys in Brazil and perspectives in digital soil mapping. Soil Horizons 56. https://doi.org/10.2136/sh14-01-0002

Ostovari, Y., Ghorbani-Dashtaki, S., Bahrami, H.-A., Abbasi, M., Dematte, J.A.M., Arthur, E., Panagos, P., 2018. Towards prediction of soil erodibility, SOM and CaCO3 using laboratory Vis-NIR spectra: A case study in a semi-arid region of Iran. Geoderma 314, 102–112. https://doi.org/https://doi.org/10.1016/j.geoderma.2017.11.014

Ostovari, Y., Ghorbani-Dashtaki, S., Bahrami, H.-A., Naderi, M., Dematte, J.A.M., Kerry, R., 2016. Modification of the USLE K factor for soil erodibility assessment on calcareous soils in Iran. Geomorphology 273, 385–395. https://doi.org/https://doi.org/10.1016/j.geomorph.2016.08.003

Panagos, P., Meusburger, K., Ballabio, C., Borrelli, P., Alewell, C., 2014. Soil erodibility in Europe: A high-resolution dataset based on LUCAS. Sci. Total Environ. 479–480, 189–200. https://doi.org/https://doi.org/10.1016/j.scitotenv.2014.02.010

Pebesma, E.J., 2009. The meuse data set: a tutorial for the gstat R package.

Phinzi, K., Ngetar, N.S., 2019. The assessment of water-borne erosion at catchment level using GIS-based RUSLE and remote sensing: A review. Int. Soil Water Conserv. Res. 7, 27–46. https://doi.org/https://doi.org/10.1016/j.iswcr.2018.12.002

Poppiel, Raúl R., Lacerda, M.P.C., Demattê, J.A.M., Oliveira Jr, M.P., Gallo, B.C., Safanelli, J.L., 2019a. Pedology and soil class mapping from proximal and remote sensed data. Geoderma 348, 189–206. https://doi.org/10.1016/j.geoderma.2019.04.028

Poppiel, Raúl R, Lacerda, M.P.C., Demattê, J.A.M., Oliveira, M.P., Gallo, B.C., Safanelli, J.L., 2019a. Pedology and soil class mapping from proximal and remote sensed data. Geoderma 348, 189–206. https://doi.org/https://doi.org/10.1016/j.geoderma.2019.04.028

Poppiel, Raúl R, Lacerda, M.P.C., Safanelli, J.L., Rizzo, R., Oliveira, M.P., Novais, J.J., Demattê, J.A.M., 2019b. Mapping at 30 m Resolution of Soil Attributes at Multiple Depths in Midwest Brazil. Remote Sens. https://doi.org/10.3390/rs11242905

Quinlan, J., 1992. Learning with continuous classes, in: Adams, A., Sterling, L. (Eds.), Proceedings AI'92, 5th Australian Conference on Artificial Intelligence.World Scientific. Singapure, pp. 343–348.

Ramesh, T., Bolan, N.S., Kirkham, M.B., Wijesekara, H., Kanchikerimath, M., Rao, C.S., et al., 2019. Soil organic carbon dynamics: impact of land use changes and management practices: a review. Adv. Agron. 156, 1–107.

Rogge, D., Bauer, A., Zeidler, J., Mueller, A., Esch, T., Heiden, U., 2018. Building an exposed soil composite processor (SCMaP) for mapping spatial and temporal characteristics of soils with Landsat imagery (1984–2014). Remote Sens. Environ. 205, 1–17. https://doi.org/10.1016/J.RSE.2017.11.004

Rosewell, C.J., Loch, R.J., 2002. Estimation of the RUSLE soil erodibility factor. Soil Phys. Meas. Interpret. L. Eval. 361–369.

Rossel, R.A.V., Chen, C., 2011. Digitally mapping the information content of visible–near infrared spectra of surficial Australian soils. Remote Sens. Environ. 115, 1443–1455. https://doi.org/https://doi.org/10.1016/j.rse.2011.02.004

Safanelli, J.L., Chabrillat, S., Ben-Dor, E., Demattê, J.A.M., 2020. Multispectral Models from Bare Soil Composites for Mapping Topsoil Properties over Europe. Remote Sens. https://doi.org/10.3390/rs12091369

Salehi-Varnousfaderani, B., Honarbakhsh, A., Tahmoures, M., Akbari, M., 2022. Soil erodibility prediction by Vis-NIR spectra and environmental covariates coupled with GIS, regression and PLSR in a watershed scale, Iran. Geoderma Reg. 28, e00470. https://doi.org/https://doi.org/10.1016/j.geodrs.2021.e00470

Schürz, C., Mehdi, B., Kiesel, J., Schulz, K., Herrnegger, M., 2020. A systematic assessment of uncertainties in large-scale soil loss estimation from different representations of USLE input factors – a case study for Kenya and Uganda. Hydrol. Earth Syst. Sci. 24, 4463–4489. https://doi.org/10.5194/hess-24-4463-2020

Shabou, M., Mougenot, B., Chabaane, Z.L., Walter, C., Boulet, G., Aissa, N.B., Zribi, M., 2015. Soil Clay Content Mapping Using a Time Series of Landsat TM Data in Semi-Arid Lands. Remote Sens. . https://doi.org/10.3390/rs70506059

Silva, E.F. da., 2000. Mapas de solos produzidos em escalas e épocas distintas (Doctoral Thesis). University of São Paulo. https://doi.org/10.11606/T.11.2020.tde-20200111-152157

Silvero, Nélida Elizabet Quiñonez, Demattê, J.A.M., Amorim, M.T.A., Santos, N.V. dos , Rizzo, R., Safanelli, J.L., Poppiel, R.R., Mendes, W. de S., Bonfatti, B.R., 2021. Soil variability and quantification based on Sentinel-2 and Landsat-8 bare soil images: A comparison. Remote Sens. Environ. 252, 112117. https://doi.org/https://doi.org/10.1016/j.rse.2020.112117

Silvero, Nélida E Q, Demattê, J.A.M., Vieira, J. de S., Mello, F.A. de O., Amorim, M.T.A., Poppiel, R.R., Mendes, W. de S., Bonfatti, B.R., 2021. Soil property maps with satellite images at multiple scales and its impact on management and classification. Geoderma 397, 115089. https://doi.org/https://doi.org/10.1016/j.geoderma.2021.115089

Sparovek, G., Schnug, E., 2001. Temporal Erosion-Induced Soil Degradation and Yield Loss. Soil Sci. Soc. Am. J. 65, 1479–1486. https://doi.org/10.2136/SSSAJ2001.6551479X

Sparovek, G., Weill, M.M., Ranieiri, S.B.L., Schnug, E., Silva, E.F., 1997. The life-time concept as a tool for erosion tolerance definition. Sci. Agric. 54, 130–135. https://doi.org/10.1590/S0103-90161997000300015

Steinmetz, A.A., Cassalho, F., Caldeira, T.L., Oliveira, V.A. de, Beskow, S., Timm, L.C., 2018. Assessment of soil loss vulnerability in data-scarce watersheds in southern Brazil. Ciência e Agrotecnologia.

Stenberg, B., Viscarra Rossel, R.A., Mouazen, A.M., Wetterlind, J., 2010. Chapter Five - Visible and Near Infrared Spectroscopy in Soil Science, in: Sparks, D.L.B.T.-A. in A. (Ed.), Academic Press, pp. 163–215. https://doi.org/https://doi.org/10.1016/S0065-2113(10)07005-7

Tang, Y., Jones, E., Minasny, B., 2020. Evaluating low-cost portable near infrared sensors for rapid analysis of soils from South Eastern Australia. Geoderma Reg. 20, e00240. https://doi.org/https://doi.org/10.1016/j.geodrs.2019.e00240

Teixeira, P.C., Donagemma, G.K., Fontana, A., Teixeira, W.G., 2017. Manual de métodos de análise de solo. Rio Janeiro, Embrapa. 573p.

Teng, H., Viscarra Rossel, R.A., Shi, Z., Behrens, T., Chappell, A., Bui, E., 2016. Assimilating satellite imagery and visible–near infrared spectroscopy to model and map soil loss by water erosion in Australia. Environ. Model. Softw. 77, 156–167. https://doi.org/https://doi.org/10.1016/j.envsoft.2015.11.024

Tian, Z., Liu, F., Liang, Y., Zhu, X., 2022. Mapping soil erodibility in southeast China at 250 m resolution: Using environmental variables and random forest regression with limited samples. Int. Soil Water Conserv. Res. 10, 62–74. https://doi.org/https://doi.org/10.1016/j.iswcr.2021.06.005

Vaezi, A.R., Hasanzadeh, H., Cerdà, A., 2016. Developing an erodibility triangle for soil textures in semi-arid regions, NW Iran. CATENA 142, 221–232. https://doi.org/https://doi.org/10.1016/j.catena.2016.03.015

Viscarra Rossel, R.A., Rizzo, R., Demattê, J.A.M., Behrens, T., 2010. Spatial Modeling of a Soil Fertility Index using Visible–Near-Infrared Spectra and Terrain Attributes. Soil Sci. Soc. Am. J. 74, 1293–1300. https://doi.org/https://doi.org/10.2136/sssaj2009.0130

Walkley, A., Black, I.A., 1934. An examination of the Degtjareff method for determining soil organic matter, and a proposed modification of the chromic acid titration method. Soil Sci. 37, 29–38.

Weil, R.R., Brady, N.C., 2017. The nature and properties of soils, 15th ed. Pearson Press, Upper Saddle River NJ.

Weill, M. de A.M., Sparovek, G., 2008. Estudo da erosão na microbacia do Ceveiro (Piracicaba, SP): I - Estimativa das taxas de perda de solo e estudo de sensibilidade dos fatores do modelo EUPS. Rev. Bras. Ciência do Solo 32, 801–814. https://doi.org/10.1590/S0100-06832008000200034

Zhang, K., Yu, Y., Dong, J., Yang, Q., Xu, X., 2019. Adapting & testing use of USLE K factor for agricultural soils in China. Agric. Ecosyst. Environ. 269, 148–155. https://doi.org/https://doi.org/10.1016/j.agee.2018.09.033

Zhu, X., Liang, Y., Tian, Z., Zhang, Yi, Zhang, Yugang, Du, J., Wang, X., Li, Y., Qu, L., Dai, M., 2021. Simulating soil erodibility in southeastern China using a sequential Gaussian algorithm. Pedosphere 31, 715–724. https://doi.org/https://doi.org/10.1016/S1002-0160(20)60021-2

4. DETECTION OF BARE SOILS IN SUGARCANE AREAS BY TEMPORAL SATELLITE IMAGES: A MONITORING TECHNIQUE FOR SOIL SECURITY

Abstract

Bare soil triggers several undesirable processes for its quality and remote sensing can be a powerful tool to monitoring its occurrence. This work aims to apply multi-temporal satellite image techniques to detect bare soil areas under sugarcane cultivation and relate with soil security. The study was carried out in an area of 2,574 km² located in Brazil. The MapBiomas land use and cover collection was used to know the sugarcane area changes from 1985 to 2019. A collection of Landsat images over 35 years (1985 to 2019) were used to create Synthetic Soil Images (SYSIs) and the Bare Soil Frequency Images (BSF) of the area. SYSIs were generated annually, in the rainy and dry season. BSFs was generated in the total period and every five years by dry and rainy season. Thus, the land use changes and bare soil occurrence were compared to categorical maps of soil types, surface clay classes and slope, and also with economic, social and political changes in the period. In general, the bare soil increased from 1985 to 2006, and began to decline thereafter because of "Agro-environmental Protocol' that anticipated the end of pre-harvest burning in sugarcane crop. BSF in the rainy season decreased over the period motivated by knowledge of farmers and changes in management. Despite this, many prone to erosion soils classes (Arenosols, Lixisols/Acrisols) remain under conventional tillage in the rainy season. We concluded that the use of multi-temporal satellite images is an important approach to monitoring soil management contributing to soil security.

Keywords: Remote Sensing, Soil Degradation, Sustainability, Soil Management, Erosion, Multi-temporal images

Published as: Campos, L.R., Demattê, J.A.M., Bellinaso, H., Poppiel, R.R., Greschuk, L.T., Rizzo, R., Rosin, N.A., Rosas, J.T.F., 2022. Detection of bare soils in sugarcane areas by temporal satellite images: A monitoring technique for soil security. Soil Secur. 7, 100057. https://doi.org/10.1016/j.soisec.2022.100057

4.1. Introduction

Sugarcane is cultivated in over 100 countries (Aparecido et al. 2021; Paungfoo-Lonhienne et al. 2021), on about 26 M ha (Dias et al. 2021b) and is one of the most important crops for the global economy (Arruda et al. 2021). In the actual global demand for renewable energy, where more than 64 countries have national programs to stimulate biofuels use (Caldarelli and Gilio, 2018), it is one of the most sustainable crops for biofuel production (Bordonal et al., 2018; Barbosa et al. 2019). Brazil is the largest sugarcane producer (Cherubin et al 2021a; Marin et al. 2021), India, China, Thailand and Australia are other important producing countries (Han et al. 2022; Som-ard et al. 2021).

Brazil with approximately 376 sugarcane mills (Hernandes et al., 2021) is the second-largest bioethanol producer in the world (Carvalho et al. 2019; Gmach et al. 2020), producing 2,348,591.8 thousand liters from sugarcane (CONAB, 2021). Ethanol is present in the consumer's daily life, mainly as a clean and renewable fuel (Coelho et al., 2006; Antunes et al., 2019), it begins in the 1970s, with the "Pro-Álcool" (Pro-Ethanol), the National Alcohol Program (Chavegatti-Gianotto et al. 2011) and nowadays, around 71.4% of vehicles are flex-fuel (Sindipeças and Abipeças, 2021). In addition, Brazil produces 29,795.7 thousand tons of sugar (CONAB, 2021), around of 10% of national electricity demand (20 TWh of bioelectricity) is generate by co-generation (Gmach et al. 2020; Nechet et al. 2021) and sugarcane or its by-products have numerous other uses (Chavegatti-Gianotto et al. 2011; Dias et al. 2021b). Brazil has been grown sugarcane since the colonial period (Dias et al. 2021a), cultivating around 10 million ha mainly in two traditional regions: the center-south (92% of the production) and the northeast (Carvalho et al. 2019; Almeida et al. 2021; Cherubin et al. 2021b). In center-south region, São Paulo State concentrates 55% of sugarcane national production (Cherubin et al. 2021b; Teixeira et al. 2021; Valente e Laurini et al. 2021).

At the 21st Conference of the Parties (COP21), Brazil commits to reducing greenhouse gas emissions (Tenelli et al. 2019; Sanchez et al. 2021;). For this, it is estimated that the country will need to double the production of Ethanol by 2030 (Almeida et al. 2021; Silva et al. 2021) and increase the production of other bioenergy produced from sugarcane by-products (Silva et al. 2021; Dos Santos et al. 2022). To this end, the recent biofuel policy of the country, denominated "Renovabio" was created (Gonçalves et al. 2021; Grangeia et al. 2022).

Although sugarcane is considered a sustainable crop for biofuel production (Barbosa et al. 2019; Dos Santos et al. 2022) and its expansion in Brazil a solution to reduce CO2 emissions (Jaiswal et al. 2017; Hernandes et al. 2021), some problems related to its soil management have been reported: degradation of the soil structure (Canisares et al. 2019), compaction (Esteban et al. 2019; Jimenez et al. 2021) excessive use of conventional tillage (Barbosa et al. 2019; Martini et al. 2021) and erosion (Medeiros et al. 2016). Soil erosion can cause lower sugar cane yield, due to diminishing the accumulation and transformation of soil organic matter (SOM), supply nutrients, infiltration, retention, and supply water (FAO & ITPS, 2015). In addition, carry sediment and nutrients to water bodies (Melland et al. 2022; Portinho et al. 2021; Santos et al. 2021). Keeping the soil uncovered (bare soil/ exposed soil) is considered one of the main causes of erosion (Morgan, 2005). The maintenance of soil cover (i.e. straw maintained in sugarcane areas) reduces soil erosion by dissipating the kinetic energy of raindrops, decreasing the flow velocity (Bordonal et al. 2018; Li et al. 2021) and reduces the pressure from agricultural machinery on the soil, attenuating the increase of compaction (Martini et al. 2021). Maintaining 50 and 100% of the sugarcane straw on the soil surface reduces soil erosion by 68 and 89% respectively (Martins Filho et al. 2009). Thus, efficient techniques are necessary for soil monitoring, preventing and minimizing soil threats and promoting soil security in sugarcane production.

The traditional ways of monitoring soil management are mostly through fieldwork (Oliveira et al., 1995; Ceddia et al., 1999; Prado and Centurion, 2001; Biddoccu et al., 2016), which are slow, and with low potential for spatial analysis. More recently, new techniques have emerged, like site-specific fertilizer management (Sanchez et al. 2021), kriging to map compaction areas (Arruda et al., 2021), magnetic susceptibility to create management zones (Catelani et al. 2021), among others (Almeida et al. 2021; Hernandes et al. 2021; Luciano et al. 2021; Som-ard et al. 2021). Another technique approach is to relate erosion susceptibility maps to land use (Azareh et al., 2019; Cerri et al., 2013; Krishna Bahadur, 2009; Weill and Sparovek, 2008). All of them do not include in their scope evaluate how many times the soil was bare in a certain period, a possible indication of potential degradation. Especially in agricultural areas where bare soils are related to management practices such as tillage (Demattê et al. 2018)

In this aspect, remote sensing (RS) is a powerful environmental monitoring technique (Ben-Dor et al., 2009; Aguiar et al. 2011; Som-ard et al. 2021). The RS is based in the interaction of electromagnetic energy with matter, for example soil (Chabrillat et al. 2019). Viscarra Rossel et al., (2016) present these relationships at the laboratory level, followed by Diek et al. (2016) at airplane level and finally at satellite level with (Mulder et al., 2011). All these researches prove the important relationship between the bare soil and the reflected energy, allowing, through multi-temporal images, to detect bare soil for multiples applications (Demattê et al., 2020; Minhoni et al. 2021). Therefore, the RS by multi-temporal strategies allows relating and evaluating the presence of bare soils with management aspects that can make it more prone to erosion or degradation (Nascimento et al. 2021). This work strategy for monitoring soil management is even more relevant in countries with large territorial extension and high agricultural demand, due to high costs (Dube et al., 2017).

Therefore, our hypothesis is: the use of multi-temporal satellite images makes it possible to evaluate aspects of soil management and their changes, in sugarcane areas, and to relate them to soil security, especially those linked

to erosion. It is expected that: i) The expansion of sugarcane occurred mainly in soils more prone to erosion and was influenced by public policies and economic factors; ii) the amount of bare soils decreased after the implementation of the public environmental policy "Agro-environmental Protocol – Green Ethanol", which anticipated the end of sugarcane pre-harvest burning; iii) many areas with different levels of soil degradation propensity will be detected by satellite sensors during the crop field reform iv) Due to the expansion of sugarcane areas and crop management changes, there was an increase in bare soil areas in the rainy season.

4.2. Material and methods

4.2.1. Study area

The study area (Figure 1) has about 2,574 km² and is located in the Piracicaba region, a traditional sugarcane production area, in São Paulo State, Brazil (Brinkman et al. 2018; Cervone et al. 2018). The region's climate, according to the Köppen system, is classified as Cwa, a Humid Subtropical with dry winter and hot summer, with rainfall in the driest month in the winter minor than 40 mm, temperature of the coldest month between -3°C and 18°C and temperature of the hottest month grater equal 22°C (Alvares et al. 2013). Using climate data from the conventional meteorological station from the "Luiz de Queiroz College of Agriculture" (ESALQ/USP) from 1917 to 2021, we obtained that the mean annual precipitation is 1274 mm, being the wettest period (November to February) with a mean of 740 mm of rainfall and the driest period (June to August) with a mean of 102 mm of rainfall. The mean annual temperature is 21.7 °C. The mean temperature of the coldest month (July) is 17.6° C and of the hottest month is 24.8 (February).

The predominant soils of the region are Lixisols/Acrisols (~58%), Ferralsols (~19%), Leptosols (~13%) and Arenosols (~6%) with occurrence also of Cambisols, Nitisols and Gleysols (Oliveira et al., 1989).

4.2.2. Sugarcane crop management in study area

Sugarcane is a semi-perennial crop, harvested annually during an average of five years before replanting (Aguiar et al. 2011; Cheavegatti-Gianotto et al. 2011). The harvest season occurs from April to December (Dias and Sentelhas, 2017; Marin et al. 2021) (Fig. S1). The traditional period of sugarcane renewal (replanting) is carried out during two seasons in the center-south region, during February to April and September to November, being called "one year-and-half cane" or "18 months- cane", and "one-year cane" or "12 months-cane", respectively (Pagani et al., 2017). However, currently, with the increase of production areas and the longer period of harvests, sugarcane is planted throughout all year, thus, the terms "winter cane", and "two-summers cane" were created for sugarcane areas planted between May to August and December to January, respectively (De Maria et al. 2016). However, in center-south region, planting carried out in January can be incorporated into the 18 months-cane system (De Maria et al. 2016) (Fig. S2). Soil preparation (tillage) practices are performed only in replanting period (Barbosa et al. 2018), usually a conventional tillage (Cheavegatti-Gianotto et al. 2011; Barbosa et al. 2018). More details about the crop's production system in the center-south region are described by Aguiar et al. (2011) and Cheavegatti-Gianotto et al. (2011).

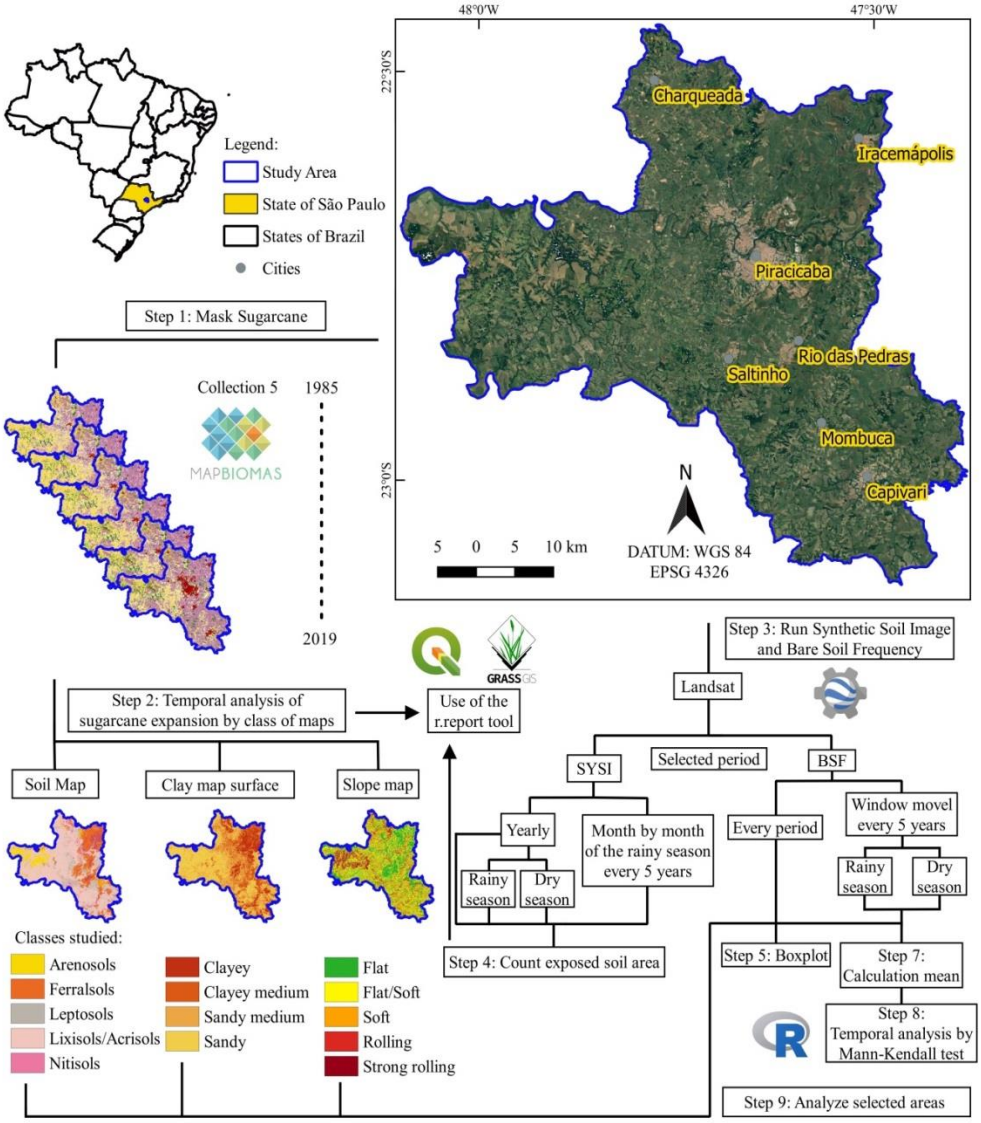

Figure 1. Study area and flowchart of methodology

4.2.3. Identification of sugarcane expansion

The identification of sugarcane cultivation areas from 1985 to 2019 was carried out using the annual land use and land cover classification maps available in Collection 5 of the Annual Use and Coverage Mapping Project of the Earth in Brazil - MapBiomas (MapBiomas, 2021). The maps with a spatial resolution of 30 m were used to select only areas with sugarcane and mask out other land uses/covers from the images. Finally, the sugarcane areas were separated into soil, granulometric and slope classes.

For it, we used a soil legacy map produced by Oliveira et al. (1989) (scale of 1: 100,000) rasterized by Mendes et al. (2021), with a spatial resolution of 30 m to select the main soil orders used for sugarcane cultivation. Therefore, soil orders found were Argissolos, Latossolos, Neossolos Litólicos, Neossolos Quartzarênicos, and Nitossolos (Santos, 2018), which are equivalent to Lixisols/Acrisols, Ferralsols, Leptosols, Arenosols, and Nitisols (WRB, 2014), respectively. The soil clay content map (0-20 cm) was also obtained from Mendes et al. (2021) and classified into five granulometric classes, usually used for sugarcane soil management in São Paulo State (Bellinaso et

al., 2021), as followed: sandy (<150 g kg-¹), medium-sandy (≥150 g kg-¹ to <250 g kg-¹), medium-clay (≥250 g kg-¹ to <350 g kg-¹) and clayey (≥350 g kg-¹). The slope map was obtained from the Shuttle Radar Topography Mission (SRTM) digital elevation model, using the algorithm proposed by Safanelli et al. (2020a) in the Google Earth Engine (Gorelick et al., 2017). Based on the slope values used for definition of soil conservation practices in sugarcane cultivation adopted in most of the center-south region, such as definition of the types of terraces used (Donzelli et al. 2018; Rotta and Zuquette, 2021)(Fig. S3), as well as the maximum slopes recommended for mechanized harvesting (15-17%) (Cheavegatti-Gianotto et al. 2011) and the characteristics of the study area (Sparovek and Schug, 2001; Pinto et al. 2003), the slope was classified as: flat (<6%), flat/soft (≥6% and <10%), soft (≥10% and <15%), rolling (≥15% and <20%) and strong rolling (≥20%).

4.2.4. Synthetic Soil Images and Bare Soil Frequency Images

We used a time series of satellite images from the Landsat 4 to 8 and the Geospatial Soil Sensing System (GEOS3) method, described in detail by Demattê et al., (2018) and Demattê et al. (2020), to obtain images of bare soil, called Synthetic Soil Images (SYSI) and images with the frequency of pixels with bare soil, called Bare Soil Frequency (BSF) in a pre-determined period between 1985 and 2019 (Figure 1) (i.e.: from 1985 to 2019, or from 1985 to 1989, or from January to December in a specific year, or from all January months from 1985 to 1989, etc.). For each chosen time interval a specific SYSI was created. To identify bare soil pixels from single satellite images, a set of rules were used based in spectral indices. These rules, coupled with quality assessment bands, removed cloud, cloud shadow, inland water, photosynthetic vegetation, and non-photosynthetic vegetation (crop residues) (Safanelli et al.2020b). Each pixel was classified as soil based on spectral indices: The Normalized Difference Vegetation Index (NDVI), with a threshold between −0.15 and 0.20 to mask out green vegetation, Normalized Burning Ratio (NBR2), with a − 0.15 and 0.15 to mask out crop residues, difference between bands 1 and 2 (B2 – B1) and bands 2 and 3 (B3 – B2) (Demattê et al., 2020; Demattê et al., 2018). Afterwards, the bare soil pixels were used to calculate, pixel-by-pixel, the median values of topsoil reflectance for single bands and obtain the final reflectance value (Demattê et al., 2020, Demattê et al., 2018). In addition, bare soil pixels within the time-series determined, were counted to create bare soil frequency image, representing the times that the soil was bare (Nascimento et al. 2021). SYSI had 30 m spatial resolution and six spectral bands harmonized as blue (0.45 - 0.52 μm), green (0.52 - 0.60 μm), red (0.63 - 0.69 μm), near-infrared (0.76 - 0.90 μm), short-wave infrared 1 (1.55 - 1.75 μm) and short-wave infrared 2 (2.08 - 2.35 μm).

First, we obtained annual SYSIs from 1985 to 2019 (called SYSI_1985, SYSI_1986, ..., SYSI_2019). For example, the SYSI_1985, is a Synthetic Soil Image created using bare soil pixels from Landsat images obtained between January 1, 1985 and December 31, 1985. A second step was to obtain annual SYSIs of specific periods classified as wet and dry seasons. We consider the four months with the highest historical average of rainfall as the rainy season (November to February) and the three months with the lowest historical average of rainfall (June to August) as the dry season. For example, the SYSI of wet season of 1990 (called SYSI_1990wet), is a SYSI created using bare soil pixels from Landsat images obtained in the months of January, February, November and December of 1990.

Finally, to assess whether there was an increase in the area of bare soil in the rainy season between 1985 and 2019, SYSIs were created for the months of November, December, January and February. As the rainy season corresponds to the period of greatest presence of clouds, which makes it difficult to detect bare soil pixels, these SYSIs were created for a period of five years (1985-1989, 1990-1994, 1995-1999, 2000-2004, 2005-2009, 2010-2014,

2015-2019) to minimize annual variations, reducing the effect of possible extreme years. In addition, this 5-year interval was chosen because it corresponds to the average period of crop replanting (section 2.2) and it has been used in other sugarcane crop monitoring studies (Aguiar et al. 2011). For example, the SYSI of January from 1985 to 1989 (Called SYSI_Jan_19851989), is a SYSI created using bare soil pixels from Landsat images obtained in the months of January 1985, January 1986, January 1987, January 1988 and January 1989, a similar approach was taken by Mzid et al. 2021, to create an average bare soil frequency image for the month of September across years 2016 and 2019.

The acquisition and use of bare soil images obtained by multi-temporal satellite images has been consolidated in recent years, varying only in some methodological aspects of acquisition (Shabou et al. 2015; Diek et al. 2017; Demattê et al. 2018; Fongaro et al. 2018; Rogge et al. 2018; Loiseau et al. 2019; Roberts et al. 2019; Demattê et al. 2020; Poppiel et al. 2020; Safanelli et al. 2020b; Silvero et al. 2021a; Tziolas et al. 2020). However, obtaining and using them in different periods within a certain time interval (as proposed in this work) was only addressed by Zepp et al. (2021) that generated bare soil masks covering Germany for seven time periods from 1984 to 2019.

Although the BSF is an image that represents how many times a single pixel was bare soil in a determined period. The calculation of the BSF, according to Demattê et al., (2020), is obtained by dividing the number of pixels classified as bare soil by the number of the same pixels with valid information, i.e., pixels that have clouds, shadows, or inconsistent values are masked (excluded) in the calculation. First, to relate the frequency of bare soil and classes of the thematic maps, we use the previous time series of Landsat images to create a BSF image of the period from 1985 to 2019. In addition, to analyze trends of increase or decrease of bare soil in specific periods (rainy and dry seasons described above), we also obtained BSF images by the 5-year moving count of bare soil pixels, that is, counting the bare pixels every 5-year + 1. For instance, the BSF for dry season of the year 1989 was obtained using images from the months of June, July, August and September of years 1985 to 1989, and the BSF for dry season of the year 1990 from images from the months of June, July, August and September of years 1986 to 1990.

The most used methodologies for creating bare soil images mentioned above also generate BSF images (Demattê et al. 2018; Rogge et al. 2018). However, there are still few works that have used this resource to monitor and analyze the frequency of bare soil (Demattê et al. 2018; Demattê et al. 2020; Mzid et al. 2021).

Both the BSF images and the SYSIs were generated using the Google Earth Engine (GEE) cloud platform (Gorelick et al., 2017), which provided the processing structure and the Landsat series collection of surface reflectance images from 1985 to 2019 (Landsat 4 Thematic Mapper (TM) (1985-1993), Landsat 5 TM (1985–2012), Landsat 7 Enhanced Thematic Mapper Plus (ETM+) (1999–2019) and the Landsat 8 Operational Land Manager (OLI) (2013–2019).

4.2.5. Data analysis

4.2.5.1 Land use and bare soil areas

Initially the areas of sugarcane, pasture and mosaic of agriculture and pasture classes were calculated, for each year from 1985 to 2019, using the Collection 5 of the Annual Use and Coverage Mapping Project of the Earth in Brazil - MapBiomas (MapBiomas, 2021). In a second moment, the sugarcane annual area (1985 to 2019) was calculated for each class of each thematic map (Soil, Granulometry and Relief). Using each annual SYSI and the map of sugarcane areas for the same year, the area of bare soil in the sugarcane crop for each year was calculated. With this information, the percentage of bare soil areas in the sugarcane areas was calculated for each year. The same approach was carried out with the rainy and dry period SYSIs from 1985 to 2019 and in the SYSIs of de wet season

months from periods of five years. To perform the sum of these areas, the *r.report* tool present in the Qgis 3.16.10 software was used.

4.2.5.2 Bare Soil Frequency and thematic map classes

Using the BSF image from 1985 to 2019 and the Soil, Granulometric Classes and Relief maps, boxplots were obtained using the *ggplot2* package in R software (Wickham, 2016). In addition, a Pearson correlation test was performed between BSF values and clay content and slope, for which the *corrplot* package in R software was used (Wei and Simko, 2021).

4.2.5.3 Temporal analysis of the Bare Soil Frequency

We calculate the mean value of BSF from 1989 to 2019, for each class of each thematic map, using the BSF images obtained by the 5-year window moving count for the two periods, the wet and the dry seasons. The 5-year window was chosen for the same reasons as described above (section 2.4). To obtain the mean values we used the *zonal statistics tool of the raster layer* present in the Qgis 3.16.10 software. Then, we submitted the time series to the test of tendency of Mann-Kendall (MK) (Kendall, 1975; Mann, 1945). The test defines if a variable consistently changes through time or has an increasing or decreasing trend and can be performed on normally or not normally distributed data, which makes it a robust test.

The MK test started by applying an indicator function (sgn) on the difference between all possible pairs of measurements (Eq. 1). The value measured in time j (xj) was subtracted from the values previously observed (xi), considering that time j > i. Then, these differences were used to define Kendall's statistics S (Eq. 2):

$$sgn(\theta) = \begin{cases} +1 & for(\theta) < 0 \\ 0 & for(\theta) = 0 \\ -1 & for(\theta) > 0 \end{cases} \quad (1)$$

$$S = \sum_{i=1}^{n-1} \sum_{j=i+1}^{n} sgn(xj - xi) \quad (2)$$

where n is the length of the dataset. Based on S, the variance V (S) (Eq. 3) and the normalized test statistics Z (Eq. 4) were calculated:

$$V(S) = \frac{1}{18}[n(n-1)(2n+5)] \quad (3)$$

$$Z = \begin{cases} \dfrac{S-1}{\sqrt{V(S)}} & ifS > 0 \\ 0 & ifS = 0 \\ \dfrac{S+1}{\sqrt{V(S)}} & ifS < 0 \end{cases} \quad (4)$$

where the null hypothesis of no trend was rejected, if the absolute value of Z was higher than the theoretical value of $Z(1-\alpha/2)$ (at 0.05 level of significance). A positive S value indicated an increasing trend while a negative S indicates a decreasing trend. The magnitude of the trend was represented by the Sen's slope (Sen, 1968) calculated over the time period. To perform the MK test the *rkt* package in R software was used (Marchetto, 2021).

4.3. Results and Discussion

4.3.1. Expansion of sugarcane land use

The cultivation of sugarcane in the studied region has expanded over the years, from a planted area of 78 thousand ha in 1985 to almost 116 thousand ha in 2019 (an increase of 48% - Figure 2a), lower than Brazil increase since the 1980s (150%) (Cherubin et al. 2021b). The most part of this expansion occurred in São Paulo State (Franco et al. 2015; Cherubin et al. 2021b). Meanwhile the pasture dimension was reduced, from 75 to 38 thousand ha in the same period. Today, the areas classified as agriculture and pasture remained without major changes. Results are in agreement with other regions evaluation (Loarie et al. 2011; Hernandes et al. 2021; Cherubin et al. 2021b). Adami et al. (2012) for whom the expansion of sugarcane over pasture in center-southern Brazil occurring 70% in degraded pastureland. Jaiswal et al. (2017), Spera et al. (2017), and Oliveira et al. (2019) consider that the most sustainable way for Brazil to expand sugarcane areas would be to occupy areas of degraded pastures. Different authors point out that the culture tends to expand in areas close to the mills, to reduce harvesting and logistic costs, even if this implies expanding a wide range of soil and slope conditions (Caldarelli and Gilio 2018; Hernandes et al. 2021; Rocha and Sparovek et al. 2021).

The increase in sugarcane areas occurred mainly in the sandy and medium sandy soils types, with the expansion of approximately 248.5 and 64.4%, respectively (Figure 2b). In the loam-clayey, the increase was only 9.1% and in the clayey one, there was a reduction of 4.6% (Figure 2b). Catelan et al. 2022 correlated crop productivity with soil magnetic susceptibility, which is closely linked to the amount and type of clay. Regarding soil types (classification), sugarcane advanced significantly in the Lixisols/Acrisols, Leptosols, and Arenosols, with 92.9, 72.2, and 540.6%, respectively (Figure 2c-d). In the Ferralsols, there was an increase of only 2.5% and in Nitisols we see a reduction of 11.9% (Figure 2c-d). These expansions are in agreement with (Donagemma et al., 2016) for whom the main central Brazilian area is expanding under sandy soils. These soils are extremely fragile and need special necessities such as soil conservation, different management, fertilizers and carbon care, cover crops, to consolidate its use in this expansion frontier of agriculture, and maintain its health (Carneiro et al., 2020). Despite this, other soils are under threat such as because results indicate the expansion of sugarcane to areas of greater susceptibility to water erosion (98.4% Strong rolling). Indeed, these areas have presence of textural gradients (Lixisols/Acrisols), shallow (Leptosols, figure 2d), lower clay contents (Arenosols), and higher slopes (Sparovek and Schnug, 2001). The result of the expansion in these types of soils are impacts on less soil water infiltration, low soil water storage volume, low aggregation, and higher surface runoff speed and strength, respectively. Lixisols/Acrisols are the most ones prone to erosion (Figure 2c) (Corrêa et al., 2019). Oliveira-Andreoli et al. (2021) consider sugarcane areas associated with sandy soils and high declivity to be of high fragility. Silva et al. (2021) evaluating the production of sediments in a watershed, showed that areas with sugarcane cultivation in undulating terrain, were the ones that generated the greatest amount of sediments. Therefore, conservation agriculture practices and the renewal of sugarcane plantations must be prioritized in these areas at the ideal time for each type of soil class.

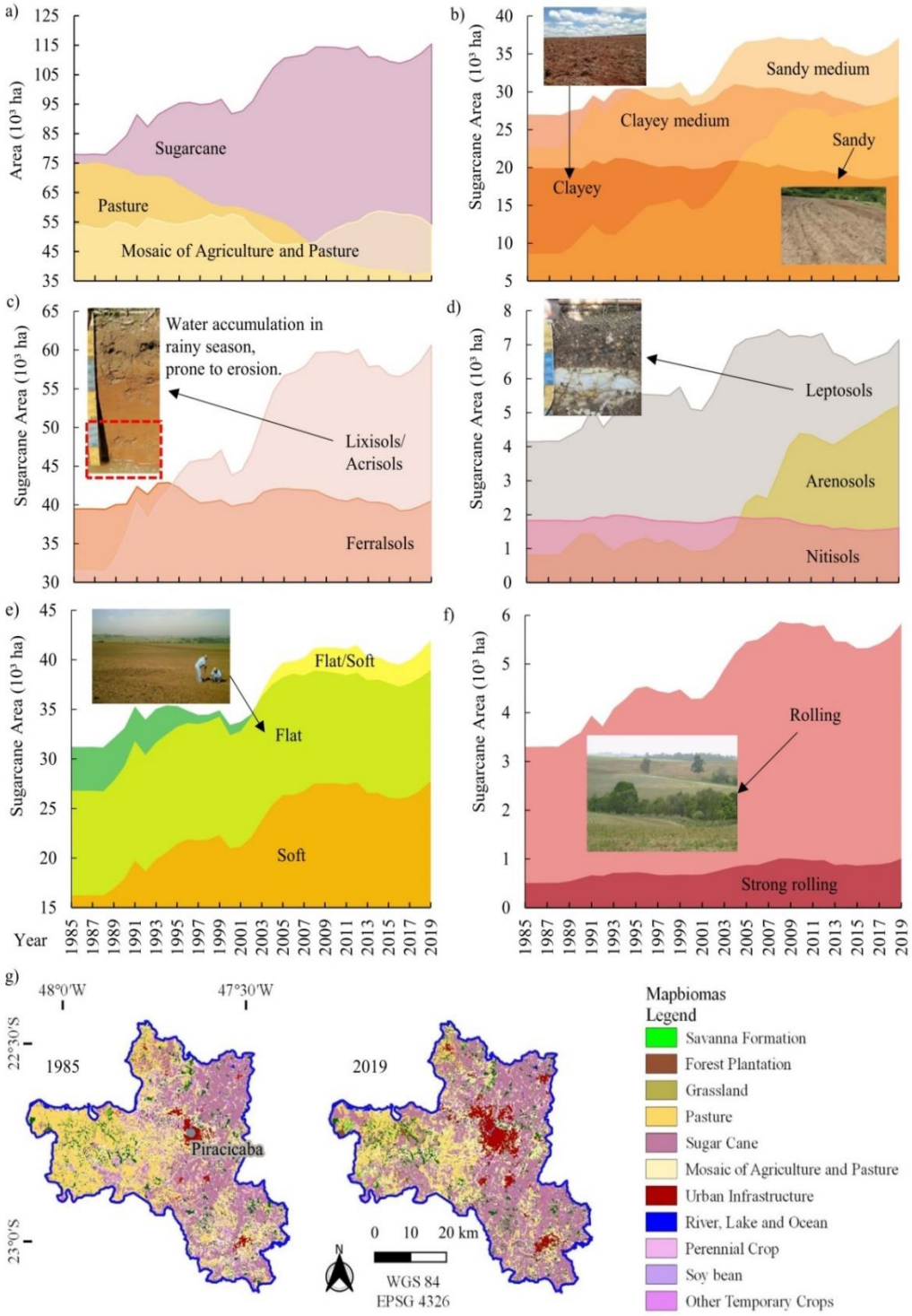

Figure 2. Area of the main land use classes from 1985 to 2019 (a); sugarcane cultivation area in clay (b), soil (c-d) and slope (e-f) classes from 1985 to 2019; Land use and land cover map for the year 1985 and 2019 (g).

4.3.2. Historical moments and bare soil area

Figure 3a shows a temporal alteration on sugarcane management, for which needs an historical explanation. The sugarcane production systems (Vitti and Prado, 2012) have undergone adaptations over the years, mainly motivated by the advance of mechanized harvesting in the sugarcane fields (Aguiar et al., 2011; Demattê and Demattê, 2009). This initiative began in 1996, and intensified after the creation of state law 11.241 in 2002, that

established a deadline for the end of pre-harvest burning, and mainly due to the Agro-environmental Protocol ("Green Ethanol Protocol") for the sugar-energy sector signed in 2007, which essentially provided the anticipation of this deadline (Aguiar et al., 2011).

This intensification is proven in the comparison of burning and non-burning area studies in the state of São Paulo (de Aguiar et al., 2009; Rudorff et al., 2010). Authors presented in the 2006/2007 33.5% of the area harvested without the use of fire and in the 2008/2009 increased to 49.1%. Valente and Laurin et al. (2021) highlight the effectiveness that the protocol had in reducing fires. Although it was not the main objective, the effectiveness of the Green Ethanol Protocol brought as another benefit, the maintenance of soil covers through the residue left after harvest (straw). Today, harvest 2020/2021 authorizations for burning were only 0.20% of the total sugarcane area in the state of São Paulo (Secretary of Infrastructure and Environment, 2021). Also, according to UNICA, (2021), there was an increase of 398% in the number of harvesting machines in the state of São Paulo from 2007/2008 to 2016/2017. Recently, other public policies have been gaining prominence and may contribute to the improvement of soil conservation management in the crop, such as the "Greener Ethanol Protocol" (Secretary of Infrastructure and Environment, 2021) and the Renovabio (Klein et al., 2019; Carvalho et al. 2021; Grangeia et al. 2022).

These historical facts and public policies explains the increase of raw sugarcane that allows the presence of straw covering the ground (Figure 3a). After 2006 a process of reducing areas with bare soil began, leaving an annual average of 53% in the period 1999-2006 to an average of 23% in the period 2012-2019. This information is also perceived when analyzing the dry season that is inserted in the harvest period (Figure 3b), whereas in the rainy season this tendency does not exist (Figure 3c), as part of the culture practices. In the off harvest season (rainy period) the area of bare soil is a consequence of the renovation (replanting) of the culture (renovation is about each 5 years), or areas that suffered pre-harvest burning and crop regrowth was not enough to cover the soil. Thus, in the past, despite the soil not being prepared, it was exposed between harvesting and regrowth, so the GEOS3 method (SYSI creation) detected these areas.

The increment of crop residue (Figure 3b) brought benefits for soil conservation and quality. According to Bezerra and Cantalice, (2006) and Valim et al. (2016), straw promotes a reduction in the impact of raindrops and surface runoff, thus resulting in less disaggregation of soil particles and reduction of erosion processes. Martins Filho et al., (2009) found that the water infiltration rate in a Red-Yellow Lixisol is higher in areas with 50 and 100% coverage by sugarcane plant residues than in areas with its absence. A reduction in the maximum temperature of the soil is also observed (Santos et al. 2022; Corrêa et al., 2019), and larger soil moisture conservation (Gmach et al., 2019). In addition, over the cycles, the increase in soil organic carbon (SOC), and CEC contents occurs, thus improving the chemical quality of the soil (Correia and Alleoni, 2011; Signor et al., 2016, 2014).

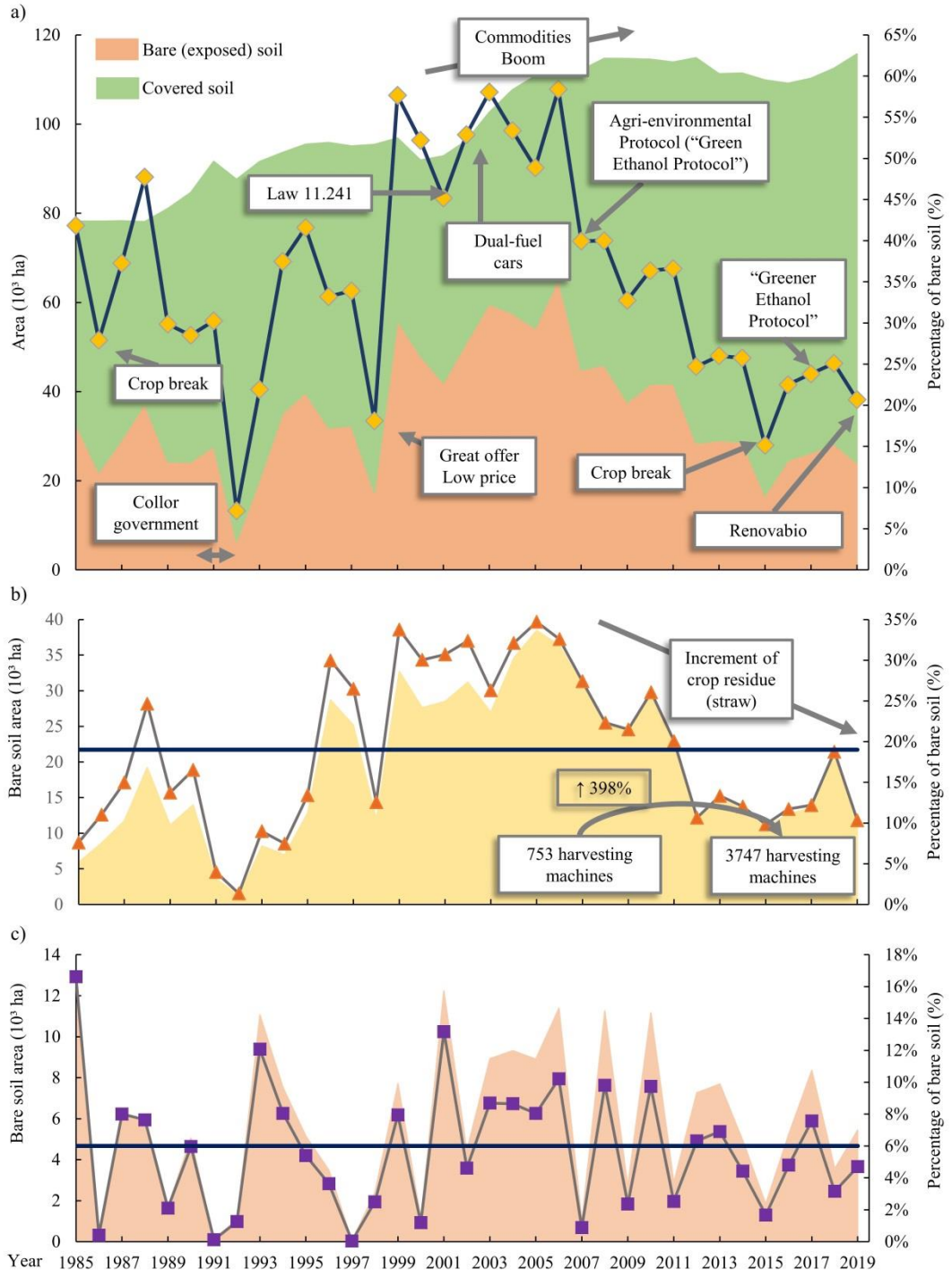

Figure 3. Area of bare and covered soil (colored areas) and percentage of bare soil (line with points) in sugarcane area (a); area and percentage of bare soil in sugarcane areas in the dry season (b); and in the rainy season (c).

In addition to the changes presented as a result of the advance of mechanization in sugarcane fields, the annual variation in the area and percentage of bare soil is affected by climatic and economic moments that occurred during the period (Fig. 3). In years of low rainfall, as occurred in the region in 1985 and 2014, the low area of soil discovered in the following year is notorious due to the crop failure. Low production leads to a reduction in the income of the producer, who, without capital, reduces the areas of renewal (replanting). (Fig. 3a). The fall of bare soil in 1986 is also motivated by the severe economic crisis that Brazil was going through and the drop in oil prices, which led the government to reduce incentives for ethanol production (Stolf and de Oliveira, 2020; UNICA, 2021).

During the Collor government (1990-1992), Brazil was going through a serious economic crisis (Fig. 3a). Thus, in the sugarcane sector, there was a reduction in incentives, high production cost, and a process of deregulation, which began with the extinction of the IAA (Institute of Sugar and Alcohol). The IAA was responsible for the quota system, which defined how much each mill could produce during the harvest, so the IAA planned and monitored all that production (Bray et al., 2000). Thus, with the extinction of the institute, the quota system was abolished, thus generating a period of instability in the sector until they managed to coordinate on their own (Stolf and de Oliveira, 2020). So, all these factors motivated the reduction of bare soils in this period.

In Figure 3a, it is possible to observe the moments of bare soil increase, as occurred in the years 1999 to 2006. This was motivated by the high perspective that the sector was going through with the increase in the prices of agricultural commodities worldwide. This was also impacted by the insertion of commercial dual-fuel cars (ethanol and gas, the called ´flex´) in 2003 (Caldarelli and Gillio, 2018). Schlindwein et al. (2021) point out that the main cause of sugarcane expansion in Brazil is due to the successful adoption of flex-fuel vehicles. Thus, new areas were transformed for the cultivation of sugarcane, and the renovation areas were greater, since the producers wanted to guarantee higher yields as a result of the good prices at the time. The early 2000s are known in the agricultural sector as the "Commodities Boom". Between 2007 and 2008 occurred a rapid internationalization of the sector, which also contributed to the expansion (Caldarelli and Gilio, 2018). The 2009 economic crisis that brought stagnation and soon after (Caldarelli and Gilio, 2018), in 2012, the government interference in gas prices, which impacted on alcohol and broke more than 100 mills. In 2018, this policy changed again and ethanol started new increasing era. Therefore, it is possible to verify that economic factors, laws and public policies have a direct impact on sugarcane production, corroborating with Catañeda-Ayarza and Godoi (2021), which ends up interfering more or less sharply with soil safety in sugarcane-producing areas.

4.3.3. Distribution of bare soils in months of risk

The three situation of surface (bare soil, straw after harvesting and adult sugar cane) are illustrated in figure 4a. The rainy season in São Paulo State concentrates 60% of the intra-annual erosivity, with the highest mean monthly values observed in January (Teixeira et al. 2021). It is possible to verify a change over time in the distribution of areas with bare soil during the rainy season (Fig. 4b). For the month of November there is a reduction in the area over time. Although, November continues to be the month, of the rainy season, with the highest area of bare soil. This can be explained for two reasons, due to the increase in mechanized harvesting along the time, which led to a decrease in bare soil areas due to pre-harvest fire in October and November, or a change in the management of crop planting in the region, leaving a system from "12 months-cane" planting to "18 months-cane". This second point can be reinforced by the increase, along the time, of bare soil areas in December, January and February. The planting season is considered the most impacting for soil conservation in the sugarcane crop (Machado et al. 2021). Li et al. (2021) demonstrated that erosion and nutrient losses were 2–3-fold higher in plant cane than in rattons. Teixeira et al. (2021) reinforced the importance of information on rainfall erosivity and erosivity density in soil conservation planning for sugarcane activity in the State of São Paulo.

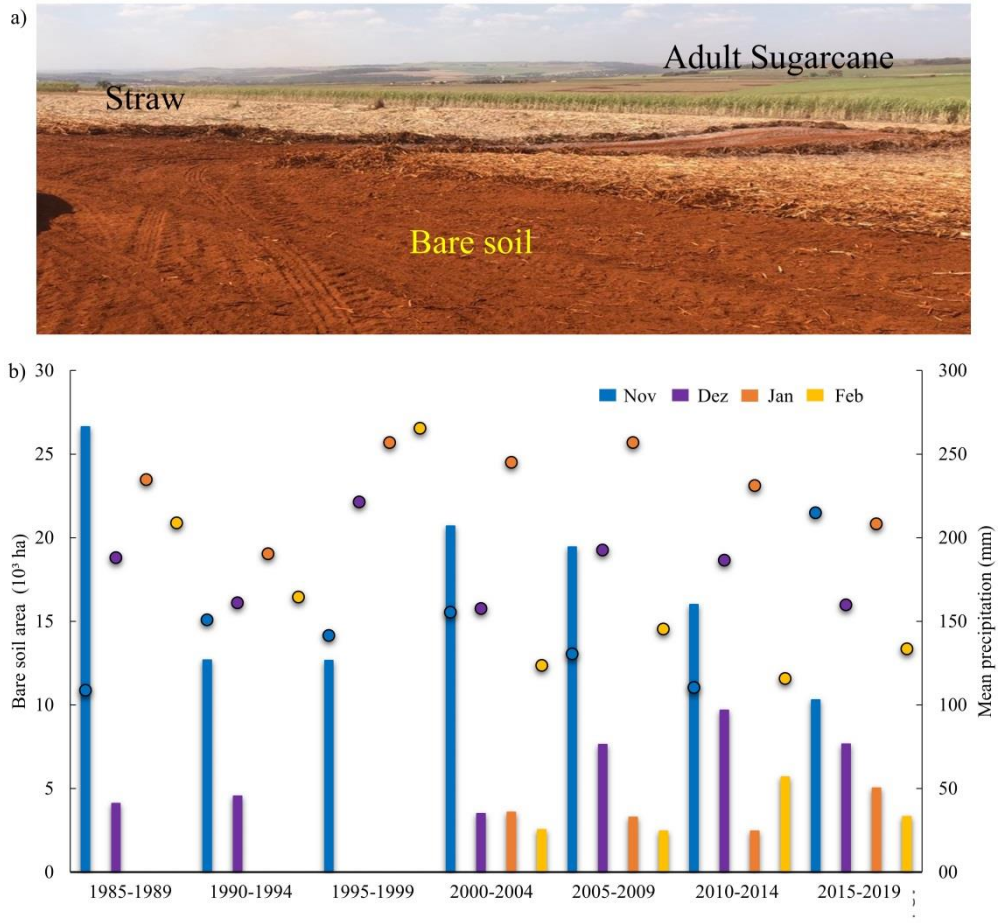

Figure 4. Illustration of three situations, bare soil, straw after harvesting and adult sugar cane (a). The bare soil area (bar) during the rainy season over the years every 5 years, and historical average precipitation (point) (b).

The progress of renovation (replanting) areas, especially in December and January, which present intense rainfall and a greater volume of precipitation, requires the correct planning that will be reformed due to the high propensity to erosion (De Maria et al., 2016). It is recommended that only flat, clayey, fertile, and high CAD areas be replanted in these months (De Maria et al., 2016). Traditionally, in the renovation of a sugarcane area, the first step is to turn the soil over, (plowing, subsoiling and harrowing) due to physical, chemical, or biological problems (conventional tillage), which promotes the breakdown of soil particles and soil organic carbon oxidation (Cerri et al., 2011; Bolonhezi et al., 2019; da Luz et al., 2020). But the presence of bare soil in the rainy season could increase soil lost by erosion (Corrêa et al., 2019). Then, minimum, no-tillage or localized tillage (preparing the soil only in the planting line, promoting greater maintenance of the straw) and use of cover crops should be considered (Carneiro et al., 2020). According to studies by Prove et al. (1995), the average soil loss for conventional tillage systems was 148 t ha^{-1} $year^{-1}$, whereas in the no-tillage system it was less than 15 t ha^{-1} $year^{-1}$. Also, according to studies in the Ferralsols during 44 days, the conventional tillage releases 954.79 kg ha^{-1} of carbon to the atmosphere, while that reduced tillage and minimum tillage releases 141 and 15.2 kg ha^{-1}, respectively (Silva-Olaya et al., 2013). However, some authors report that the sector still resists the adoption of more conservationist soil preparation methodologies (Fuentes-Llanillo et al. 2021).

Different studies have pointed out the importance of soil conservation practices in the sugarcane crop, mainly due to the production of sediments and pollutant transport by runoff. Amorim et al. (2021) studying the

origin of sediments from a basin in northeastern Brazil, detected that the second largest source of sediments was the sugarcane crop. Machado et al. (2021) studying the variation of runoff coefficient in a watershed in Piracicaba region, largely occupied with sugarcane, pointed out the impact of soil management on the runoff produced. Anjinho et al. (2021) pointed to agriculture (sugarcane) and soil type were key factors to the erosion and sedimentation susceptibility. Furlan et al. (2021) evaluated the impact of sediments from sugarcane area on wetlands. In Australia, there is great concern about soil management practices in the sugarcane crop, mainly due to the potential impact of sediments and polluting compounds on the Great Barrier Reef (Vilas et al. 2022).

4.3.4. Soil types and bare soil frequency: vulnerability to degradation

We observed a high spatial variation in the frequency of bare soil in the period from 1985 to 2019 in sugarcane areas (Fig. 5a). In the northeast there is a lower bare soil frequency (lower exposure frequency) when compared to the northwest and southwest sites, which have higher frequencies related to the predominant soil types and clay contents (Fig. 5b-c). The distribution of BSF in relation to clay contents presented a negative correlation of -0.34, while, relating to slope, was -0.08, thus showing a greater dependence on the clay (Fig. 5c-d). Catelan et al. (2021) and Marques et al. (2014) pointed out a positive correlation between sugarcane yield and soil clay content. Productivity is the main factor considered in the need to replant sugarcane (Cheavegatti-Gianotto et al. 2011), then, the maintenance of productivity implies, as a consequence, less soil tillage over time. Therefore, any practice that contributes to the increase in the longevity of the sugarcane crop, will imply a greater number of ratoons and will reduce the need for replanting, when there is more disturbance of the soil, and consequently less environmental impact (Chagas et al. 2016). May be cited as practices that contribute to increased longevity: compaction control (Lima et al. 2022; Panziera et al. 2022), use of varieties in suitable production environments (Barbosa et al. 2021), adequate fertilization (Pancelli et al. 2015), harvest performed with adequate speed (Martins et al. 2022), irrigation (Walter et al. 2014), among others

The Arenosols, present in the northwest region (Fig. 5b), are located in flat to soft undulating reliefs and present a high rate of water infiltration into the soil. However, these soils require attention because they are sandy texture and low levels of SOM, therefore, they have a low particle aggregation capacity, which gives them a high propensity to erosion, especially rill and gully erosion (Carneiro et al., 2020; Cunha et al., 2011; Santos, 2018; Thomaz and Fidalski, 2020). The low levels of SOM plays a fundamental role in its quality, such as low CEC, slow release of P, N, S nutrients, lower availability of micronutrients and water retention (Cunha et al., 2011). This soil type had the highest BSF mean, 7.02% (Figure 5e), which is harmful to the maintenance or increase of SOM, since maintain the soil uncovered promotes SOM decomposition and other impacts (Cerri et al., 2011; Cherubin et al., 2021; Morais et al., 2020; Popin et al., 2020). Sayão et al. (2020) demonstrated that bare sandy soils, from the same region of our study, had the highest surface temperature which contributes to an even greater SOM mineralization.

These observations are alarming since the management adopted for Arenosols, in the studied region, indicate a soil degradation cycle (Fig. 6). Breaking this cycle can be promoted through the adoption of management practices such as: greater input of organic and mineral fertilizers, as vinasse and filter cake, cover crops/green manure, intercropping (Shen et al. 2019; Singh et al. 2021), minimum or no-tillage (Martíni et al. 2021), practices that enable an increase in the number of ratoons (longevity) and maintenance of the straw. Cherubin et al. (2021a) concluded that sandy soils were more prone to soil health degradation, when straw is removed and the healthier soils were associated with higher sugarcane yields. Shukla et al. (2020) emphasize that maintaining soil organic carbon and

increasing crop productivity is an inseparable issue, without addressing both issues simultaneously, the sustainability of production system could not be achieved.

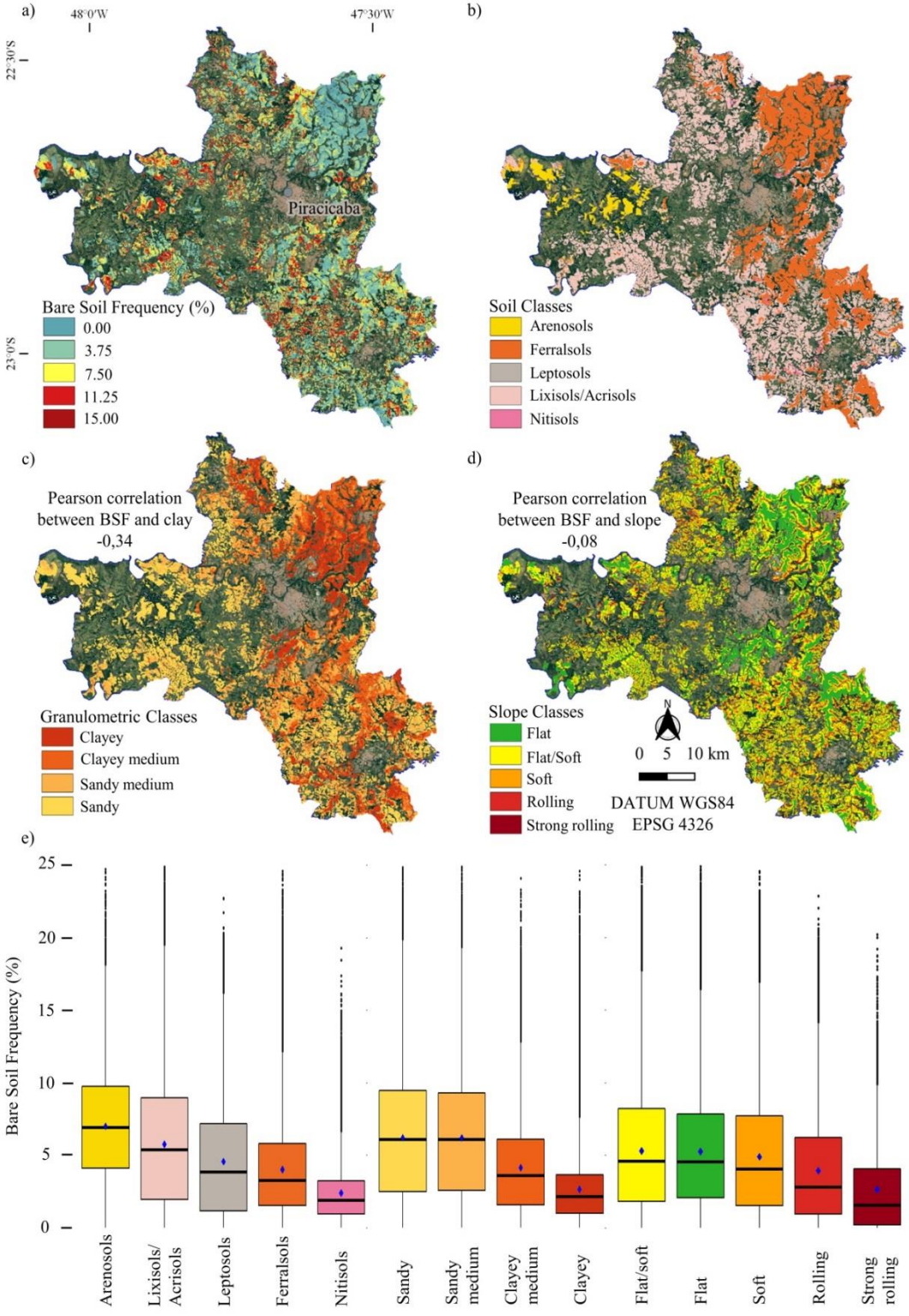

Figure 5. Bare soil frequency map from 1985 to 2019 for sugarcane areas (a); Soil (b), Granulometric classes (c) and Slope classes (d) maps for sugarcane areas; Boxplot of bare soil frequency for maps classes (e).

In the northwest and southwest regions, Lixisols/Acrisols are the main soil classes (Fig. 5b), and present the second highest average of the BSF (5.78%). These soil types are susceptible to erosive processes, as they are located in more rugged reliefs and have increase of clay in-depth, resulting in a textural gradient, which makes it difficult for water to infiltrate, and increasing surface runoff (Fig. 2a), to finally transport the eroded sediment (Jarbas et al., n.d.; Santos et al., 2018; Zaroni and Santos, n.d.). According to Martins Filho et al. (2009) an Lixisol without vegetation cover, there is an enrichment ratio in the eroded sediment of 2.7 (SOM), 3.8 (P), 1.3 (K), 3.9 (Ca), and 2.9 (Mg) times when compared to soil 100% covered, i.e., resulting in a greater loss of SOM and nutrients when to bare.

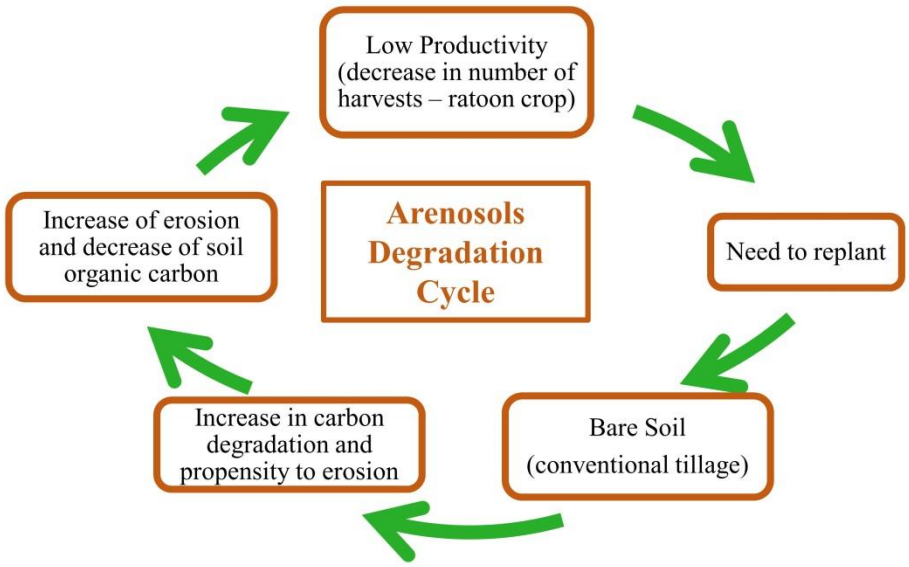

Figure 5. Bare soil frequency map from 1985 to 2019 for sugarcane areas (a); Soil (b), Granulometric classes (c) and Slope classes (d) maps for sugarcane areas; Boxplot of bare soil frequency for maps classes (e).

Leptosols (Fig. 2d) located in 6.21% of the area (Fig. 5b) are soils with a low degree of pedogenetic development, and low depth due to the mandatory contact of the A horizon to the R/C/Cr horizons within 50 cm of the surface and are found in strong declivity reliefs. Such characteristics increase the propensity to erosion (Curcio et al., n.d.; Santos et al., 2018). The presence of lithic contact prevents water infiltration into the soil and results in a low storage volume, favoring surface runoff. This gains strength due to the high declivity, so its BSF mean of 4.58% in the period, (Fig. 5e) favors it is degradation (Weill and Sparovek, 2008).

Finally, the Ferralsols and Nitisols had the lowest BSF averages, 4.02 and 2.42%, respectively (Fig. 5e). Ferralsols are deep, well-drained, with strong profile percolation and low fertility. Clay contents range from 150 to 800 g kg-1 and are mostly found in flat to soft undulating reliefs (Fig. 5b) (Santos, 2018; Sousa and Lobato, n.d.). Due to these characteristics, the propensity to degradation, such as nutrient deficiency and erosion, occurs mainly in sandy-medium Ferralsols, which have lower aggregation and lower SOM (Carneiro et al., 2020; Donagemma et al., 2016; Sousa and Lobato, n.d.). Thus, as with Arenosols, greater coverage of these soils is necessary to promote the maintenance and increase of SOM, as well as water retention to reduce nutrient leaching. In the northeast sector are found most of the Ferralsols (Fig. 5b) with higher clay contents (Fig. 5c) and lowest BSF (Fig. 5a). It is in agreement with that was pointed out previously, that, there is a high correlation between clay contents, productivity and the need of replant.

On the other hand, Nitisols are also deep and well-drained soils with good structure, and clay contents (above 350 g kg^{-1}), without the presence of textural gradient, and are found in smooth wavy to strong wavy reliefs (Santos and Zaroni, n.d.; Santos, 2018). In areas with more sloping relief, there is greater susceptibility to erosion processes, so keep the soil uncovered in these regions must be associated with other conservation practices to ensure soil security (Santos and Zaroni, 2021). Mechanized harvesting without previous burning provided the maintenance of cover in these soils, however brought problems with soil compaction, especially in clayey soils, harming its porosity and density (Braunack et al., 2006; Oliveira et al., 1995). Some authors point out that, in some cases, up to 60% of the area may be affected by compaction (Souza et al., 2014; Esteban et al. 2019). The physical impediment caused by the high traffic of machines impairs the infiltration of water into the soil, promoting a greater volume of surface runoff, which can result in erosive processes (Ceddia et al., 1999; Fiorio et al., 2000; Prado and Centurion, 2001). This surface runoff with the presence of sediments is harmful also to aquatic systems, as the deposition of these sediments in rivers, lakes or reservoirs impacts water quality and ecosystem biodiversity (Politano and Pissarra, 2005). In addition, compacted soils present unfavorable conditions for the growth and development of the sugarcane root system (De Sousa et al. 2019), thus resulting in lower productivity (Arruda et al. 2021) that will contribute to the producer's decision-making for the anticipation of sugarcane replant, i.e., reducing longevity. Marin et al. (2019), appointment that the negative effects of mechanical harvest on soil structure is one aspect related to yield decline in commercial sugarcane areas. Another negative aspect is that conventional soil preparation is often seen as the main way to reduce compaction, although different studies have shown its low effectiveness, especially after the first harvest (Guimarães Júnnyor et al. 2019; Martíni et al. 2021). Some compaction mitigation practices are: the adoption of controlled traffic (De Sousa et al. 2019; Barbosa et al. 2021), spacing and machine gauge adjustment (Rossi Neto et al. 2018; Esteban et al. 2019)

4.3.5. Monitoring the bare soil frequency

Monitoring the average frequency of bare soil in two different seasons, rainy (Fig. 7a,c,e) and dry (Fig. 7b,d,f), showed a downward trend in the two periods, i.e., the BSF average has declined over the years (Fig. 7g). In the dry season, only in the second period there was a downward trend, and in the first, there was an upward (Fig. 7g). The Arenosols did not trend in the first periods of the dry and rainy season and the Nitisols either did not in the second period of the rainy season.

The tendency to reduce the frequency of bare soil in the rainy season is of great importance for their conservation and soil security. This reduction shows the better planning and understanding of the sector in which lands can be bare at certain times of the year. This could be related to the advancement of the concept of "Production Environments", that considers the interaction between soil, climate, and plant (Barbosa et al. 2021; Catelan et al., 2021; Demattê and Demattê, 2009), use of cover crops (Carneiro et al., 2020); migration from 12 months-cane planting, to 18 months-cane, adoption of MEIOSI (Portuguese acronym for Methods Inter-rotacional Ocurring Simultaneously) planting system when it is possible (Oliveira et al. 2018). According to Landell et al. (2003), for adequate knowledge of the production environment in sugarcane culture, it is necessary, first, to classify the given soil. Besides, Donzelli et al. (2018) emphasizes the importance of an adequate soil mapping for production environments classification and soil groups for agricultural management.

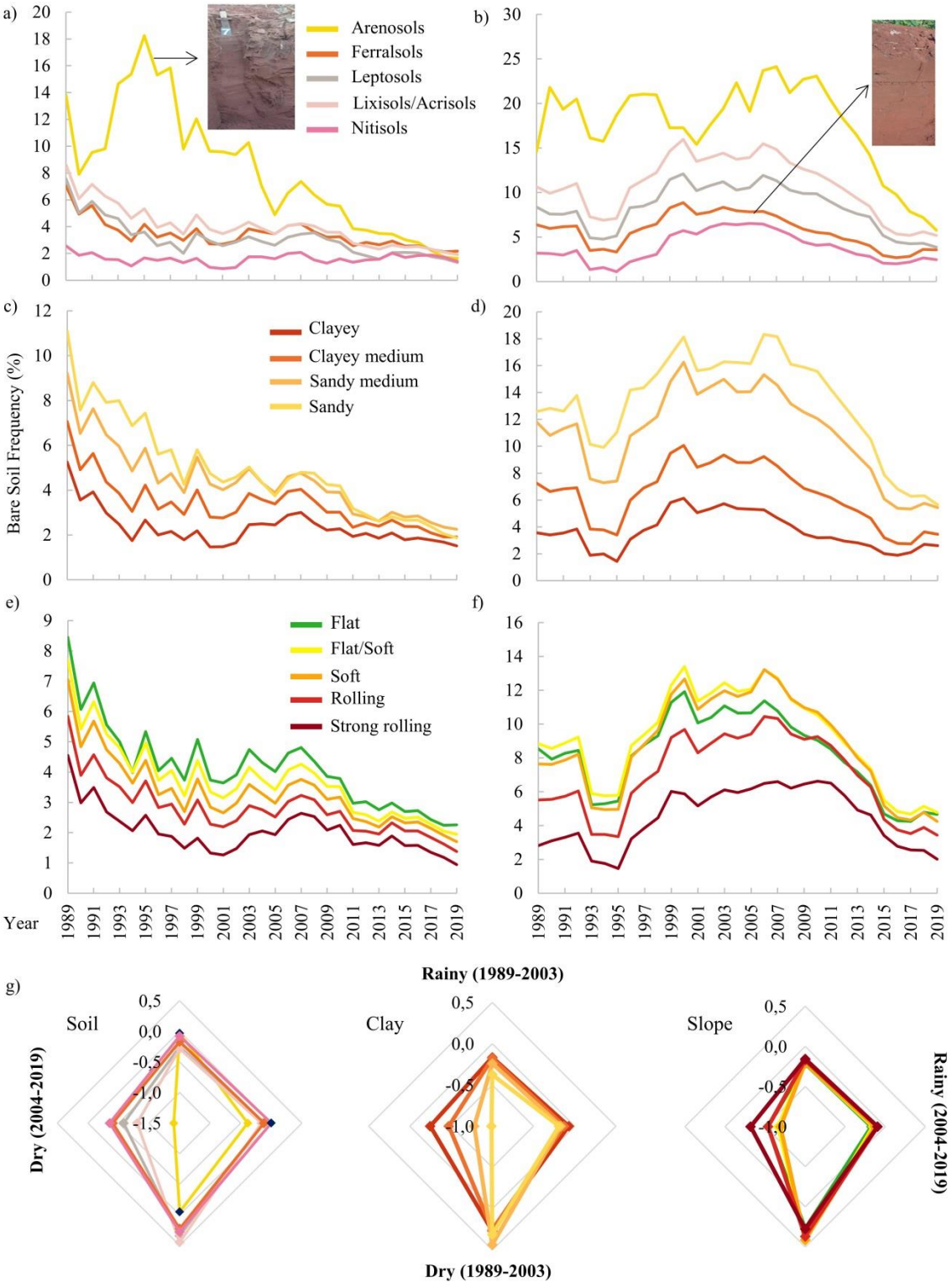

Figure 7. Mean Bare soil frequency in rainy season (a-c-e) and dry season (b-d-f); Magnitude of the trend by Sen's slope (g).

In particular, the Lixisols/Acrisols and Leptosols (Fig. 2c,d), that presents a high propensity to degradation when bare (Corrêa et al., 2019; De Maria et al., 2016), presented a downward trend of 0.28 and 0.25% rainy season^{-1} year^{-1} in the first period and 0.16 and 0.14% rainy season^{-1} year^{-1} in the second period, respectively (Table 1). The Arenosols (Fig. 7a), indicated a significant downward trend of 0.38% in the second rainy season^{-1} year^{-1} (Table 1). However, it is the soil class with the highest BSF for all period. Ferralsols presented low variation (Fig. 7a,b). To

keep the soils uncovered promotes an increase in temperature, which leads to the acceleration of SOM decomposition (Silva-Olaya et al., 2013), and consequently, affecting soil biota (Demattê et al., 2020). Therefore, the upward trend presented in the first period, motivated by the increase of newly cultivated areas, was detrimental to soil conservation. However, the downward trend in the second period, caused mainly by the advance of mechanized harvesting, shows the improvement in the biological and chemical conditions that the sector has been providing to its soils. In particular, soils of the sandy and sandy medium clay classes showed a downward trend of 0.99 and 0.78 dry season^{-1} year^{-1}, respectively (Table 1). In general, such classes do not have high levels of SOM, therefore, promoting their maintenance or increase is of paramount importance for soil quality, providing greater particle aggregation, increasing CEC and nutrient release and increasing water retention.

4.3.6. Site-specific monitoring in an eroded area

We made a site-specific evaluation regarding the erosion identification (Fig. 8a). The site had a surface with clay content of 170 g kg^{-1}, a slope of 11.5%, and classified as Lixisols/Acrisols. This information infers that it is an area of great erosion susceptibility, which is seen in the satellite image. The observed erosive furrow proves that the soil management was not adequate in this area and the control practices, such as the presence of contour lines and terracing (Fig. 8a), were not sufficient or poorly dimensioned.

Also, this region had high BSF in the period from 1985 to 2019 (Fig. 8b). We observed that until 2014, in almost every year, at the same site-specific the soil was bare, except for the years 1986, 1992, and 1998. It was caused by the sugarcane pre-harvest burning that occurred in the past or by the conventional tillage during the period of sugarcane replanting. Thus, analyzing from 1985 to 2014, 9% of exposures (soil was bare) occurred in months considered restricted, 44% in unsuitable and 47% in adequate periods. The exposure in restricted and unsuitable months may have favored the erosive process. On the other hand, after 2015 (despite the short period of analysis), it is observed that the number of years without bare soil presence increases, which could be explained by the introduction of mechanized harvesting. In any case, and for this region, planting and harvesting should be prioritized between May and August, which are considered suitable for the exhibition in agreement with De Maria et al. (2016). In this simple site-specific evaluation, it is possible to observe that BSF is a good tool to identify areas with a high propensity to soil degradation, promoting information for soil security through its efficacy such as a technique for soil monitoring.

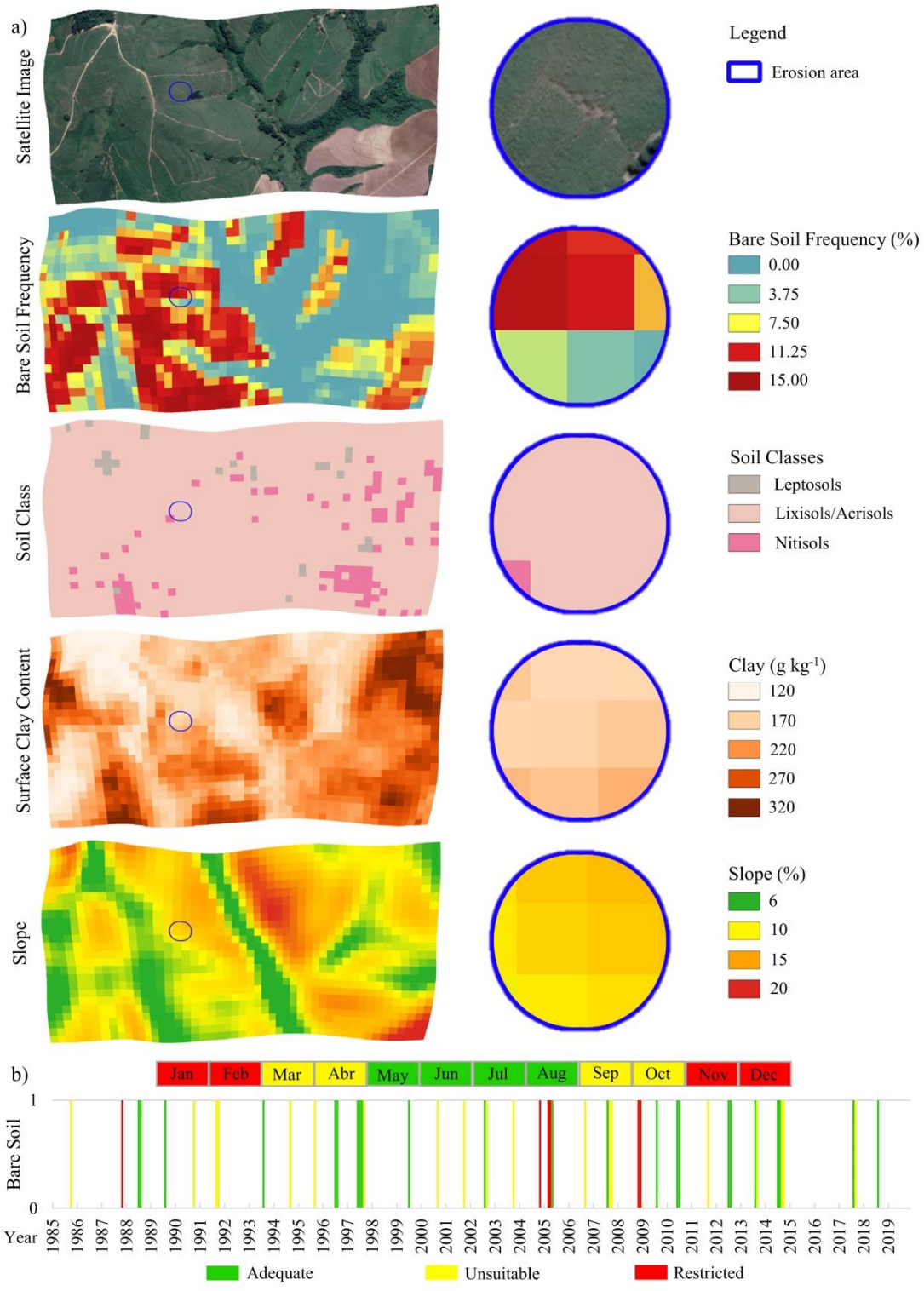

Figure 8. Satellite Image, Bare Soil Frequency, Soil Unit Class, surface clay content and Slope map in an area with the presence of erosion (a); Moments of soil was bare per month from 1985 to 2019 (b).

4.3.7. Limitations and advantages

Some points can be pointed out as the main limitations related to the creation of images of bare soil and bare soil frequency. The definition of threshold values for the indices used to mask unexposed (soil covered) pixels varies with the region and scale (Demattê et al. 2020; Silvero et al. 2021a). Zepp et al. (2021) pointed out as not

robust enough the threshold values previously pointed out by Rogge et al. (2018). The high presence of clouds and shadows in a certain region and/or the season are another limitation (Silvero et al. 2021b; Mzid et al. 2021). Silvero et al. (2021a) obtained percentage of bare soil pixels lower than 15% in the moist season in a tropical area and concludes that twenty images from the dry period would provide barer soil pixels than twenty images from the moist season. Another issue is the satellite´s temporal resolution, the shorter the revisit time, more images can be obtained and, consequently, barer soil pixels (Silvero et al. 2021a; Silvero et al. 2021b; Mzid et al. 2021).

Despite these limitations, the use of multi-temporal images for environmental monitoring has been consolidated and pointed out as having a high potential for use (Canata et al. 2021; Som-ard et al 2021; Zepp et al. 2021). As mentioned before, several works have shown solid results (Silvero et al. 2021b). Furthermore, the free open access of satellite images, like Landsat and Sentinel missions, especially in cloud-based platform such as the GEE, is a great opportunity (Aguiar et al. 2011; Silvero et al. 2021a) and facilitates the study of large areas (Chikhaoui et al., 2005). A future possibility is the fusion of multi-temporal images from different sensors that would allow a greater number of images with a shorter revisiting time for an area (Silvero et al. 2020a). Finally, specifically regarding soil security, Zepp et al. (2021) conclude that the use of multi-temporal composite images contributes with the information about where and when soils are bare, that is a valuable information for soil erosion studies.

4.4. Conclusions

We confirm our hypothesis that the use of multi-temporal satellite images makes it possible to evaluate aspects of soil management and their changes in sugarcane areas, and to relate them to soil security, especially those linked to erosion. The use of SYSIs showed that the bare soils areas under sugarcane cultivation reduced after the "Agro-environmental protocol". However, we confirmed that the expansion occurred over soils more prone to erosion (Lixisols/Acrisols, Arenosols and Leptosols with sandy and sandy medium surface texture). Despite the challenges imposed by mechanized harvesting in relation to the physical properties of the soil, their cover maintenance contributes to its conservation, safety, and quality, that is, a necessary change for the development of more sustainable agriculture. Among the historical period of 35 years, the ups and down on soil tillage and bare soil area in the sugarcane culture, had several factors such as climate, commodities price, public policies, governments decisions and the learning curve of farmers.

The use of the BSF allowed verifying the reduction of the bare soil frequency in the rainy season, in particular, into the Lixisols/Acrisols, Leptosols, and Arenosols soils types. This confirms the best knowledge of the sector in relation to the best period to tillage each soil class. However, it is necessary to continue the downward trend in order to reduce the propensity to degradation, especially in Arenosols and soils with a sandy surface texture, that are soils with highest BSF in all period. In the dry season, the reduction in the average BSF in the second period confirms the importance of the aforementioned protocol for soils.

It was not possible to verify changes in the area of bare soil during the rainy season (November to February) over the years. However, there was a decrease in bare soil areas during November and an increase during the December, January and February.

Finally, the site specific temporal analysis of bare soil in a given area, confirms the importance of remote sensing in environmental monitoring. The technique, proposed by Demattê et al. (2020) has important contributions in land inspection and the adoption of public policies on sustainability and soil conservation as impacts in soil security as well. Furthermore, this approach could be applied in other regions with sugarcane crop (i.e. Brazilian Northeast, Australia) either for past analysis or for future land monitoring.

Acknowledgments

The financial support, which came from different Brazilian institutions, is hereby acknowledged: grants numbers 2014/22262-0, 2019/21002-8, 2018/23760-4 from the São Paulo Research Foundation (FAPESP), the grant number 88887.513392/2020-00 from Brazilian Federal Agency for Support and Evaluation of Graduate Education (CAPES), and the National Council for Scientific and Technological Development (CNPq). The third author thanks the Coordination of Integrate Technical Assistance (CATI/SAA) for encouraging him to pursue his doctorate. The authors are grateful to Geotechnologies on Soil Science group - GEOCIS (www.esalqgeocis.wixsite.com/geocis).

Appendices

Table A.1. Results of the trend analysis of the average bare soil frequency

Class	Rainy season						Dry season season					
	1989-2003			2004-2019			1989-2003			2004-2019		
	Tau	Slope	p-value	Tau	Slope	p-value	Tau	Slope	p-value	Tau	Slope	p-value
Arenosols	-0.09	-0.03	0.692	-0.88	-0.38	<0.001	-0.03	-0.05	0.921	-0.77	-1.40	<0.001
Ferralsols	-0.56	-0.17	0.004	-0.75	-0.12	<0.001	0.45	0.23	0.023	-0.87	-0.41	<0.001
Leptosols	-0.60	-0.25	0.002	-0.65	-0.14	<0.001	0.54	0.34	0.006	-0.88	-0.59	<0.001
Lixisol/Acrisols	-0.64	-0.28	<0.001	-0.77	-0.16	<0.001	0.54	0.45	0.006	-0.88	-0.81	<0.001
Nitisols	-0.49	-0.08	0.013	0.02	0.00	0.96	0.45	0.28	0.023	-0.82	-0.36	<0.001
Clayey	-0.58	-0.17	0.003	-0.77	-0.07	<0.001	0.49	0.27	0.013	-0.82	-0.25	<0.001
Clayey medium	-0.60	-0.18	0.002	-0.77	-0.13	<0.001	0.43	0.26	0.029	-0.87	-0.47	<0.001
Sandy medium	-0.62	-0.24	<0.001	-0.73	-0.17	<0.001	0.47	0.44	0.018	-0.85	-0.78	<0.001
Sandy	-0.68	-0.37	<0.001	-0.77	-0.19	<0.001	0.62	0.31	0.002	-0.92	-0.99	<0.001
Flat	-0.60	-0.21	0.002	-0.80	-0.17	<0.001	0.54	0.28	0.006	-0.83	-0.53	<0.001
Flat/Soft	-0.62	-0.21	<0.001	-0.75	-0.15	<0.001	0.56	0.42	0.004	-0.87	-0.66	<0.001
Soft	-0.66	-0.20	<0.001	-0.73	-0.13	<0.001	0.60	0.41	0.002	-0.88	-0.69	<0.001
Rolling	-0.70	-0.17	<0.001	-0.70	-0.10	<0.001	0.60	0.37	0.002	-0.82	-0.54	<0.001
Strong rolling	-0.77	-0.16	<0.001	-0.68	-0.10	<0.001	0.58	0.28	0.003	-0.63	-0.32	<0.001

References

Adami, M., Rudorff, B.F.T., Freitas, R.M., Aguiar, D.A., Sugawara, L.M., Mello, M.P., 2012. Remote Sensing Time Series to Evaluate Direct Land Use Change of Recent Expanded Sugarcane Crop in Brazil. Sustain. 2012, Vol. 4, Pages 574-585 4, 574–585. https://doi.org/10.3390/SU4040574

Aguiar, D.A., Rudorff, B.F.T., Silva, W.F., Adami, M., Mello, M.P., 2011. Remote sensing images in support of environmental protocol: Monitoring the sugarcane harvest in São Paulo State, Brazil. Remote Sens. 3, 2682–2703. https://doi.org/10.3390/rs3122682

Aguilera Esteban, D.A., de Souza, Z.M., Tormena, C.A., Lovera, L.H., de Souza Lima, E., de Oliveira, I.N., de Paula Ribeiro, N., 2019. Soil compaction, root system and productivity of sugarcane under different row spacing and controlled traffic at harvest. Soil Tillage Res. 187, 60–71. https://doi.org/https://doi.org/10.1016/j.still.2018.11.015

Almeida, G.M. de, Pereira, G.T., Bahia, A.S.R. de S., Fernandes, K., Marques Júnior, J., 2021. Machine learning in the prediction of sugarcane production environments. Comput. Electron. Agric. 190, 106452. https://doi.org/https://doi.org/10.1016/j.compag.2021.106452.

Alvares, C.A., Stape, J.L., Sentelhas, P.C., de Moraes Gonçalves, J.L., Sparovek, G., 2013. Köppen's climate classification map for Brazil. Meteorol. Zeitschrift 22. https://doi.org/10.1127/0941-2948/2013/0507

Amorim, F. F., Jacques Agra Bezerra da Silva, Yuri, Cabral Nascimento, R., Jacques Agra Bezerra da Silva, Ygor, Tiecher, T., Williams Araújo do Nascimento, C., Paolo Gomes Minella, J., Zhang, Y., Ram Upadhayay, H., Pulley, S., Collins, A.L., 2021. Sediment source apportionment using optical property composite signatures in a rural catchment, Brazil. CATENA 202, 105208. https://doi.org/https://doi.org/10.1016/j.catena.2021.105208

Anjinho, P. da S., Barbosa, M.A.G.A., Costa, C.W., Mauad, F.F., 2021. Environmental fragility analysis in reservoir drainage basin land use planning: A Brazilian basin case study. Land use policy 100, 104946. https://doi.org/https://doi.org/10.1016/j.landusepol.2020.104946

Antunes F.A.F., Chandel, A. K., Terán-Hilares, R., Milessi, T.S.S, Travalia, B.M., Ferrari, F.A., Hernandez-Pérez, A.F., Ramos, L., Marcelino, P.F., Brumano, L.P., Silva, G.M., Forte, M.B.S, Santos, J.C., Felipe, M.G.A., da Silva, S.S., 2019. Biofuel Production from Sugarcane in Brazil. In: Khan M., Khan I. (Eds.), Sugarcane Biofuels. Springer, Cham. https://doi.org/10.1007/978-3-030-18597-8_5

Aparecido, L.E. de O., de Moraes, J.R. da S.C., de Meneses, K.C., Torsoni, G.B., Costa, C.T.S. e, Mesquita, D.Z., 2021. Climate Efficiency for Sugarcane Production in Brazil and its Application in Agricultural Zoning. Sugar Tech 23, 776–793. https://doi.org/10.1007/s12355-020-00949-1

Arruda, A.B., Souza, R.F. de, Brito, G.H.M., Moura, J.B. de, Oliveira, M.H.R. de, Santos, J.M. dos, Dutra e Silva, S., 2021. Resistance of soil to penetration as a parameter indicator of subsolation in crop areas of sugar cane. Sci. Rep. 11, 11780. https://doi.org/10.1038/s41598-021-91186-3

Azareh, A., Rahmati, O., Rafiei-Sardooi, E., Sankey, J.B., Lee, S., Shahabi, H., Ahmad, B. Bin, 2019. Modelling gully-erosion susceptibility in a semi-arid region, Iran: Investigation of applicability of certainty factor and maximum entropy models. Sci. Total Environ. 655, 684–696. https://doi.org/10.1016/J.SCITOTENV.2018.11.235

Barbosa, L.C., Magalhães, P.S.G., Bordonal, R.O., Cherubin, M.R., Castioni, G.A., Rossi Neto, J., Franco, H.C.J., Carvalho, J.L.N., 2021. Untrafficked furrowed seedbed sustains soil physical quality in sugarcane mechanized fields. Eur. J. Soil Sci. 72, 2150–2164. https://doi.org/https://doi.org/10.1111/ejss.13107

Barbosa, L.C., Magalhães, P.S.G., Bordonal, R.O., Cherubin, M.R., Castioni, G.A.F., Tenelli, S., Franco, H.C.J., Carvalho, J.L.N., 2019. Soil physical quality associated with tillage practices during sugarcane planting in south-central Brazil. Soil Tillage Res. 195, 104383. https://doi.org/https://doi.org/10.1016/j.still.2019.104383

Barbosa, L.C., Souza, Z.M. de, Franco, H.C.J., Otto, R., Rossi Neto, J., Garside, A.L., Carvalho, J.L.N., 2018. Soil texture affects root penetration in Oxisols under sugarcane in Brazil. Geoderma Reg. 13, 15–25. https://doi.org/https://doi.org/10.1016/j.geodrs.2018.03.002

Bellinaso, H., Silvero, N.E.Q., Ruiz, L.F.C., Accorsi Amorim, M.T., Rosin, N.A., Mendes, W. de S., Sousa, G.P.B. de Sepulveda, L.M.A., Queiroz, L.G. de, Nanni, M.R., Demattê, J.A.M., 2021. Clay content prediction using spectra data collected from the ground to space platforms in a smallholder tropical area. Geoderma 399. https://doi.org/10.1016/j.geoderma.2021.115116

Ben-Dor, E., Chabrillat, S., Demattê, J.A.M., Taylor, G.R., Hill, J., Whiting, M.L., Sommer, S., 2009. Using Imaging Spectroscopy to study soil properties. Remote Sens. Environ. 113. https://doi.org/10.1016/j.rse.2008.09.019

Bezerra, S.A., Cantalice, J.R.B., 2006. Erosão entre sulcos em diferentes condições de cobertura do solo, sob cultivo da cana-de-açúcar. Rev. Bras. Ciência do Solo 30. https://doi.org/10.1590/S0100-06832006000300016

Biddoccu, M., Ferraris, S., Opsi, F., Cavallo, E., 2016. Long-term monitoring of soil management effects on runoff and soil erosion in sloping vineyards in Alto Monferrato (North–West Italy). Soil Tillage Res. 155. https://doi.org/10.1016/j.still.2015.07.005

Bolonhezi, D., Vischi Filho, O. J., Ivo, W.M.P. de Mello, Vitti, A.C., Bolonhezi, A.C., Brancalião, S.R., 2019. Manejo e conservação do solo em cana-de-açúcar, in: Bertol, I., De Maria, I.C., Souza, L. da S. (Eds.), Manejo e conservação do solo e da água. Sociedade Brasileira de Ciência do Solo, Viçosa, pp. 1029-1080.

Bray, S.C., Ferreira, E.R., Ruas, D.G.G., 2000. As políticas da agroindústria canavieira e o Proálcool no Brasil. Unesp Marília Publicações, Marília. https://doi.org/10.36311/2000.85-86738-14-X

Bordonal, R. de O., Carvalho, J.L.N., Lal, R., de Figueiredo, E.B., de Oliveira, B.G., La Scala, N., 2018. Sustainability of sugarcane production in Brazil. A review. Agron. Sustain. Dev. 38, 13. https://doi.org/10.1007/s13593-018-0490-x

Braunack, M. V., Arvidsson, J., Håkansson, I., 2006. Effect of harvest traffic position on soil conditions and sugarcane (Saccharum officinarum) response to environmental conditions in Queensland, Australia. Soil Tillage Res. 89, 103–121. https://doi.org/10.1016/J.STILL.2005.07.004

Brinkman, M.L.J., da Cunha, M.P., Heijnen, S., Wicke, B., Guilhoto, J.J.M., Walter, A., Faaij, A.P.C., van der Hilst, F., 2018. Interregional assessment of socio-economic effects of sugarcane ethanol production in Brazil. Renew. Sustain. Energy Rev. 88, 347–362. https://doi.org/https://doi.org/10.1016/j.rser.2018.02.014

Caldarelli, C.E., Gilio, L., 2018. Expansion of the sugarcane industry and its effects on land use in São Paulo: Analysis from 2000 through 2015. Land use policy 76, 264–274. https://doi.org/https://doi.org/10.1016/j.landusepol.2018.05.008

Canata, T.F., Wei, M.C., Maldaner, L.F., Molin, J.P., 2021. Sugarcane Yield Mapping Using High-Resolution Imagery Data and Machine Learning Technique. Remote Sens. . https://doi.org/10.3390/rs13020232

Canisares, L.P., Cherubin, M.R., da Silva, L.F.S., Franco, A.L.C., Cooper, M., Mooney, S.J., Cerri, C.E.P., 2020. Soil microstructure alterations induced by land use change for sugarcane expansion in Brazil. Soil Use Manag. 36, 189–199. https://doi.org/https://doi.org/10.1111/sum.12556

Carneiro, L.F., de Oliveira, R.A., Weber, H., Daros, E., Berton, G.S., Rodrigues, F.V., 2020. Alternative sugarcane production for conservation of sandy soils: Sugarcane straw, intercropping and nitrogen. Cienc. e Agrotecnologia 44, 1–9. https://doi.org/10.1590/1413-7054202044009920

Carvalho, J.L.N., Oliveira, B.G., Cantarella, H., Chagas, M.F., Gonzaga, L.C., Lourenço, K.S., Bordonal, R.O., Bonomi, A., 2021. Implications of regional N2O–N emission factors on sugarcane ethanol emissions and granted decarbonization certificates. Renew. Sustain. Energy Rev. 149, 111423. https://doi.org/https://doi.org/10.1016/j.rser.2021.111423

Carvalho, J.L.N., Menandro, L.M.S., de Castro, S.G.Q., Cherubin, M.R., Bordonal, R. de O., Barbosa, L.C., Gonzaga, L.C., Tenelli, S., Franco, H.C.J., Kolln, O.T., Castioni, G.A.F., 2019. Multilocation Straw Removal Effects on Sugarcane Yield in South-Central Brazil. BioEnergy Res. 12, 813–829. https://doi.org/10.1007/s12155-019-10007-8

Castañeda-Ayarza, J.A., Godoi, B.A., 2021. Macro-environmental influence on the development of Brazilian fuel ethanol between 1975 and 2019. Renew. Sustain. Energy Rev. 137, 110457. https://doi.org/https://doi.org/10.1016/j.rser.2020.110457

Catelan, M.G., Marques Júnior, J., Siqueira, D.S., Gomes, R.P., Bahia, A.S.R. de S., 2022. Sugarcane yield and quality using soil magnetic susceptibility. Sci. Agric. 79. https://doi.org/10.1590/1678-992x-2020-0329

Ceddia, M.B., dos Anjos, L.H.C., Lima, E., Ravelli Neto, A., da Silva, L.A., 1999. Sistemas de colheita da cana-de-açúcar e alterações nas propriedades físicas de um solo podzólico amarelo no estado do espírito santo. Pesq. agropec. Bras. 34, 1467–1473.

Cerri, C.C., Galdos, M. V., Maia, S.M.F., Bernoux, M., Feigl, B.J., Powlson, D., Cerri, C.E.P., 2011. Effect of sugarcane harvesting systems on soil carbon stocks in Brazil: An examination of existing data. Eur. J. Soil Sci. 62, 23–28. https://doi.org/10.1111/j.1365-2389.2010.01315.x

Cerri, C.E.P., Demattě, J.A.M., Ballester, M.V.R., Martinelli, L.A., Victoria, R.L., Roose, E., 2013. GIS erosion risk assessment of the piracicaba river basin, southeastern brazil. 38, 157–171. https://doi.org/10.1080/07493878.2001.10642173

Cervone, C. O. F. de O., Walter, A., Guarenghi, M. M., Favero, C., 2018. Resident perceptions of the impacts of large-scale sugarcane production on ecosystem services in two regions of Brazil. Biomass and Bioenergy 114, 63–72. https://doi.org/https://doi.org/10.1016/j.biombioe.2017.08.029

Chabrillat, S., Ben-Dor, E., Cierniewski, J., Gomez, C., Schmid, T., van Wesemael, B., 2019. Imaging Spectroscopy for Soil Mapping and Monitoring. Surv. Geophys. https://doi.org/10.1007/s10712-019-09524-0

Chagas, C. da S., de Carvalho Junior, W., Bhering, S.B., Calderano Filho, B., 2016. Spatial prediction of soil surface texture in a semiarid region using random forest and multiple linear regressions. CATENA 139, 232–240. https://doi.org/10.1016/j.catena.2016.01.001

Cheavegatti-Gianotto, A., de Abreu, H.M.C., Arruda, P., Bespalhok Filho, J.C., Burnquist, W.L., Creste, S., di Ciero, L., Ferro, J.A., de Oliveira Figueira, A.V., de Sousa Filgueiras, T., Grossi-de-Sá, M. de F., Guzzo, E.C., Hoffmann, H.P., de Andrade Landell, M.G., Macedo, N., Matsuoka, S., de Castro Reinach, F., Romano, E., da Silva, W.J., de Castro Silva Filho, M., César Ulian, E., 2011. Sugarcane (Saccharum X officinarum): A Reference Study for the Regulation of Genetically Modified Cultivars in Brazil. Trop. Plant Biol. 4, 62–89. https://doi.org/10.1007/s12042-011-9068-3

Cherubin, M.R., Bordonal, R.O., Castioni, G.A., Guimarães, E.M., Lisboa, I.P., Moraes, L.A.A., Menandro, L.M.S., Tenelli, S., Cerri, C.E.P., Karlen, D.L., Carvalho, J.L.N., 2021a. Soil health response to sugarcane straw removal in Brazil. Ind. Crops Prod. 163, 113315. https://doi.org/https://doi.org/10.1016/j.indcrop.2021.113315

Cherubin, M.R., Carvalho, J.L., Cerri, C.E., Nogueira, L.A., Souza, G.M., Cantarella, H., 2021b. Land Use and Management Effects on Sustainable Sugarcane-Derived Bioenergy. L. https://doi.org/10.3390/land10010072

Chikhaoui, M., Bonn, F., Bokoye, A.I., Merzouk, A., 2005. A spectral index for land degradation mapping using ASTER data: Application to a semi-arid Mediterranean catchment. Int. J. Appl. Earth Obs. Geoinf. 7, 140–153. https://doi.org/https://doi.org/10.1016/j.jag.2005.01.002

Coelho, S.T., Goldemberg, J., Lucon, O., Guardabassi, P., 2006. Brazilian sugarcane ethanol: lessons learned. Energy for Sustainable Development 10, 2, 26-39. https://doi.org/10.1016/S0973-0826(08)60529-3

CONAB, 2021. Acompanhamento da safra brasileira: Cana-de-açúcar. v. 7- Safra 2020/21, n. 4 - Quarto levantamento. Brasília.

Corrêa, S.T.R., Barbosa, L.C., Menandro, L.M.S., Scarpare, F.V., Reichardt, K., Moraes, L.O. de, Hernandes, T.A.D., Franco, H.C.J., Carvalho, J.L.N., 2019. Straw Removal Effects on Soil Water Dynamics, Soil Temperature, and Sugarcane Yield in South-Central Brazil. BioEnergy Res. 124 12, 749–763. https://doi.org/10.1007/S12155-019-09981-W

Correia, B.L., Alleoni, L.R.F., 2011. Conteúdo de carbono e atributos químicos de Latossolo sob cana-de-açúcar colhida com e sem queima. Pesqui. Agropecuária Bras. 46. https://doi.org/10.1590/S0100-204X2011000800022

Cunha, F.N., Colodro, G., Silva, N.F. da, Maia, G.A., Bastos, F.J. de C., Silva, F.C. da, Oliveira, R.C. de, Cunha, G.N., 2011. Aptidão agrícola dos neossolos quartzarênicos, in: V Congresso de Iniciação Científica Da Universidade de Rio Verde. Rio Verde, pp. 7–11.

Curcio, G.R., Bonnet, A., Kacharouski, M., n.d. NEOSSOLOS LITÓLICOS DO SUBPLANALTO DE CASCAVEL [WWW Document]. Programa Nac. Solos - PronaSolos Paraná. URL http://www.pronasolos.pr.gov.br/pagina-20.html (accessed 7.12.21).

Da Luz, F.B., Carvalho, M.L., de Borba, D.A., Schiebelbein, B.E., de Lima, R.P., Cherubin, M.R., 2020. Linking soil water changes to soil physical quality in sugarcane expansion areas in Brazil. Water (Switzerland) 12, 1–18. https://doi.org/10.3390/w12113156

De Aguiar, D.A., Rudorff, B.F.T., Adami, M., Shimabukuro, Y.E., 2009. Remote sensing images for monitoring the sugarcane harvest. Eng. Agric. 29, 440–451. https://doi.org/10.1590/s0100-69162009000300011

De Lima, R.P., Rolim, M.M., Toledo, M.P.S., Tormena, C.A., da Silva, A.R., e Silva, I.A.C., Pedrosa, E.M.R., 2022. Texture and degree of compactness effect on the pore size distribution in weathered tropical soils. Soil Tillage Res. 215, 105215. https://doi.org/https://doi.org/10.1016/j.still.2021.105215

De Maria, I.C., Drugowich, M.I., Bortoletti, J.O., Vitti, A.C., Rossetto, R., Fontes, J.L., Tcatchenco, J., Margatho, S.M.F., 2016. Recomendações gerais para a conservação do solo na cultura da canade-açúcar. Campinas.

De Sousa, A.C.M., Farhate, C.V.V., de Souza, Z.M., Torres, J.L.R., da Silva, R.B., 2019. Soil Load-Bearing Capacity and Development of Root System in Area Under Sugarcane with Traffic Control in Brazil. Sugar Tech 21, 153–161. https://doi.org/10.1007/s12355-018-0636-9

Demattê, J.A.M., Fongaro, C.T., Rizzo, R., Safanelli, J.L., 2018. Geospatial Soil Sensing System (GEOS3): A powerful data mining procedure to retrieve soil spectral reflectance from satellite images. Remote Sens. Environ. 212. https://doi.org/10.1016/j.rse.2018.04.047

Demattê, J.A.M., Safanelli, J.L., Poppiel, R.R., Rizzo, R., Silvero, N.E.Q., Mendes, W. de S., Bonfatti, B.R., Dotto, A.C., Salazar, D.F.U., Mello, F.A. de O., Paiva, A.F. da S., Souza, A.B., Santos, N.V. dos, Maria Nascimento, C., Mello, D.C. de, Bellinaso, H., Gonzaga Neto, L., Amorim, M.T.A., Resende, M.E.B. de, Vieira, J. da S., Queiroz, L.G. de, Gallo, B.C., Sayão, V.M., Lisboa, C.J. da S., 2020. Bare Earth's Surface Spectra as a Proxy for Soil Resource Monitoring. Sci. Rep. 10. https://doi.org/10.1038/s41598-020-61408-1

Demattê, J.L.I., Demattê, J.A.M., 2009. Ambientes de produção como estratégia de manejo na cultura da cana-de-açúcar. Informações Agronômicas 10–18.

Dias, H.B., Inman-Bamber, G., Sentelhas, P.C., Everingham, Y., Bermejo, R., Christodoulou, D., 2021a. High-yielding sugarcane in tropical Brazil – Integrating field experimentation and modelling approach for assessing variety performances. F. Crop. Res. 274, 108323. https://doi.org/https://doi.org/10.1016/j.fcr.2021.108323

Dias, H.B., Sentelhas, P.C., 2017. Evaluation of three sugarcane simulation models and their ensemble for yield estimation in commercially managed fields. F. Crop. Res. 213, 174–185. https://doi.org/https://doi.org/10.1016/j.fcr.2017.07.022

Dias, H.B., Sentelhas, P.C., Inman-Bamber, G., Everingham, Y., 2021b. Sugarcane yield future scenarios in Brazil as projected by the APSIM-Sugar model. Ind. Crops Prod. 171, 113918. https://doi.org/https://doi.org/10.1016/j.indcrop.2021.113918

Diek, S., Fornallaz, F., Schaepman, M.E., de Jong, R., 2017. Barest Pixel Composite for agricultural areas using landsat time series. Remote Sens. 9, 1245. https://doi.org/10.3390/rs9121245

Diek, S., Schaepman, M., de Jong, R., 2016. Creating Multi-Temporal Composites of Airborne Imaging Spectroscopy Data in Support of Digital Soil Mapping. Remote Sens. 8. https://doi.org/10.3390/rs8110906

Donagemma, G.K., de Freitas, P.L., Balieiro, F. de C., Fontana, A., Spera, S.T., Lumbreras, J.F., Viana, J.H.M., Filho, J.C. de A., dos Santos, F.C., de Albuquerque, M.R., Macedo, M.C.M., Teixeira, P.C., Amaral, A.J., Bortolon, E., Bortolon, L., 2016. Characterization, agricultural potential, and perspectives for the management of light soils in Brazil. Pesqui. Agropecu. Bras. 51, 1003–1020. https://doi.org/10.1590/S0100-204X2016000900001

Donzelli, J.L., Bertolani, F.C., de Campos Trombeta, N., 2018. Chapter 1 - Sugarcane Cultivation: Soil Mapping, Environmental Effects, and New Sugarcane Varieties, in: Chandel, A.K., Luciano Silveira, M.H.B.T.-A. in S.B. (Eds.), . Elsevier, pp. 1–15. https://doi.org/https://doi.org/10.1016/B978-0-12-804534-3.00001-X

Dube, T., Mutanga, O., Sibanda, M., Seutloali, K., Shoko, C., 2017. Use of Landsat series data to analyse the spatial and temporal variations of land degradation in a dispersive soil environment: A case of King Sabata Dalindyebo local municipality in the Eastern Cape Province, South Africa. Phys. Chem. Earth, Parts A/B/C 100, 112–120. https://doi.org/10.1016/J.PCE.2017.01.023

FAO & ITPS, 2015. Intergovernmental Technical Panel on Soils. Status of the World's Soil Resources., Intergovernmental Technical Panel on Soils.

Fiorio, P.R., Demattê, J.A.M., Sparovek, G., 2000. Cronologia e impacto ambiental do uso da terra na Microbacia Hidrográfica do Ceveiro, em Piracicaba, SP. Pesqui. Agropecuária Bras. 35, 671–679. https://doi.org/10.1590/S0100-204X2000000400001

Fongaro, C.T., Demattê, J.A.M., Rizzo, R., Safanelli, J.L., Mendes, W. de S., Dotto, A.C., Vicente, L.E., Franceschini, M.H.D., Ustin, S.L., Lucas Safanelli, J., Mendes, W. de S., Dotto, A.C., Vicente, L.E., Franceschini, M.H.D., Ustin, S.L., 2018. Improvement of clay and sand quantification based on a novel approach with a focus on multispectral satellite images. Remote Sens. 10, 1555. https://doi.org/10.3390/rs10101555

Franco, A.L.C., Cherubin, M.R., Pavinato, P.S., Cerri, C.E.P., Six, J., Davies, C.A., Cerri, C.C., 2015. Soil carbon, nitrogen and phosphorus changes under sugarcane expansion in Brazil. Sci. Total Environ. 515–516, 30–38. https://doi.org/https://doi.org/10.1016/j.scitotenv.2015.02.025

Fuentes-Llanillo, R., Telles, T.S., Soares Junior, D., de Melo, T.R., Friedrich, T., Kassam, A., 2021. Expansion of no-tillage practice in conservation agriculture in Brazil. Soil Tillage Res. 208, 104877. https://doi.org/https://doi.org/10.1016/j.still.2020.104877

Furlan, L. M., Moreira, C.A., de Alencar, P.G., Rosolen, V., 2021. Environmental monitoring and hydrological simulations of a natural wetland based on high-resolution unmanned aerial vehicle data (Paulista Peripheral Depression, Brazil). Environ. Challenges 4, 100146. https://doi.org/https://doi.org/10.1016/j.envc.2021.100146

Gasmi, A., Gomez, C., Lagacherie, P., Zouari, H., Laamrani, A., Chehbouni, A., 2021. Mean spectral reflectance from bare soil pixels along a Landsat-TM time series to increase both the prediction accuracy of soil clay content and mapping coverage. Geoderma 388, 114864. https://doi.org/https://doi.org/10.1016/j.geoderma.2020.114864

Gmach, M.R., Scarpare, F.V., Cherubin, M.R., Lisboa, I.P., Santos, A.K.B. dos, Cerri, C.E.P., Cerri, C.C., 2019. Sugarcane straw removal effects on soil water storage and drainage in southeastern Brazil. J. Soil Water Conserv. 74, 466–476. https://doi.org/10.2489/JSWC.74.5.466

Gmach, M.R., Kaiser, K., Cherubin, M.R., Cerri, C.E.P., Lisboa, I.P., Vasconcelos, A.L.S., Siqueira-Neto, M., 2021. Soil dissolved organic carbon responses to sugarcane straw removal. Soil Use Manag. 37, 126–137. https://doi.org/https://doi.org/10.1111/sum.12663

Gonçalves, F., Perna, R., Lopes, E., Maciel, R., Tovar, L., Lopes, M., 2021. Strategies to improve the environmental efficiency and the profitability of sugarcane mills. Biomass and Bioenergy 148, 106052.

Gorelick, N., Hancher, M., Dixon, M., Ilyushchenko, S., Thau, D., Moore, R., 2017. Google Earth Engine: Planetary-scale geospatial analysis for everyone. Remote Sens. Environ. 202. https://doi.org/10.1016/j.rse.2017.06.031

Grangeia, C., Santos, L., Lazaro, L.L.B., 2022. The Brazilian biofuel policy (RenovaBio) and its uncertainties: An assessment of technical, socioeconomic and institutional aspects. Energy Convers. Manag. X 13, 100156. https://doi.org/https://doi.org/10.1016/j.ecmx.2021.100156

Han, S.Y., Bishop, T.F.A., Filippi, P., 2022. Data-driven, early-season forecasts of block sugarcane yield for precision agriculture. F. Crop. Res. 276, 108360. https://doi.org/https://doi.org/10.1016/j.fcr.2021.108360

Hernandes, T.A.D., Duft, D.G., Luciano, A.C. dos S., Leal, M.R.L.V., Cavalett, O., 2021. Identifying suitable areas for expanding sugarcane ethanol production in Brazil under conservation of environmentally relevant habitats. J. Clean. Prod. 292, 125318. https://doi.org/https://doi.org/10.1016/j.jclepro.2020.125318

Jaiswal, D., De Souza, A.P., Larsen, S., LeBauer, D.S., Miguez, F.E., Sparovek, G., Bollero, G., Buckeridge, M.S., Long, S.P., 2017. Brazilian sugarcane ethanol as an expandable green alternative to crude oil use. Nat. Clim. Chang. 7, 788–792. https://doi.org/10.1038/nclimate3410

Jarbas, T., Sá, I.B., Petrere, V.G., Taura, T.A., n.d. Argissolos [WWW Document]. URL https://www.agencia.cnptia.embrapa.br/gestor/bioma_caatinga/arvore/CONT000g5twggzi02wx5ok01edq5sp172540.html (accessed 7.12.21).

Jimenez, K.J., Rolim, M.M., Gomes, I.F., de Lima, R.P., Berrío, L.L.A., Ortiz, P.F.S., 2021. Numerical analysis applied to the study of soil stress and compaction due to mechanised sugarcane harvest. Soil Tillage Res. 206, 104847. https://doi.org/https://doi.org/10.1016/j.still.2020.104847

Júnnyor, W. da S.G., Maria, I.C. De, Araujo-Junior, C.F., Lima, C.C. de , Vitti, A.C., Figueiredo, G.C., Dechen, S.C.F., 2019. Soil compaction on traffic lane due to soil tillage and sugarcane mechanical harvesting operations. Sci. Agric. 76, 509–517. https://doi.org/10.1590/1678-992x-2018-0052

Kendall, M.G., 1975. Rank correlation methods.

Klein, B.C., Chagas, M.F., Watanabe, M.D.B., Bonomi, A., Maciel Filho, R., 2019. Low carbon biofuels and the New Brazilian National Biofuel Policy (RenovaBio): A case study for sugarcane mills and integrated sugarcane-microalgae biorefineries. Renew. Sustain. Energy Rev. 115, 109365. https://doi.org/10.1016/j.rser.2019.109365

Krishna Bahadur, K.C., 2009. Mapping soil erosion susceptibility using remote sensing and GIS: a case of the Upper Nam Wa Watershed, Nan Province, Thailand. Environ. Geol. 57, 695–705. https://doi.org/10.1007/s00254-008-1348-3

Landell, M.G. de A., do Prado, H., de Vasconcelos, A.C.M., Perecin, D., Rossetto, R., Bidoia, M.A.P., Silva, M.deA., Xavier, M.A, 2003. Oxisol subsurface chemical attributes related to sugarcane productivity. Sci. agric. https://doi.org/10.1590/S0103-90162003000400020

Li, Y., Mo, Y., Are, K.S., Huang, Z., Guo, H., Tang, C., Abegunrin, T.P., Qin, Z., Kang, Z., Wang, X., 2021. Sugarcane planting patterns control ephemeral gully erosion and associated nutrient losses: Evidence from hillslope observation. Agric. Ecosyst. Environ. 309, 107289. https://doi.org/https://doi.org/10.1016/j.agee.2020.107289

Loarie, S.R., Lobell, D.B., Asner, G.P., Mu, Q., Field, C.B., 2011. Direct impacts on local climate of sugar-cane expansion in Brazil. Nat. Clim. Chang. 1, 105–109. https://doi.org/10.1038/nclimate1067

Loiseau, T., Chen, S., Mulder, V.L., Román Dobarco, M., Richer-de-Forges, A.C., Lehmann, S., Bourennane, H., Saby, N.P.A., Martin, M.P., Vaudour, E., Gomez, C., Lagacherie, P., Arrouays, D., 2019. Satellite data integration for soil clay content modelling at a national scale. Int. J. Appl. Earth Obs. Geoinf. 82, 101905. https://doi.org/https://doi.org/10.1016/j.jag.2019.101905

Luciano, A.C. dos S., Picoli, M.C.A., Duft, D.G., Rocha, J.V., Leal, M.R.L.V., le Maire, G., 2021. Empirical model for forecasting sugarcane yield on a local scale in Brazil using Landsat imagery and random forest algorithm. Comput. Electron. Agric. 184, 106063. https://doi.org/https://doi.org/10.1016/j.compag.2021.106063

Machado, R.E., Cardoso, T.O., Mortene, M.H., 2021. Determination of runoff coefficient (C) in catchments based on analysis of precipitation and flow events. Int. Soil Water Conserv. Res. https://doi.org/https://doi.org/10.1016/j.iswcr.2021.09.001

Mann, H.B., 1945. Nonparametric Tests Against Trend. Econometrica 13, 245. https://doi.org/10.2307/1907187

MapBiomas. MapBiomas plataform—Uso e cobertura do solo. 2021. Available online: https://plataforma.mapbiomas.org/ (accessed on 03 June 2021).

Marchetto, A. 2021. rkt package: Mann-Kendall Test, Seasonal and Regional Kendall Tests (Version 1.6), https://CRAN.R-project.org/package=rkt (accessed 30 June 2021).

Marin, F.R., Rattalino Edreira, J.I., Andrade, J., Grassini, P., 2019. On-farm sugarcane yield and yield components as influenced by number of harvests. F. Crop. Res. 240, 134–142. https://doi.org/10.1016/j.fcr.2019.06.011

Marin, F.R., Rattalino Edreira, J.I., Andrade, J.F., Grassini, P., 2021. Sugarcane Yield and Yield Components as Affected by Harvest Time. Sugar Tech 23, 819–826. https://doi.org/10.1007/s12355-020-00945-5

Marques, J., Siqueira, D.S., Camargo, L.A., Teixeira, D.D.B., Barrón, V., Torrent, J., 2014. Magnetic susceptibility and diffuse reflectance spectroscopy to characterize the spatial variability of soil properties in a brazilian haplustalf. Geoderma 219–220, 63–71. https://doi.org/10.1016/j.geoderma.2013.12.007

Martíni, A.F., Valani, G.P., da Silva, L.F., Bolonhezi, D., Di Prima, S., Cooper, M., 2021. Long-Term Trial of Tillage Systems for Sugarcane: Effect on Topsoil Hydrophysical Attributes. Sustain. . https://doi.org/10.3390/su13063448

Martins, M.B., Testa, J.V.P., Drudi, F.S., Sandi, J., Ramos, C.R.G., Lancas, K.P., 2022. Interference of speed at cutting height and damage to rootstock in mechanical harvesting of sugarcane. Aust. J. Crop Sci. https://doi.org/10.3316/informit.755498156985902

Martins Filho, M. V., Liccioti, T.T., Pereira, G.T., Marques Júnior, J., Sanchez, R.B., 2009. Perdas de solo e nutrientes por erosão num Argissolo com resíduos vegetais de cana-de-açúcar. Eng. Agrícola 29. https://doi.org/10.1590/S0100-69162009000100002

Medeiros, G. de O.R., Giarolla, A., Sampaio, G., Marinho, M. de A., 2016. Estimates of Annual Soil Loss Rates in the State of São Paulo, Brazil. Rev. Bras. Ciência do Solo 40. https://doi.org/10.1590/18069657rbcs20150497

Melland, A.R., Bosomworth, B., Cook, F.J., Silburn, D.M., Eyles, M., 2022. Impacts of sugarcane (Saccharum sp.) soil and fertiliser management practices on nutrients and sediment in plot-scale runoff from simulated rainfall. Soil Tillage Res. 216, 105259. https://doi.org/https://doi.org/10.1016/j.still.2021.105259

Mendes, W. de S., Demattê, J.A.M., Silvero, N.E.Q., Rabelo Campos, L., 2021. Integration of multispectral and hyperspectral data to map magnetic susceptibility and soil attributes at depth: A novel framework. Geoderma 385. https://doi.org/10.1016/j.geoderma.2020.114885

Minhoni, R.T. de A., Scudiero, E., Zaccaria, D., Saad, J.C.C., 2021. Multitemporal satellite imagery analysis for soil organic carbon assessment in an agricultural farm in southeastern Brazil. Sci. Total Environ. 784, 147216. https://doi.org/https://doi.org/10.1016/j.scitotenv.2021.147216

Morais, M.C., Siqueira-Neto, M., Guerra, H.P., Satiro, L.S., Soltangheisi, A., Cerri, C.E.P., Feigl, B.J., Cherubin, M.R., 2020. Trade-Offs between Sugarcane Straw Removal and Soil Organic Matter in Brazil. Sustain. 2020, Vol. 12, Page 9363 12, 9363. https://doi.org/10.3390/SU12229363

Morgan, R.P.C., 2005. Soil Erosion and Conservation, 3rd edition. ed. Blackwell Publishing, Oxford.

Mulder, V.L., de Bruin, S., Schaepman, M.E., Mayr, T.R., 2011. The use of remote sensing in soil and terrain mapping — A review. Geoderma 162, 1–19. https://doi.org/10.1016/J.GEODERMA.2010.12.018

Mzid, N., Pignatti, S., Huang, W., Casa, R., 2021. An Analysis of Bare Soil Occurrence in Arable Croplands for Remote Sensing Topsoil Applications. Remote Sens. . https://doi.org/10.3390/rs13030474

Nascimento, C.M., de Sousa Mendes, W., Quiñonez Silvero, N.E., Poppiel, R.R., Sayão, V.M., Dotto, A.C., Valadares dos Santos, N., Accorsi Amorim, M.T., Demattê, J.A.M., 2021. Soil degradation index developed by multitemporal remote sensing images, climate variables, terrain and soil atributes. J. Environ. Manage. 277, 111316. https://doi.org/https://doi.org/10.1016/j.jenvman.2020.111316

Nechet, K.L., Ramos, N.P., Halfeld-Vieira, B.A., 2021. Impact of conservation practices on the severity of sugarcane foliar diseases. Australas. Plant Pathol. 50, 487–494. https://doi.org/10.1007/s13313-021-00801-4

Oliveira-Andreoli, E.Z., Moraes, M.C.P. de, Faustino, A. da S., Vasconcelos, A.F., Costa, C.W., Moschini, L.E., Melanda, E.A., Justino, E.A., Di Lollo, J.A., Lorandi, R., 2021. Multi-temporal analysis of land use land cover interference in environmental fragility in a Mesozoic basin, southeastern Brazil. Groundw. Sustain. Dev. 12, 100536. https://doi.org/https://doi.org/10.1016/j.gsd.2020.100536

Oliveira, D.M.S., Cherubin, M.R., Franco, A.L.C., Santos, A.S., Gelain, J.G., Dias, N.M.S., Diniz, T.R., Almeida, A.N., Feigl, B.J., Davies, C.A., Paustian, K., Karlen, D.L., Smith, P., Cerri, C.C., Cerri, C.E.P., 2019. Is the expansion of sugarcane over pasturelands a sustainable strategy for Brazil's bioenergy industry? Renew. Sustain. Energy Rev. 102, 346–355. https://doi.org/https://doi.org/10.1016/j.rser.2018.12.012

Oliveira, H.P. de, de Melo, R.O., Baldotto, M.A., Andrade, M. A., Baldotto, L.E.B., 2018. Performance of pre-sprouted sugarcane seedlings in response to the application of humic acid and plant growth-promoting bactéria. Semina. 39, n3, 1365-1370. http://dx.doi.org/10.5433/1679-0359.2018v39n3p1365

Oliveira, J.B., Prado, H., Bejar, O.I.G., Oliveira, E.R., Nogobardi, R.C., Assis, E.A., 1989. Carta Pedológica Semidetalhada do Estado de São Paulo: Piracicaba. São Paulo, Secretaria da Agricultura/CPA/IA, Secretaria da Economia e Planejamento/CAR/IGC. (Mapa escala 1:100.000)

Oliveira, J.C.M. de, Vaz, C.M.P., Reichardt, K., 1995. Efeito do cultivo contínuo da cana-de-açúcar em propriedades físicas de um Latossolo Vermelho Escuro. Sci. Agric. 52, 50–55. https://doi.org/10.1590/S0103-90161995000100009

Pagani, V., Stella, T., Guarneri, T., Finotto, G., van den Berg, M., Marin, F.R., Acutis, M., Confalonieri, R., 2017. Forecasting sugarcane yields using agro-climatic indicators and Canegro model: A case study in the main production region in Brazil. Agric. Syst. 154, 45–52. https://doi.org/10.1016/j.agsy.2017.03.002

Pancelli, M.A., Prado, R. de M., Flores, R.A., Almeida, H.J. de, Moda, L.R., Souza, J.P. de, 2022. Growth, yield and nutrition of sugarcane ratoon as affected by potassium in a mechanized harvesting system. Aust. J. Crop Sci. https://doi.org/10.3316/informit.659779009697335

Panziera, W., Rodrigues de Lima, C.L., Timm, L.C., Aquino, L.S., Barros, W.S., Stumpf, L., dos Anjos e Silva, S.D., Moura-Bueno, J.M., Junior, L.A.D., Pauletto, E.A., 2022. Investigating the relationships between soil and sugarcane attributes under different row spacing configurations and crop cycles using the state-space approach. Soil Tillage Res. 217, 105270. https://doi.org/https://doi.org/10.1016/j.still.2021.105270

Paungfoo-Lonhienne, C., Wang, W., Yeoh, Y.K., Reeves, S., Halpin, N., Daly, J., 2021. Effects of different rotational legume crops and residue management regimes on soil microbial properties and functions in a sugarcane farming system. J. Plant Nutr. Soil Sci. 184, 398–408. https://doi.org/https://doi.org/10.1002/jpln.202000535

Pinto, L.F.G., Bernardes, M.S., Sparovek, G., 2003. Feasibility of cultivation of sugarcane in agroforestry systems. Sci. Agric. 60, 489–493. https://doi.org/10.1590/S0103-90162003000300012

Politano, W., Pissarra, T.C.T., 2005. Avaliação por fotointerpretação das áreas de abrangência dos diferentes estados da erosão acelerada do solo em canaviais e pomares de citros. Eng. Agrícola 25, 242–252. https://doi.org/10.1590/S0100-69162005000100027

Popin, G. V., Santos, A.K.B., Melo, P.L.A., Cherubin, M.R., Cerri, C.E.P., Siqueira-Neto, M., Popin, G. V., Santos, A.K.B., Melo, P.L.A., Cherubin, M.R., Cerri, C.E.P., Siqueira-Neto, M., 2020. Importance of sugarcane straw maintenance to prevent soil organic matter depletion in a Nitisol in the central-southern region of Brazil. Soil Res. 59, 119–129. https://doi.org/10.1071/SR20013

Poppiel, R.R., Lacerda, M.P., Rizzo, R., Safanelli, J.L., Bonfatti, B.R., Silvero, N.E., Demattê, J.A., 2020. Soil Color and Mineralogy Mapping Using Proximal and Remote Sensing in Midwest Brazil. Remote Sens. https://doi.org/10.3390/rs12071197

Portinho, J.L., Gomes, A.C.C., Koga-Vicente, A., Milani, F.C.C., Pentean, R.B., Manzatto, C.V., Spinelli-Araujo, L., Vicente, L.E., 2021. The pathways influence of agricultural expansion on water quality of fish farming in Ilha Solteira reservoir, São Paulo, Brazil. Aquaculture 536, 736405. https://doi.org/https://doi.org/10.1016/j.aquaculture.2021.736405

Prado, R. de M., Centurion, J.F., 2001. Alterações na cor e no grau de floculação de um Latossolo Vermelho-Escuro sob cultivo contínuo de cana-de-açúcar. Pesqui. Agropecuária Bras. 36, 197–203. https://doi.org/10.1590/S0100-204X2001000100024

Prove, B.G., Googan, V.J., Truong, P.N. V., 1995. Nature and magnitude of soil erosion in sugarcane land on the wet tropical coast of north-eastern. Austr J Exper Agric.

Roberts, D., Wilford, J., Ghattas, O., 2019. Exposed soil and mineral map of the Australian continent revealing the land at its barest. Nat. Commun. 10, 5297. https://doi.org/10.1038/s41467-019-13276-1

Rocha, G.C. da, Sparovek, G., 2021. Scientific and technical knowledge of sugarcane cover-management USLE/RUSLE factor. Sci. Agric. 78. https://doi.org/10.1590/1678-992x-2020-0234

Rogge, D., Bauer, A., Zeidler, J., Mueller, A., Esch, T., Heiden, U., 2018. Building an exposed soil composite processor (SCMaP) for mapping spatial and temporal characteristics of soils with Landsat imagery (1984–2014). Remote Sens. Environ. 205, 1–17. https://doi.org/10.1016/J.RSE.2017.11.004

Rossi Neto, J., de Souza, Z.M., Kölln, O.T., Carvalho, J.L.N., Ferreira, D.A., Castioni, G.A.F., Barbosa, L.C., de Castro, S.G.Q., Braunbeck, O.A., Garside, A.L., Franco, H.C.J., 2018. The Arrangement and Spacing of Sugarcane Planting Influence Root Distribution and Crop Yield. BioEnergy Res. 11, 291–304. https://doi.org/10.1007/s12155-018-9896-1

Rotta, C.M. dos S., Zuquette, L.V., 2021. Assessment of environmental degradation due to anthropogenic processes based on critical zones: a study in a basin in southern Brazil. Environ. Earth Sci. 80, 215. https://doi.org/10.1007/s12665-021-09475-z

Rudorff, B.F.T., de Aguiar, D.A., da Silva, W.F., Sugawara, L.M., Adami, M., Moreira, M.A., 2010. Studies on the rapid expansion of sugarcane for ethanol production in São Paulo state (Brazil) using Landsat data. Remote Sens. 2, 1057–1076. https://doi.org/10.3390/rs2041057

Safanelli, J., Poppiel, R., Ruiz, L., Bonfatti, B., Mello, F., Rizzo, R., Demattê, J., 2020a. Terrain Analysis in Google Earth Engine: A Method Adapted for High-Performance Global-Scale Analysis. ISPRS Int. J. Geo-Information 9. https://doi.org/10.3390/ijgi9060400

Safanelli, J.L., Chabrillat, S., Ben-Dor, E., Demattê, J.A.M., 2020b. Multispectral Models from Bare Soil Composites for Mapping Topsoil Properties over Europe. Remote Sens. . https://doi.org/10.3390/rs12091369

Sanches, G.M., Magalhães, P.S.G., Kolln, O.T., Otto, R., Rodrigues, F., Cardoso, T.F., Chagas, M.F., Franco, H.C.J., 2021. Agronomic, economic, and environmental assessment of site-specific fertilizer management of Brazilian sugarcane fields. Geoderma Reg. 24, e00360. https://doi.org/https://doi.org/10.1016/j.geodrs.2021.e00360

Santos, A.K.B. dos, Popin, G.V., Gmach, M.R., Cherubin, M.R., Siqueira Neto, M., Cerri, C.E.P., 2022. Changes in soil temperature and moisture due to sugarcane straw removal in central-southern Brazil. Sci. Agric. 79. https://doi.org/10.1590/1678-992x-2020-0309

Santos, J.Y.G. dos, Montenegro, S.M.G.L., Silva, R.M. da, Santos, C.A.G., Quinn, N.W., Dantas, A.P.X., Ribeiro Neto, A., 2021. Modeling the impacts of future LULC and climate change on runoff and sediment yield in a strategic basin in the Caatinga/Atlantic forest ecotone of Brazil. CATENA 203, 105308. https://doi.org/https://doi.org/10.1016/j.catena.2021.105308

Santos, H.G. dos, Zaroni, M.J., n.d. Agência Embrapa de Informação Tecnológica - Nitossolos [WWW Document]. URL https://www.agencia.cnptia.embrapa.br/gestor/solos_tropicais/arvore/CONTAG01_17_2212200611543.html (accessed 7.12.21).

Santos, H.G., 2018. Sistema brasileiro de classificação de solos, 5th ed, Embrapa Solos. Brasília.

Sayão, V.M., dos Santos, N.V., de Sousa Mendes, W., Marques, K.P.P., Safanelli, J.L., Poppiel, R.R., Demattê, J.A.M., 2020. Land use/land cover changes and bare soil surface temperature monitoring in southeast Brazil. Geoderma Reg. 22. https://doi.org/10.1016/j.geodrs.2020.e00313

Schlindwein, S.L., Feitosa de Vasconcelos, A.C., Bonatti, M., Sieber, S., Strapasson, A., Lana, M., 2021. Agricultural land use dynamics in the Brazilian part of La Plata Basin: From driving forces to societal responses. Land use policy 107, 105519. https://doi.org/https://doi.org/10.1016/j.landusepol.2021.105519

Secretaria de Infraestrutura e Meio Ambiente, 2021. Etanol Verde [WWW Document]. URL https://www.infraestruturameioambiente.sp.gov.br/etanolverde/ (accessed 7.12.21).

Sen, P.K., 1968. Estimates of the Regression Coefficient Based on Kendall's Tau. J. Am. Stat. Assoc. 63, 1379–1389. https://doi.org/10.1080/01621459.1968.10480934

Shabou, M., Mougenot, B., Chabaane, Z.L., Walter, C., Boulet, G., Aissa, N.B., Zribi, M., 2015. Soil Clay Content Mapping Using a Time Series of Landsat TM Data in Semi-Arid Lands. Remote Sens. https://doi.org/10.3390/rs70506059

Shen, X.-F., Zhao, Z.-H., Chen, Y., 2019. Effects of Intercropping with Peanut and Silicon Application on Sugarcane Growth, Yield and Quality. Sugar Tech 21, 437–443. https://doi.org/10.1007/s12355-018-0667-2

Shukla, S.K., Jaiswal, V.P., Sharma, L., Pathak, A.D., Singh, A.K., Gupta, R., Awasthi, S.K., Gaur, A., Zubair, A., Tiwari, R., 2020. Sugarcane Yield Using Minimum Tillage Technology Through Subsoiling: Beneficial Impact on Soil Compaction, Carbon Conservation and Activity of Soil Enzymes. Sugar Tech 22, 987–1006. https://doi.org/10.1007/s12355-020-00860-9

Signor, D., Czycza, R.V., Milori, D.M.B.P., Cunha, T.J.F., Cerri, C.E.P., 2016. Atributos químicos e qualidade da matéria orgânica do solo em sistemas de colheita de cana-de-açúcar com e sem queima. Pesqui. Agropecuária Bras. 51. https://doi.org/10.1590/s0100-204x2016000900042

Signor, D., Zani, C.F., Paladini, A.A., Deon, M.D., Cerri, C.E.P., 2014. Estoques de carbono e qualidade da matéria orgânica do solo em áreas cultivadas com cana-de-açúcar. Rev. Bras. Ciência do Solo 38, 1402–1410. https://doi.org/10.1590/S0100-06832014000500005

Silva-Olaya, A.M., Cerri, C.E.P., La Scala Jr, N., Dias, C.T.S., Cerri, C.C., 2013. Carbon dioxide emissions under different soil tillage systems in mechanically harvested sugarcane. Environ. Res. Lett. 8. https://doi.org/10.1088/1748-9326/8/1/015014

Silva, A.F.R., Brasil, Y.L., Koch, K., Amaral, M.C.S., 2021. Resource recovery from sugarcane vinasse by anaerobic digestion – A review. J. Environ. Manage. 295, 113137. https://doi.org/https://doi.org/10.1016/j.jenvman.2021.113137

Silvero, Nélida Elizabet Quiñonez, Demattê, J.A.M., Amorim, M.T.A., Santos, N.V. dos, Rizzo, R., Safanelli, J.L., Poppiel, R.R., Mendes, W. de S., Bonfatti, B.R., 2021a. Soil variability and quantification based on Sentinel-2 and Landsat-8 bare soil images: A comparison. Remote Sens. Environ. 252, 112117. https://doi.org/https://doi.org/10.1016/j.rse.2020.112117

Silvero, Nélida E Q, Demattê, J.A.M., Vieira, J. de S., Mello, F.A. de O., Amorim, M.T.A., Poppiel, R.R., Mendes, W. de S., Bonfatti, B.R., 2021b. Soil property maps with satellite images at multiple scales and its impact on management and classification. Geoderma 397, 115089. https://doi.org/https://doi.org/10.1016/j.geoderma.2021.115089

SINDIPEÇAS, ABIPEÇAS, 2021. Relatório da Frota Circulante. São Paulo.

Singh, S.R., Yadav, P., Singh, D., Shukla, S.K., Tripathi, M.K., Bahadur, L., Mishra, A., Kumar, S., 2021. Intercropping in Sugarcane Improves Functional Diversity, Soil Quality and Crop Productivity. Sugar Tech 23, 794–810. https://doi.org/10.1007/s12355-021-00955-x

Som-ard, J., Atzberger, C., Izquierdo-Verdiguier, E., Vuolo, F., Immitzer, M., 2021. Remote Sensing Applications in Sugarcane Cultivation: A Review. Remote Sens. . https://doi.org/10.3390/rs13204040

Sousa, D.M.G. de, Lobato, E., n.d. Agência de Informação Embrapa Areia Quartzosa / Neossolo Quartzarênico [WWW Document]. URL http://www.agencia.cnptia.embrapa.br/Agencia16/AG01/arvore/AG01_2_10112005101955.html (accessed 7.12.21).

Souza, G.S. de, Souza, Z.M. de, Silva, R.B. da, Barbosa, R.S., Araújo, F.S., 2014. Effects of traffic control on the soil physical quality and the cultivation of sugarcane. Rev. Bras. Ciência do Solo 38, 135–146.

Sparovek, G., Schnug, E., 2001. Temporal Erosion-Induced Soil Degradation and Yield Loss. Soil Sci. Soc. Am. J. 65, 1479–1486. https://doi.org/10.2136/SSSAJ2001.6551479X

Spera, S., VanWey, L., Mustard, J., 2017. The drivers of sugarcane expansion in Goiás, Brazil. Land use policy 66, 111–119. https://doi.org/https://doi.org/10.1016/j.landusepol.2017.03.037

Stolf, R., de Oliveira, A.P.R., 2020. The success of the brazilian alcohol program (Proalcool)-a decadeby-decade brief history of ethanol in Brazil. Eng. Agric. 40, 243–248. https://doi.org/10.1590/1809-4430-ENG.AGRIC.V40N2P243-248/2020

Teixeira, D.B. de S., Cecílio, R.A., de Oliveira, J.P.B., de Almeida, L.T., Pires, G.F., 2021. Rainfall erosivity and erosivity density through rainfall synthetic series for São Paulo State, Brazil: Assessment, regionalization and modeling. Int. Soil Water Conserv. Res. https://doi.org/https://doi.org/10.1016/j.iswcr.2021.10.002

Tenelli, S., de Oliveira Bordonal, R., Barbosa, L.C., Carvalho, J.L.N., 2019. Can reduced tillage sustain sugarcane yield and soil carbon if straw is removed? BioEnergy Res. 12, 764–777. https://doi.org/10.1007/s12155-019-09996-3

Tenelli, S., Otto, R., Bordonal, R.O., Carvalho, J.L.N., 2021. How do nitrogen fertilization and cover crop influence soil C-N stocks and subsequent yields of sugarcane? Soil Tillage Res. 211, 104999. https://doi.org/https://doi.org/10.1016/j.still.2021.104999

Thomaz, E.L., Fidalski, J., 2020. Interrill erodibility of different sandy soils increases along a catena in the caiuá sandstone formation. Rev. Bras. Cienc. do Solo 44, 1–13. https://doi.org/10.36783/18069657rbcs20190064

Tziolas, N., Tsakiridis, N., Ben-Dor, E., Theocharis, J., Zalidis, G., 2020. Employing a Multi-Input Deep Convolutional Neural Network to Derive Soil Clay Content from a Synergy of Multi-Temporal Optical and Radar Imagery Data. Remote Sens. . https://doi.org/10.3390/rs12091389

UNICA, 2021. Observatório da Cana [WWW Document]. URL https://www.observatoriodacana.com.br (accessed 7.13.21).

Valente, F., Laurini, M., 2021. Pre-harvest sugarcane burning: A statistical analysis of the environmental impacts of a regulatory change in the energy sector. Clean. Eng. Technol. 4, 100255. https://doi.org/https://doi.org/10.1016/j.clet.2021.100255

Valim, W., Valim, W.C., Panachuki, E., Pavei, D.S., Sobrinho, T.A., Almeida, W.S., 2016. Effect of sugarcane waste in the control of interrill erosion. Semin. Ciências Agrárias 37, 1155–1164. https://doi.org/10.5433/1679-0359.2016v37n3p1155

Viscarra Rossel, R.A., Behrens, T., Ben-Dor, E., Brown, D.J., Demattê, J.A.M., Shepherd, K.D., Shi, Z., Stenberg, B., Stevens, A., Adamchuk, V., Aïchi, H., Barthès, B.G., Bartholomeus, H.M., Bayer, A.D., Bernoux, M., Böttcher, K., Brodský, L., Du, C.W., Chappell, A., Fouad, Y., Genot, V., Gomez, C., Grunwald, S., Gubler, A., Guerrero, C., Hedley, C.B., Knadel, M., Morrás, H.J.M., Nocita, M., Ramirez-Lopez, L., Roudier, P., Campos, E.M.R., Sanborn, P., Sellitto, V.M., Sudduth, K.A., Rawlins, B.G., Walter, C., Winowiecki, L.A., Hong, S.Y., Ji, W., 2016. A global spectral library to characterize the world's soil. Earth-Science Rev. 155. https://doi.org/10.1016/j.earscirev.2016.01.012

Vilas, M.P., Shaw, M., Rohde, K., Power, B., Donaldson, S., Foley, J., Silburn, M., 2022. Ten years of monitoring dissolved inorganic nitrogen in runoff from sugarcane informs development of a modelling algorithm to prioritise organic and inorganic nutrient management. Sci. Total Environ. 803, 150019. https://doi.org/https://doi.org/10.1016/j.scitotenv.2021.150019

Vitti, A. C., Prado, H. do (2012). Produtividade da cana-de-açúcar em função do ambiente e disponibilidade hídrica (Sugarcane productivity as a function of the environment and water availability). Pesquisa & Tecnologia Apta regional, vol. 9, n. 2, Jul-Dez 2012. Disponível em: http://www.aptaregional.sp.gov.br/acesse-os-artigos-pesquisa-e-tecnologia/edicao-2012/julho-dezembro-2/1324-produtividade-da-cana-de-acucar-em-funcao-do-ambiente-e-disponibilidade-hidrica/file.html

Walter, A., Galdos, M.V., Scarpare, F.V., Leal, M.R.L.V., Seabra, J.E.A., da Cunha, M.P., Picoli, M.C.A., de Oliveira, C.O.F., 2014. Brazilian sugarcane ethanol: developments so far and challenges for the future. WIREs Energy Environ. 3, 70–92. https://doi.org/https://doi.org/10.1002/wene.87

Wei T, Simko V (2021). R package 'corrplot': Visualization of a Correlation Matrix. (Version 0.92), https://github.com/taiyun/corrplot. (accessed 30 June 2021).

Weill, M. de A.M., Sparovek, G., 2008. Estudo da erosão na microbacia do Ceveiro (Piracicaba, SP): I - Estimativa das taxas de perda de solo e estudo de sensibilidade dos fatores do modelo EUPS. Rev. Bras. Ciência do Solo 32, 801–814. https://doi.org/10.1590/S0100-06832008000200034

Wickham, H., 2016. ggplot2: Elegant Graphics for Data Analysis, Springer-Verlag New York. Available at: https://ggplot2.tidyverse.org (accessed 30 June 2021).

Zaroni, M.J., Santos, H.G. dos, n.d. Agência Embrapa de Informação Tecnológica - Argissolos [WWW Document]. URL https://www.agencia.cnptia.embrapa.br/gestor/solos_tropicais/arvore/CONTAG01_7_2212200611538.html (accessed 7.12.21).

Zepp, S., Jilge, M., Metz-Marconcini, A., Heiden, U., 2021. The influence of vegetation index thresholding on EO-based assessments of exposed soil masks in Germany between 1984 and 2019. ISPRS J. Photogramm. Remote Sens. 178, 366–381. https://doi.org/https://doi.org/10.1016/j.isprsjprs.2021.06.015

5. GENERAL DISCUSSIONS AND CONCLUSIONS

In this thesis, two chapters were presented that deal with the use of remote and proximal sensing technologies to map soil properties for soil management and conservation. The third chapter used Landsat multi-temporal images to monitor soil management in sugarcane areas, aiming at its application in soil security.

In the first study (Chapter 2) at the farm scale, different sensors were used for clay prediction for a smallholder area. The cubist algorithm and bootstrap (100 realizations) were applied to obtain the mean clay map and the uncertainty maps. It was tested the application of models obtained with external data, but from the same region, and models obtained within area data. For the external models the best result was obtained with Vis-NIR-SWIR data from the Fieldspec sensor. Among the models of multispectral sensors on board datellites, Sentinel 2-MSI had the best performance followed by Landsat 8-OLI, with the PlanetScope sensor being the worst result. The AISA-FÉNIX hyperspectral sensor, on the other hand, presented similar performance to Landsat 8-OLI and Sentinel 2-MSI sensors. There was a significant improvement in the performance of the models obtained from data from within the area. PlanetScope images had low spectral resolution and no spectral bands in the SWIR region, which are very important information in clay prediction.

In the second study, an approach similar to that learned in the first was developed. However, one area was studied on a regional scale. SYSI bands and terrain covariates were used as independent variables to predict soil erodibility (K factor), in a covariate-based method prediction approach. Also erodibility was predicted using Vis-NIR-SWIR data as independent variables, in a spatial autocorrelation approach (ordinary kriging). Again the Cubist algorithm was used. Two case studies were carried out to evaluate the results found. Both compared the erodibility maps obtained with erodibility maps obtained by traditional methodology, that is, from soil maps, one at a scale of 1:100,000 and the other detailed at a scale of 1:10,000. The results found showed that the digital maps obtained have greater agreement with the traditional map obtained from the detailed soil map, which demonstrates the potential of the technique to be applied to obtain erodibility maps for microbasin or farm scale.

Finally, in chapter 4, multi-temporal images from the Landsat series, from 1985 to 2019, were used to understand the dynamics of exposure of soils (bare soils) cultivated with sugarcane in the Piracicaba region. The results found that the end of pre-harvest burning provided a sharp drop in exposed soil areas over the years. They also demonstrate that sandy soils have a higher frequency of exposure than more clayey soils. The explanation for this is the lower productive potential of these soils, which leads to the need for sugarcane replanting with conventional tillage. It was also possible to verify a change over the years in the crop production system, a migration from the 12-month cane system to 18-month cane.

As general conclusions of the developed works were found that: the use of remote and proximal sensing data have high potential to contribute to the digital mapping of soil attributes, being an important tool for obtaining adequate information for management and conservation practices. In addition, the use of multi-temporal images makes it possible to monitor management practices and soil tillage over the years.